NAVAL POSTGRADUATE SCHOOL

MONTEREY, CALIFORNIA

THESIS

OPTIMIZATION OF A BACK SURFACE CONTACT COPPER INDIUM GALLIUM SELENIDE THIN FILM SOLAR CELL WITH NEARLY ORTHOGONAL LATIN HYPERCUBE AND SILVACO

by

Brandy A. Allain

June 2022

Thesis Advisor: Sherif N. Michael
Second Reader: Susan M. Sanchez

THIS PAGE INTENTIONALLY LEFT BLANK

REPORT DOCUMENTATION PAGE			*Form Approved OMB No. 0704-0188*

1. AGENCY USE ONLY *(Leave blank)*	**2. REPORT DATE** June 2022	**3. REPORT TYPE AND DATES COVERED** Master's thesis

4. TITLE AND SUBTITLE OPTIMIZATION OF A BACK SURFACE CONTACT COPPER INDIUM GALLIUM SELENIDE (CIGS) THIN FILM SOLAR CELL WITH NEARLY ORTHOGONAL LATIN HYPERCUBE AND SILVACO	**5. FUNDING NUMBERS**
6. AUTHOR(S) Brandy A. Allain	
7. PERFORMING ORGANIZATION NAME(S) AND ADDRESS(ES) Naval Postgraduate School Monterey, CA 93943-5000	**8. PERFORMING ORGANIZATION REPORT NUMBER**
9. SPONSORING / MONITORING AGENCY NAME(S) AND ADDRESS(ES) N/A	**10. SPONSORING / MONITORING AGENCY REPORT NUMBER**

11. SUPPLEMENTARY NOTES The views expressed in this thesis are those of the author and do not reflect the official policy or position of the Department of Defense or the U.S. Government.

12a. DISTRIBUTION / AVAILABILITY STATEMENT Approved for public release. Distribution is unlimited.	**12b. DISTRIBUTION CODE** A

13. ABSTRACT (maximum 200 words)

This thesis focuses on the optimization of a novel design back surface contact (BSC) copper indium gallium (di)selenide (CIGS). It introduces the Nearly Orthogonal Latin Hypercube (NOLH) design of experiments as a means of optimizing parameters to be entered into Silvaco ATLAS simulation software. By introducing a vertical p-n junction within the bulk of the solar cell the separation of charges was promoted, and with the BSC layout shadowing effects were negated. Due to these changes the optimized cell efficiency was found to be 27.1%, a relative increase of 11.5% from the previous optimal designs of prior theses. The NOLH generated data that could be run in parallel, significantly reducing simulation time, as well as giving a better understanding of the relationship between parameters within the solar cell. The NOLH design of experiments is the next step for all solar cell optimization efforts. The implications of the high-efficiency, lightweight design of the BSC CIGS solar cell ranges from terrestrial to celestial and everywhere in between. From lightweight comms recharge capabilities to unmanned aerial vehicle (UAV) power sources, and even satellites, the potential for CIGS are endless.

14. SUBJECT TERMS CIGS, optimize, solar cells, copper indium gallium (di)selenide	**15. NUMBER OF PAGES** 105
	16. PRICE CODE

17. SECURITY CLASSIFICATION OF REPORT	**18. SECURITY CLASSIFICATION OF THIS PAGE**	**19. SECURITY CLASSIFICATION OF ABSTRACT**	**20. LIMITATION OF ABSTRACT**
Unclassified	Unclassified	Unclassified	UU

NSN 7540-01-280-5500

Standard Form 298 (Rev. 2-89)
Prescribed by ANSI Std. 239-18

THIS PAGE INTENTIONALLY LEFT BLANK

Approved for public release. Distribution is unlimited.

OPTIMIZATION OF A BACK SURFACE CONTACT COPPER INDIUM GALLIUM SELENIDE (CIGS) THIN FILM SOLAR CELL WITH NEARLY ORTHOGONAL LATIN HYPERCUBE AND SILVACO

Brandy A. Allain
Lieutenant, United States Navy
BS, Norwich University, 2015

Submitted in partial fulfillment of the
requirements for the degree of

MASTER OF SCIENCE IN ELECTRICAL ENGINEERING

from the

NAVAL POSTGRADUATE SCHOOL
June 2022

Approved by: Sherif N. Michael
Advisor

Susan M. Sanchez
Second Reader

Douglas J. Fouts
Chair, Department of Electrical and Computer Engineering

THIS PAGE INTENTIONALLY LEFT BLANK

ABSTRACT

This thesis focuses on the optimization of a novel design back surface contact (BSC) copper indium gallium (di)selenide (CIGS). It introduces the Nearly Orthogonal Latin Hypercube (NOLH) design of experiments as a means of optimizing parameters to be entered into Silvaco ATLAS simulation software. By introducing a vertical p-n junction within the bulk of the solar cell the separation of charges was promoted, and with the BSC layout shadowing effects were negated. Due to these changes the optimized cell efficiency was found to be 27.1%, a relative increase of 11.5% from the previous optimal designs of prior theses. The NOLH generated data that could be run in parallel, significantly reducing simulation time, as well as giving a better understanding of the relationship between parameters within the solar cell. The NOLH design of experiments is the next step for all solar cell optimization efforts. The implications of the high-efficiency, lightweight design of the BSC CIGS solar cell ranges from terrestrial to celestial and everywhere in between. From lightweight comms recharge capabilities to unmanned aerial vehicle (UAV) power sources, and even satellites, the potential for CIGS are endless.

THIS PAGE INTENTIONALLY LEFT BLANK

TABLE OF CONTENTS

LIST OF FIGURES

LIST OF TABLES

THIS PAGE INTENTIONALLY LEFT BLANK

LIST OF ACRONYMS AND ABBREVIATIONS

A	Ampere, unit of current
a-Si	amorphous silicone
AM	air mass
ARC	anti-reflective coating
AZO	aluminum zinc oxide
BSF	back surface field
c	speed of light
C	Celsius, unit of temperature (metric scale)
CdS	cadmium sulfide
CdTe	cadmium telluride
CGS	copper gallium selenide
CIGS	copper indium gallium (di)selenide
CIS	copper indium selenide
CO_2	carbon dioxide
Cu	copper
D	diffusion constant
eV	electron volt
E_C	conduction band energy level
E_F	Fermi energy level
E_G	bandgap energy
E_V	valence band energy level
EHP	electron-hole pair
F	Fahrenheit, unit of temperature (empirical scale)
FF	fill factor
FSF	front surface field
G	Generation rate
Ga	gallium
GaAs	gallium arsenide
Ge	germanium
h	Planck's constant

$\hbar$	reduced Planck's constant
I	current
I_D	diffusion current
I_{MP}	max power peak current
I_S	drift current
I_{SC}	short circuit current
In	indium
InP	indium phosphide
J	current density
J	Joule, unit of energy
J_{SC}	short circuit current density
k	Boltzmann constant
k	wave vector
K	Kelvin, unit of temperature (absolute scale)
L_n	electron diffusion length
L_p	hole diffusion length
m	meter, unit of length (metric scale)
Mo	molybdenum
Na	sodium
O	oxygen
O_3	ozone
P	power
P_{MP}	max power peak power
PV	photovoltaic
q	electron charge
R	resistance
s	second, unit of time
Se	selenium
Si	silicon
V	voltage
V_F	turn on voltage
V_{MP}	max power peak voltage

V_{OC}	open circuit voltage
Zn	zinc
ZnO	zinc oxide
α	absorption coefficient
η	efficiency
θ_z	zenith angle
μ	mobility
μ_n	electron mobility
μ_p	hole mobility
ε	permittivity
ρ	resistivity
σ	conductivity
τ	carrier lifetime
χ	electron affinity
Ω	Ohm

THIS PAGE INTENTIONALLY LEFT BLANK

ACKNOWLEDGMENTS

Many people have assisted in the completion of this work, first and foremost Dr. Sherif Michael for his guidance and support as my advisor, and former NPS graduate Kevin Logar for assisting in the development of what became this thesis.

THIS PAGE INTENTIONALLY LEFT BLANK

I. INTRODUCTION

As the use of technology continues to advance in the modern world, the demand for clean, renewable, and inexpensive energy is on a rise. With the increase of power consumption, the effects of fossil fuel usage on the environment and political climate are causing countries to scramble for a clean, renewable source of power. Current means of renewable energy include wind turbines, hydroelectric, and geothermal. These power generation techniques, however, have environmental requirements not met in most parts of the world and have ecological impacts. Solar power is both a renewable energy source and has minimal environmental or ecological effects. To combat climate change solar energy has been integrated into everyday technology, creating extreme demands on high-efficiency cells. As the most used solar cell, silicon (Si), approaches its theoretical maximum performance, greater amounts of study have been directed at new materials in hopes of surpassing the current power and efficiency limits. As part of this research effort, novel cell designs utilizing thin film back surface contacts (BSCs) have been investigated.

Solar energy demand is not solely concentrated on societal infrastructure but is currently in use in many government and military applications. Current uses are, but not limited to, satellites, interplanetary space rovers, and charging stations for communication devices for warfighters. The diverse implementation of solar energy requires a diverse requirement for types of solar cells. Space specific solar cells must be radiation hardened (rad-hard), with increased longevity, and lightweight to decrease the cost of launch systems. For terrestrial usage by warfighters, the cell must be rugged, compact, and lightweight. A study conducted for the Marines showed that for every 15 pounds of excess weight a Marine had to carry decreases survivability in a combat scenario by 5.3% [1]. To accommodate the necessary requirements, solar cells such as copper-indium-gallium-Di-selenide (CIGS) have been investigated and proven to be great contenders for both applications with their rad-hard and efficient characteristics.

A. OBJECTIVE

The motivation of this thesis is to explore the benefits of a novel design CIGS solar cell and the impact of a BSC on efficiency and cell design. To determine the optimal parameters under terrestrial industry standard, AM1.5, this model will be optimized utilizing the Nearly Orthogonal Latin Hypercube (NOLH) and simulated in semiconductor modeling software Silvaco. This builds on the work conducted by Logar [2] in March 2022, with additional parameters being varied utilizing the NOLH.

B. RELATED WORK

The BSC architecture with CIGS has been modeled by several past Naval Postgraduate School (NPS) students. At the forefront are Herrera [3] and Logar [2], with similar models explored in this thesis. Previous work on novel designs of CIGS were conducted by Fortis [4] and Columbus [5], where a CIGS solar cell was modeled focusing on optimization by interchanging layer materials and altering thicknesses in Silvaco. Modeling of BSC designs was conducted by O'Connor [6] and Green [7] utilizing Gallium Arsenide (GaAs) and silicone (Si) solar cells, respectively. Modeling techniques, as well as the optimal performance data from these previous student works, will be utilized to meet the objective of this thesis.

C. ORGANIZATION

This thesis is organized to provide sufficient background for readers who are not familiar with semiconductor physics or solar cell specifics, Chapter II and Chapter III cover these topics in detail, respectively. Chapter IV delves into CIGS and the novel design explored in this thesis. Chapter V covers the simulation techniques used to model the solar cell, both NOLH and Silvaco. The final two chapters expound upon the results found and provide concluding remarks with focus on future applications.

II. BACKGROUND

This chapter contains the required review information for atomic physic and the nature and functionality of semiconductor physics. The fundamentals of all solar cells start at the atomic level. The reader who is familiar with the concepts described herein may wish to proceed to either Chapter III or IV for a discussion on solar cell construction and CIGS, respectively.

A. FUNDAMENTAL PHYSICS

The modern model of an atomic structure was created by Niels Bohr in 1913. His model demonstrated multiple electrons can occupy quantized energy states, known as shells. These shells surround a positively charged nucleus, creating an atom. The electrons surrounding the nucleus may transfer between the energy states, going from shell to shell, by giving up or gaining energy, as demonstrated in Figure 1. The energy required for this action is equivalent to the difference in the energy levels of the different shells.

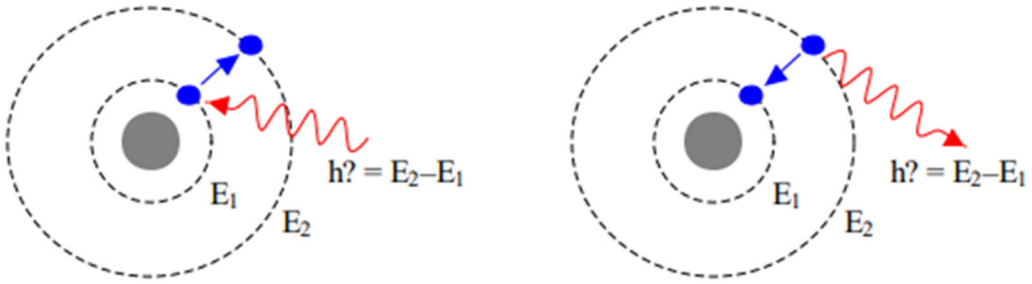

Figure 1. Transition of an electron from shell states. Source: [8].

The farther the electron is from the nucleus the higher the potential energy, and the lower the kinetic energy, giving it the weakest bond to the atomic structure. As an electron can only occupy a shell orbit, and not the space between energy states, each shell has a set number of electrons that may occupy it. This forces electrons to the valence band, the outermost band, and creates the possibility for free electrons. Free electrons are electrons that do not occupy any energy band of an atom and are cable of moving independently.

The number of free electrons is directly correlated to temperature. At 0 K, absolute zero, the movement of electrons is minimized and there is not enough energy for an electron to change state. As the temperature increases, kinetic energy is increased; this allows the electrons to break free from the valence band. Free electron movement is directly correlated to the electrical conductivity and magnetism of all materials. Bohr's model for atomic structure and the demonstration of a free electron is shown in Figure 2.

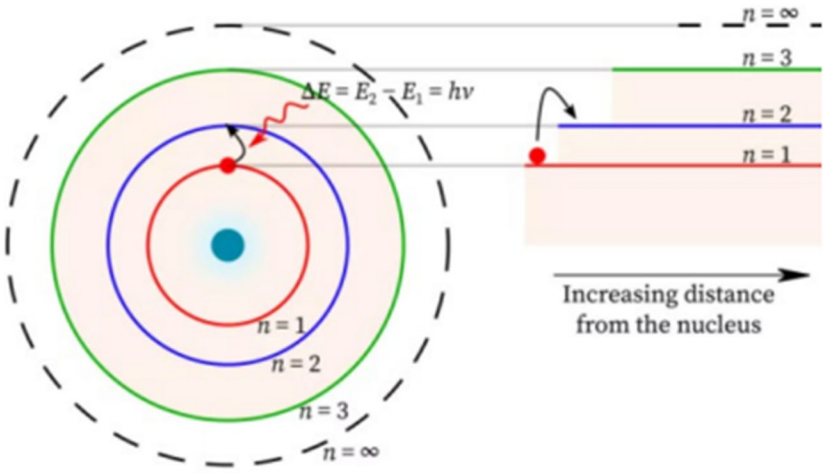

Figure 2. Bohr's model of the atomic structure. Source: [9].

B. BANDGAP

As temperature rises the energy levels in valence electrons increase and some break free from the atoms. The higher the temperature the more electrons that are capable of breaking free from the valence band. This holds true until there are no more electrons in the valence band, and then the temperature increase could hinder conductivity of the material. When the electrons leave the valence band (E_v), they enter what is known as the conduction band (E_c). Free electrons in the conduction band have higher energy than those in the valence band and can only exist in one of the two bands. The state between the two bands is known as the bandgap, (E_g), as shown in Figure 3. No energy states can exist within E_g; however, it is a vital characteristic in predicting the behavior of the materials discussed in future chapters.

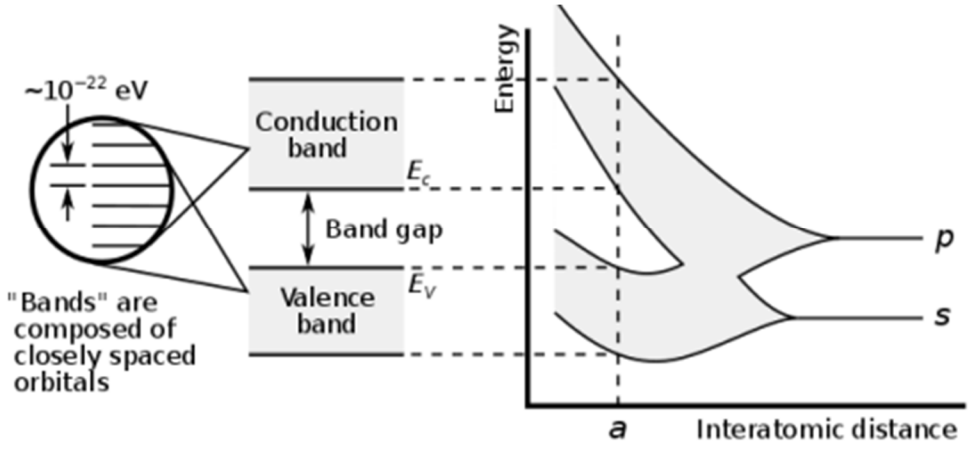

Figure 3. Bandgap construction. Source: [10].

The size of the bandgap within materials and compounds indicates the conductivity. As shown in Figure 4, materials classified as conductors have overlapping valence and conduction bands, they promote the flow of electrons, such as most metals, especially Copper. Inversely, materials classified as insulators have a large bandgap, a greater difference between the energy levels of the conduction and valence bands. These insulators inhibit the flow of electrons, this is found in materials such as rubber and plastic. Conductors have very low resistivity to electron flow, while insulators have very high resistivity. Materials with moderate bandgaps are classified as semiconductors.

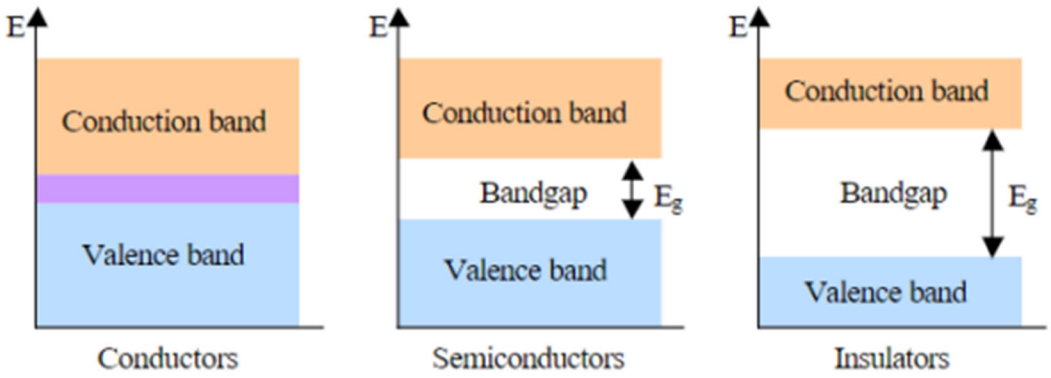

Figure 4. Bandgap effects on materials. Source: [8].

The conductivity, the number of free electrons, can be increased with the amount of energy supplied, at minimum equal to the bandgap of the material. Conductors require very little energy, while insulators require greater amounts of energy to conduct a negligible number of electrons. The true diversity is found in semiconductors, which can act as both a conductor and an insulator in the right situations. For this reason, semiconductors are often used in electrical systems in the form of diodes, transistors, and many other applications.

Natural semiconductor material is exclusively found in Group IV of the periodic table. Compound semiconductors can also be created by combining materials from various groups on the periodic table, such as III-V and II-VI compounds. The combination of these different groups of materials mimics a Group IV material, by maintaining eight electrons in the valence band, a full valence band. Materials within the Group V and VI have five and six electrons in their valence band, same with group II and III, they have the corresponding number of electrons in the valence band. When a Group V or VI material is introduced to a Group III or II material, they will give up an electron to said material, creating a net positive charge. This positive ion will now be attracted to the now electron heavy Group II or III material that will have a net negative charge, a negative ion. Once the ions of opposite polarity combine, they form an ionic bond, now having eight electrons in the outer valence shell. Figure 5 shows an abbreviated periodic table that represents most of the Group IV and compound semiconductor materials.

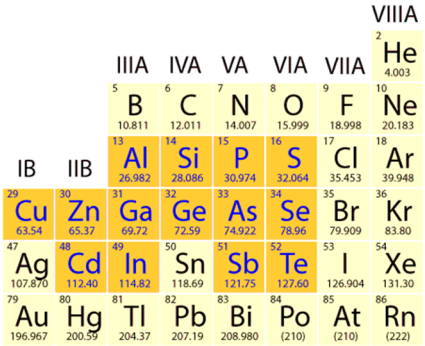

Figure 5. Abbreviated Periodic Table. Source: [11].

When an electron is released from their covalent bond, due to a rise in energy, their negative energy is removed from the location, and a resultant hole is left behind. The hole, or a vacancy of an electron, has a net positive charge of the same magnitude as the absent electron. This process happens through ionization, or generation. The now created electron hole pair (EHP) can recombine if near each other, this will cause the ions to disappear, and a neutral charge to perpetuate, this is called recombination. An electron can move through the material, and so is afforded many different opportunities to recombine. Temperature and the concentration of EHPs within a material determine the rate of generation and recombination. At thermal equilibrium there is a constant number of EHPs present within the material, due to the rate of generation and recombination being equal.

If a semiconductor contains no foreign atoms, it is called a pure or intrinsic semiconductor and can be seen in Figure 6. No EHPs exist at 0 K in intrinsic semiconductors. However, as the temperature is increased the number of EHPs will raise logarithmically. These EHPs are called intrinsic carriers, and as the number of EHPs increase so too does the conductivity of the material. The intrinsic carriers make up a small fraction of the atoms within the device and play an important role in the function of the electronic device.

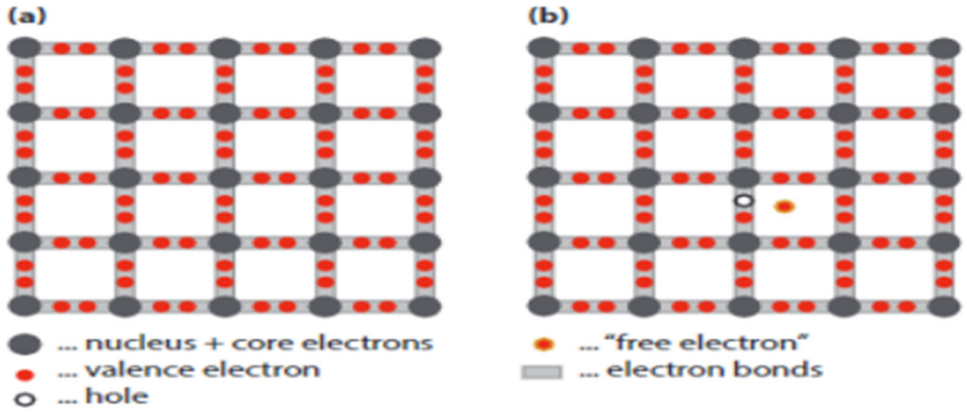

Figure 6. Intrinsic semiconductor without (a) and with (b) EHP. Source: [12].

To increase the conductivity or alter the electrical properties of materials, impurities known as dopants, can be added. Group V or above materials are classified as donors, since their predominant carriers are electrons, and they will donate an electron to a material of Group III or lower, thereby obtaining a net positive charge. Group III and lower are called acceptors, as their predominant carriers are holes, and they will accept an electron from a neighboring atom, becoming negatively charged. Materials that are doped with donors are called n-type materials, while materials doped with acceptors are p-type materials. N-type material is said to have electrons as the majority carriers, while p-type material has holes as the majority carriers. Doping a material is the process of adding these donors or acceptors to intrinsic material, thereby turning it extrinsic, as shown in Figure 7. Extrinsic material will have inherently different electrical properties than its intrinsic counterpart. Both types of doping can be used to counteract impurities that may exist in intrinsic materials, this is known as a compensated semiconductor.

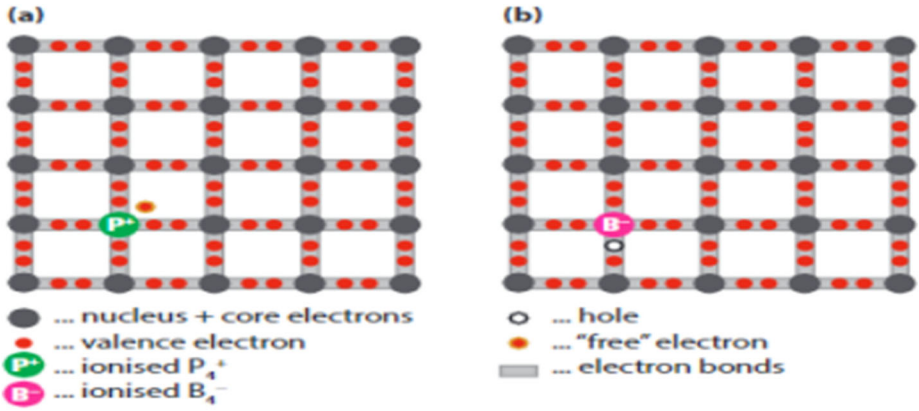

Figure 7. N-type (a) and P-type (b) doping. Source: [12].

C. FERMI LEVEL

As doping is conducted on a material, the concentration of carriers shifts and what is knowns as the fermi level, E_F, will change. The fermi level, or energy, is the electrochemical potential of the electrons in a material, and it signifies the average energy of electrons in said material [12]. This comes from the Heisenberg uncertainty principle, which states that uncertainty is inherent in measuring the characteristics of a particle, such

as velocity, momentum, position, and energy level. In an intrinsic semiconductor, when at 0°K, all electrons will have energies below the fermi level, however as temperature rises EHPs are generated and electron energy will rise above the fermi level, populating the conduction band. Equation 1 is the measure of the fermi level, known as the Fermi-Dirac distribution.

$$f(E) = \frac{1}{1 + e^{(E - E_F)/kT}} \tag{1}$$

While the fermi level is in the middle of the band gap for intrinsic semiconductors, the same is not true for extrinsic. Figure 8 shows the fermi levels of n-type and p-type materials, based upon the concentration of electrons. N-type will have a higher electron energy, forcing the fermi level higher. Conversely, p-type will have a higher positive charge, forcing the fermi level down towards the valence band.

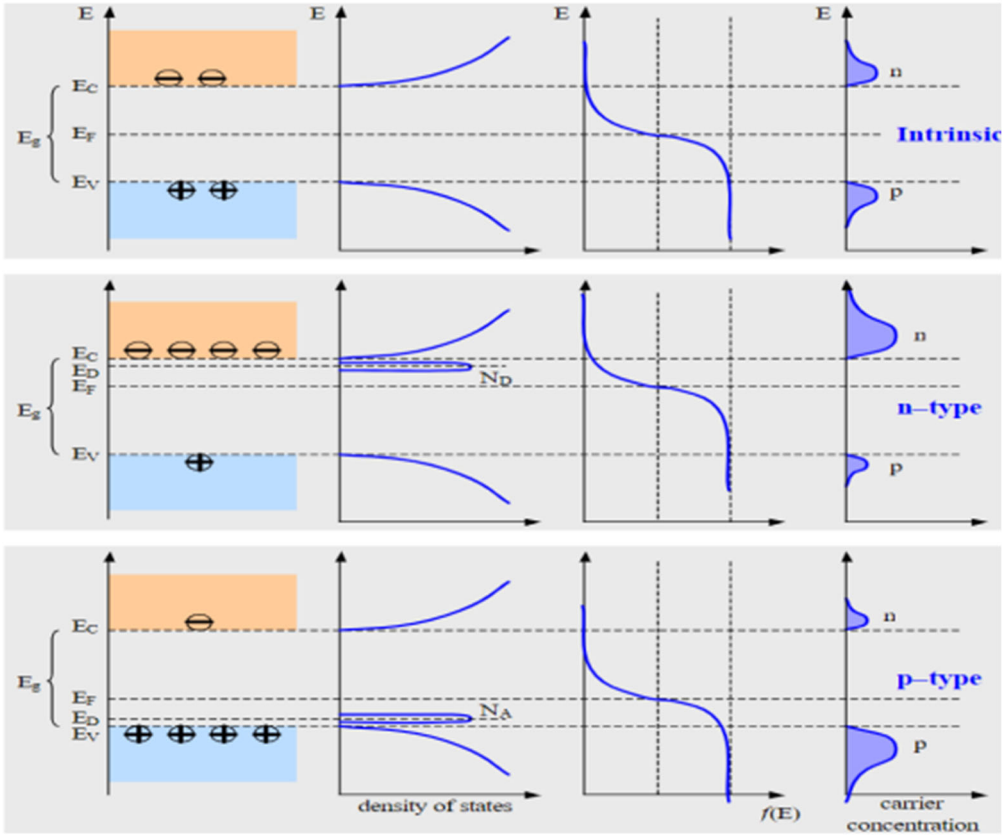

Figure 8. Carrier concentration-based fermi levels. Source: [8].

While Figure 8 demonstrates the carrier concentration effects of fermi levels, temperature is another factor that can affect the material fermi level. Not only does temperature change the conductivity of a material, the generation and recombination rates of EHPs, but also the fermi levels. Figure 9 shows the effects temperature has at generic set points above 0°K.

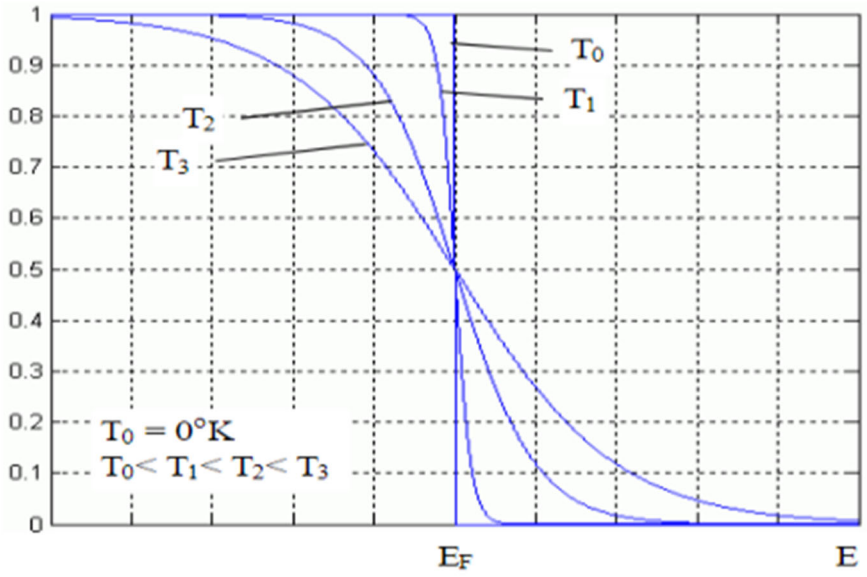

Figure 9. Temperature effect on fermi level. Source: [8].

D. P-N JUNCTION

A p-n junction, or a heterojunction, is the combination of a p-type and n-type material. The interface between the materials is responsible for the functionality and built-in voltages observed in many modern electronics such as transistors, diodes, and solar cells. These junctions have different currents that run through the semiconductors. The two discussed will be the drift and diffusion currents. Both play a vital role in the operation of the p-n junction and capability for utilization by modern electronics.

If a doped semiconductor has a higher concentration of carriers in part of it, then those carriers will diffuse, evenly spreading across the material. This action is analogous to the diffusion of dye in water. The diffusion current, I_d, is the current produced by the

movement of said carriers. This is caused by the majority carrier concentration, also called the doping of the material. Figure 10 shows the diffusion current of holes in a material, the holes move to the right, a less concentrated portion of the material.

If there is an external force, such as an electric or magnetic field, the movement of charges can create a current. This current is known as drift current, I_s. The current is proportional to the magnitude of the temperature, minority charge carrier density, and electric field. Figure 11 demonstrates drift current of holes in a material.

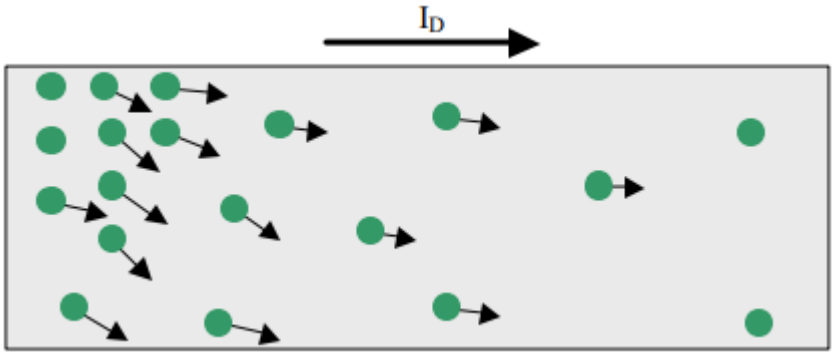

Figure 10. Diffusion current of holes. Source: [8].

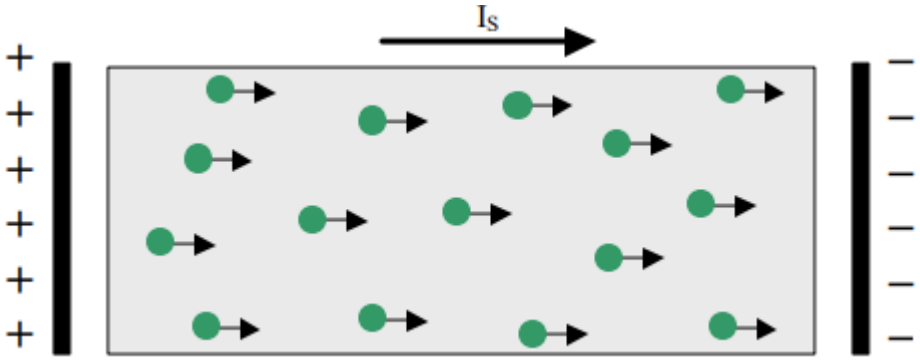

Figure 11. Drift current of holes. Source: [8].

Drift and diffusion current are both defined by the direction of motion of the holes, or positive charges, as shown in Figures 10 and 11, this is opposite the movement of

electrons. As these particles drift in the material, attempting to accelerate, collision occurs with atoms in the lattice. The collisions and the charge of the ionized impurities within the material will cause a deceleration of an electron. The electron will stop accelerating due to these forces and will attain a constant speed through the material. This is called drift speed, v_D. The ratio of the drift speed to the applied field is known as mobility, μ, and is dependent on the material. Mobility will decrease with temperature and the concentration of impurities due to carrier scattering.

At equilibrium, if two doped materials (one n-type and one p-type) are brought together, as in Figure 12, the following would occur. Majority carriers (holes for p-type and electrons for n-type) will diffuse into the other material, creating at first a large diffusion current. Upon crossing the junction, the holes and electrons will recombine with their opposite from the other material, holes crossing will combine with electrons and vice versa. The recombination will create what is known as the depletion region, a region devoid of any carriers, with negatively charged ions remaining on the p-type material and positively charged ions on the n-type material. The depletion region, with its highly concentrated 'walls' of ions creates an electric field, thereby slowing the diffusion of carriers through the material until equilibrium has been achieved.

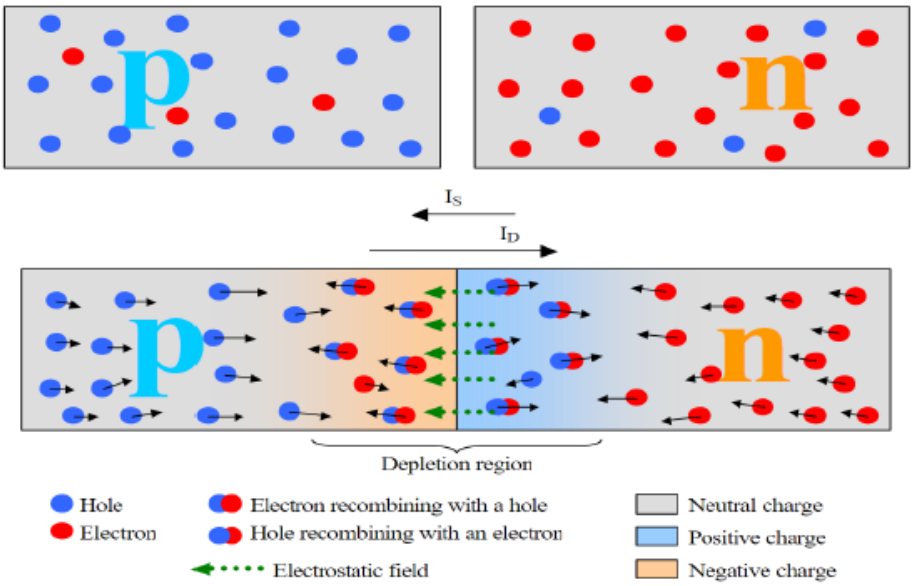

Figure 12. Depletion region of p-n junction. Source: [8].

Due to the buildup of carriers on opposite sides of the junction, an electric field will be created that will oppose the diffusion current of carriers. Minority carriers from either side of the junction will be forced by the new field to the opposite ends of their material, creating now a drift current. Equilibrium is reached when drift and diffusion current become equal in magnitude.

As demonstrated in Figure 8, n-type and p-type materials have differing natural fermi levels due to their majority carrier concentrations. When the two materials form a junction, that fermi level must remain the same. That will cause the conduction and valence band to shift, or bend around the depletion region, as shown in Figure 13.

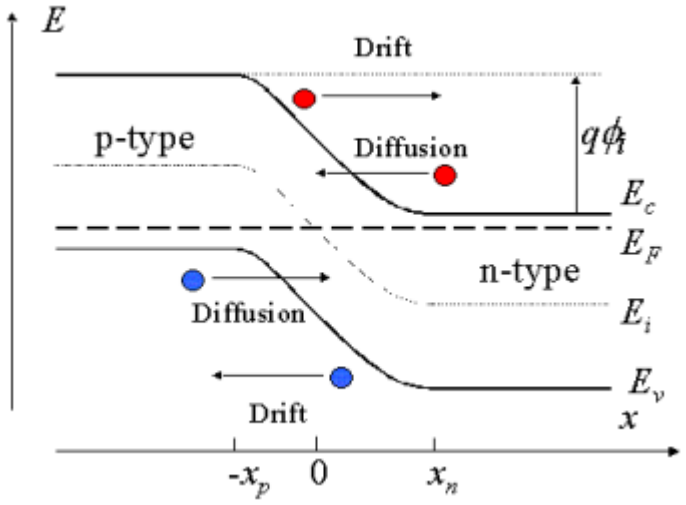

Figure 13. Band Diagram of p-n junction at equilibrium. Source: [13].

If a voltage is applied across the material, it will place the junction in either a forward or reverse biased state. A forward biased p-n junction has a positive lead connected to the p-type material and a negative lead to the n-type, this will distribute back to each region their natural majority carriers. This action minimizes the I_s and will counteract the internal voltage created by the depletion region, thereby narrowing the depletion region. Since this junction is no longer in equilibrium the fermi levels are now what are called quasi-fermi levels and are separated at the junction between the two materials. The

separation level of the two quasi-fermi levels is equivalent to the applied voltage, as is shown in Figure 14.

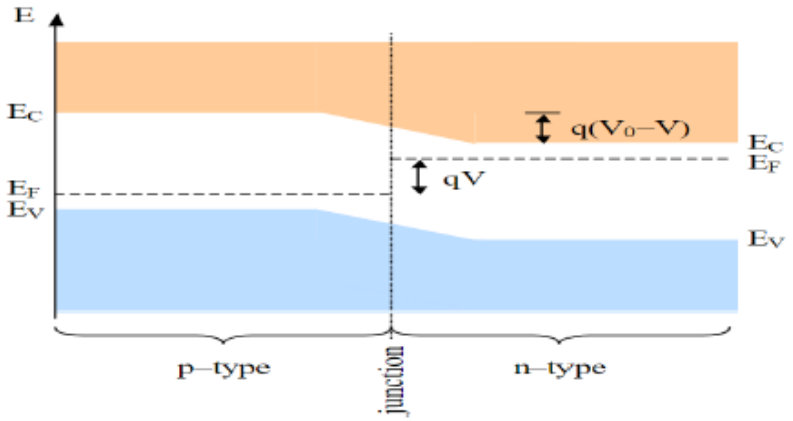

Figure 14. Forward biased p-n junction. Source: [8].

Conversely, a system is said to be reverse biased if a voltage is applied with the positive lead connected to the n-type and a negative lead connected to the p-type. A larger depletion region and an increase in barrier voltage will occur. This is due to the increase of minority carriers, as well as the decrease of majority carriers. The current will become predominately controlled by I_s as I_d will be severely decreased. The band diagram for reverse bias is shown in Figure 15.

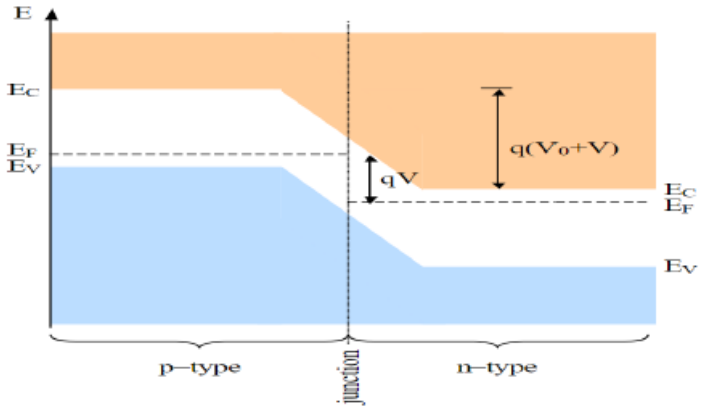

Figure 15. Reverse biased p-n junction. Source: [8].

III. SOLAR CELLS

A solar cell construction is comparable to a p-n junction on a fundamental level. Solar cells, or photovoltaic (PV) cells, are a particular form of semiconductor, with components that prioritize the generation of electricity from the radiation of the sun. This chapter will focus on the development of a modern PV system and how it operates, regarding cell construction, influence of materials, loss mechanics and limitations. To understand how a PV cell converts external energy into the generation of EHPs to provide electricity, first the source of the power must be explored.

A. SOLAR SPECTRUM

While solar radiation is the source of energy that PV cells utilize, the measurement that is utilized by PV cell industry is a concept called air mass, AM. AM is the measure of the effect of loss due to the photons increased distance from the sun and passage through the Earth atmosphere, thereby loss of irradiance. At AM0, there is no loss due to the Earth atmosphere, and irradiance is at the highest, as shown in Table 1. When the photon makes it to the earth at a 90^{o} angle it is called AM1, as shown in Figure 16, the amount of irradiance is the peak of terrestrial capabilities. However, this is not a realistic metric for PV system capability to capture the photons through a sun cycle. For this reason, the industry standard for testing of PV materials is at AM1.5, with a sun measurement of 48.2^{o} from overhead. Of note in Table 1, AM1.5 gives 900 W/m^2, however, AM1.5 will be measured at 1000 W/m^2 for this study, consistent with the industry standard.

Table 1. Spectral distribution conditions. Adapted from [2].

Location	Zenith Angle (θ_z) [deg]	Approx. Incident Power [W/m^2]	AM Condition
Outside Atmosphere	N/A	1365	AM0
Surface of Earth	90	1040	AM1
Surface of Earth	48.2	900 (1000 Standard)	AM1.5

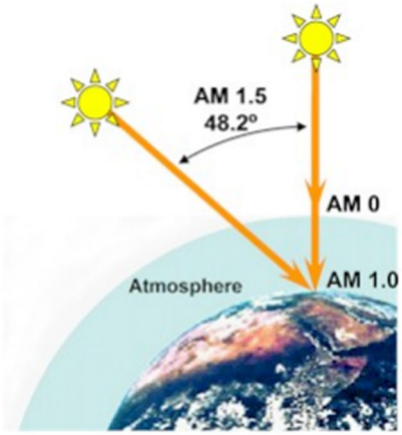

Figure 16. Air Mass 0, 1, and 1.5. Source: [14].

Wavelength also plays a crucial role in the generation of EHPs in a PV cell. Any wavelengths with energy less than that of the material bandgap do not provide sufficient energy for generation and so will pass through the cell without incident and will not be absorbed. Conversely, wavelengths that exceed the band gap energy will generate an electron, however, the excess energy will force the electron well above the conduction band. Here the electron will move around generating heat, until it stabilizes at a lower energy level. This heat generation is not beneficial to the solar cell and can lead to further losses. A spectral mismatch is when both the too short and too long wavelengths affect the solar cell, this accounts for the majority of loss in the energy conversion process [12]. Equation 2 shows the relation between wavelength and energy, and Figure17 demonstrates the corresponding energy-wavelength graph for AM0 and AM1.5.

$$E = \frac{hc}{\lambda} = \frac{1.24}{\lambda_{\mu m}} \tag{2}$$

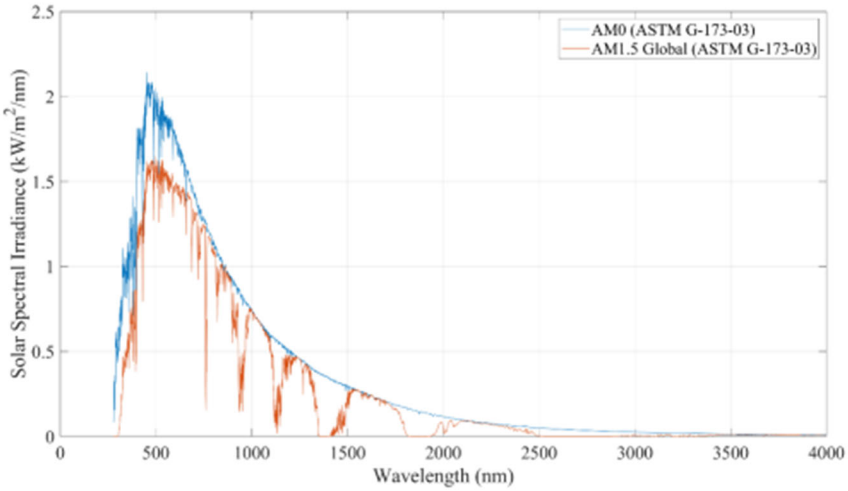

Figure 17. Solar Spectral Irradiance. Source: [4].

B. LOSS MECHANICS

Several other losses that may occur for a solar cell are light refraction, recombination, and shadowing. Refraction occurs on the surface of the cell and can account for up to 30% of total loss on an untreated PV cell [15]. Antireflective coating, ARC, and texturing are ways to counter refraction loss and promote the absorption of light. ARC thickness should be as such that it will not trap incoming photons yet promote the absorption of those that meet the bandgap requirements. Texturing is the process of creating micro-grooves on the surface of a PV cell. These pyramid-like shapes reflect light back into the substrate to be absorbed, if possible. Finally, shadowing occurs from the electrical grid on the surface of the cell blocking sunlight from absorbing into the cell, effectively casting a 'shadow' over the material. The loss can be minimized by careful construction of the microgrid to allow sufficient surface exposure, but not be too far apart as to allow recombination to occur. Another way to combat shadowing losses will be explored in Section 3D.

C. SOLAR CELL CONSTRUCTION

This section will give a brief overview of a common PV cell structure for a reference on the changes that the novel design introduced in Chapter IV will have. Figure 18 shows a generic solar cell, of note is that this design is not set in stone, there are other

factors that could come into play depending on the material used, application of cell, and layer thickness requirements.

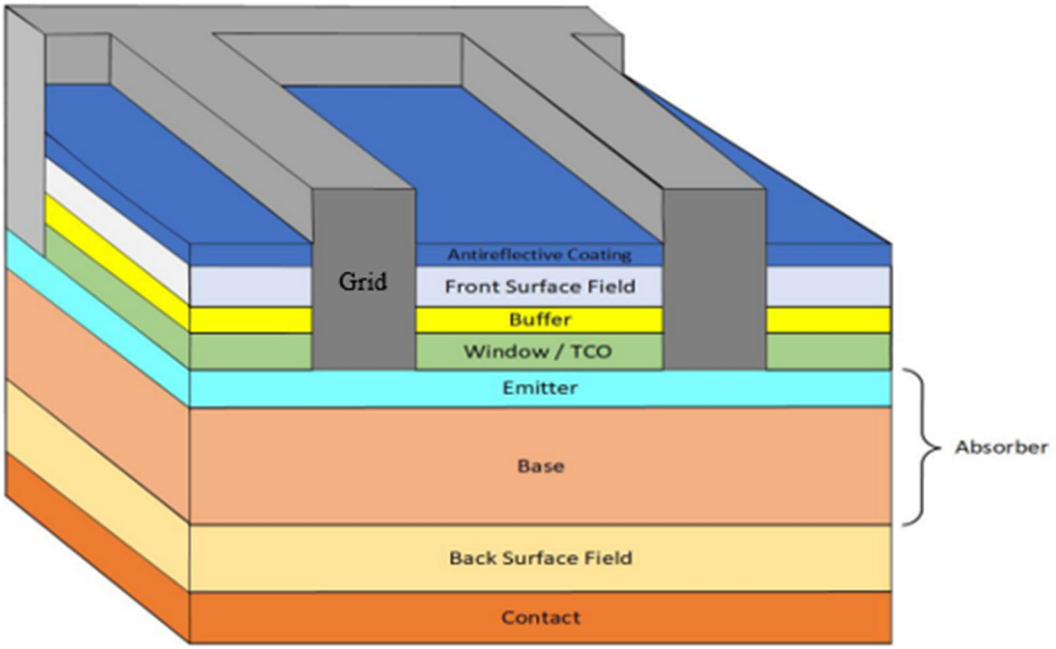

Figure 18. Layers of typical solar cell. Adapted from [2].

To conduct a proper review of the solar cell, each layer will be briefly described, with attributes and requirements for operation. First is the grid. As discussed in Section 3B, this collects the charge carriers and provides a means to transport electricity from the solar cell. Careful consideration must be made in the construction of the grid, as overly large fingers on the grid causes the shadow loss, while overly small fingers will increase recombination rates of EHPs. The ARC should be directly beneath the grid, to absorb as much irradiance as possible, and may be applied in more than one coat. This coating typically has a blue hue thanks to polysilicon.

Next is a front surface field, FSF. This is a highly resistive material that reduces the number of carriers that can make it to the surface or recombine, and instead assists in maintaining them to the lower levels to be absorbed into the grid. The fourth layer is the buffer, this portion is dependent on the material, as its main objective is to assist in

connecting two materials that are typically incompatible due to mismatched lattice constants. The window/transparent conducting oxide (TCO) layer is the final layer with the grid in it. This is a very low resistive layer that promotes the flow of carriers to maximize the collection.

The top layer of the p-n junction, the emitter, is a very thin section of only a few micrometers that most EHPs are generated from. The bottom layer of the p-n junction is called the base and is much thicker than the emitter. At 200–300 μm this layer combines with the emitter to create the p-n junction, thereby creating the internal voltage that is required to assist the creation of the EHPs. The most common base is p-type, due to electron mobility being higher, therefore reducing the chance of recombination, as electrons flow from the emitter to the grid. The base and emitter must be of opposite polarity to create the p-n junction. The two combined together is also known as the absorber layer.

The final two layers are the back surface field (BSF) and the back contact. The BSF is made of highly doped material, of the same polarity as the base. This creates a secondary, albeit smaller, internal voltage to assist in the separation of carriers and direct the flow of the ones generated deeper in the cell. The back contact collects the charge carriers of the same polarity as the BSF and base. This final layer is typically reflective to rebound photons of higher energy back into the cell in hopes of causing generation.

D. BACK SURFACE CONTACT

The traditional solar cell contains a grid on the surface of the cell for the collection of holes and electrons that break free from the material. There has been substantial study on the effects of widening, thickening, and positioning of the fingers of the grid to achieve the maximum throughput of solar radiation, while simultaneously minimizing the possibility of recombination. However, there exists an alternate method for collecting the carriers that are released by the photons, and that is called the back surface contact (BSC). BSC has many other names, such as interdigitated back contact (IBC), staggered back contact (SBC), and back alternating contact (BAC), all effectively the same concept. Figure 19 is a model of the SunPower Corp. BSC solar cell that was created in 2008. To garner a better understanding of the BSC cell, each component will be discussed briefly.

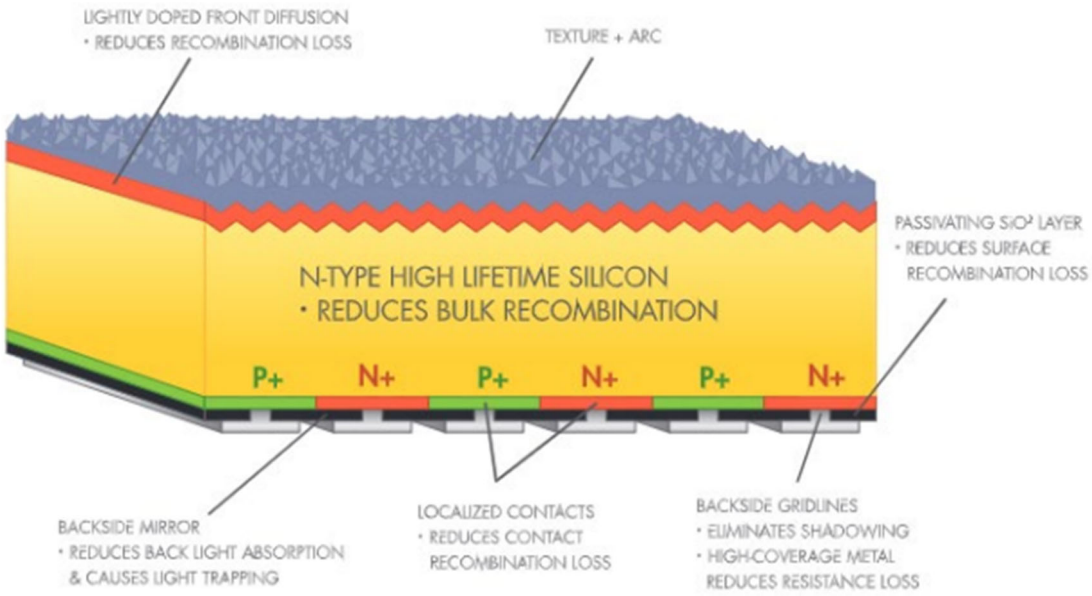

Figure 19. BSC cell. Source: [16].

The surface of the cell no longer contains the grid, thereby eliminating shadow loss and increasing the photon throughput, thereby EHP generation by approximately 10%. Without a grid on the surface the creation of a textured layer is far easier as well. Due to grid relocation, the size of the fingers is no longer a variable. Instead, there must be contacts layered on the bottom of alternating heavily doped p (p+) and n (n+) semiconductors. These alternate to capture the respective minority carriers and transport them along their respective busbar. Between each of the p+ and n+ semiconductors there must be a small gap, experimentally found to be 10 μm to prevent shorting [17]. The size of the n+ and p+ can vary depending on the bulk material makeup and mobility constants to ensure the highest throughput of minority carriers and minimize the chances of recombination. The passivation layer has the functionality as the Buffer, Window/TCO, and the FSF shown in Figure 18. Lastly, the electrons and holes now must move in the downward direction, to their respective busbars, and so there is no emitter layer near the top. Figure 20 demonstrates the movement of the minority carriers into their respective materials.

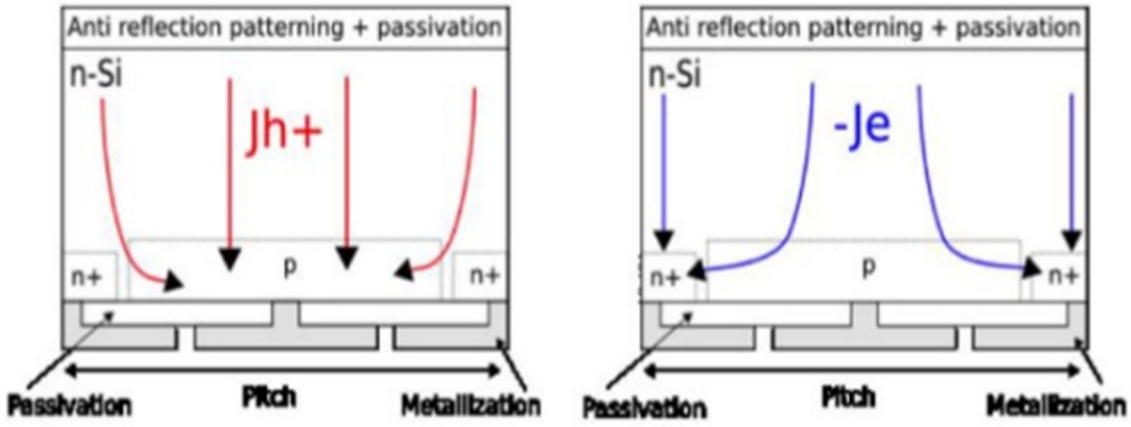

Figure 20. Movement of carriers in BSC cell. Source: [18].

E. PERFORMANCE METRICS

To truly measure the success of a solar cell there are specific parameters that are measured and considered, known as optical parameters. These are known as fill factor (FF), short-circuit current (I_{SC}), max power current (I_{mp}), max power point (P_{max}), max power voltage (V_{mp}), open-circuit current (V_{OC}), and efficiency (η). Equations 3 through 7 show how to calculate all parameters with exception of the I_{mp} and V_{mp}, which can be identified using a graph called an I-V curve, as shown in Figure 21.

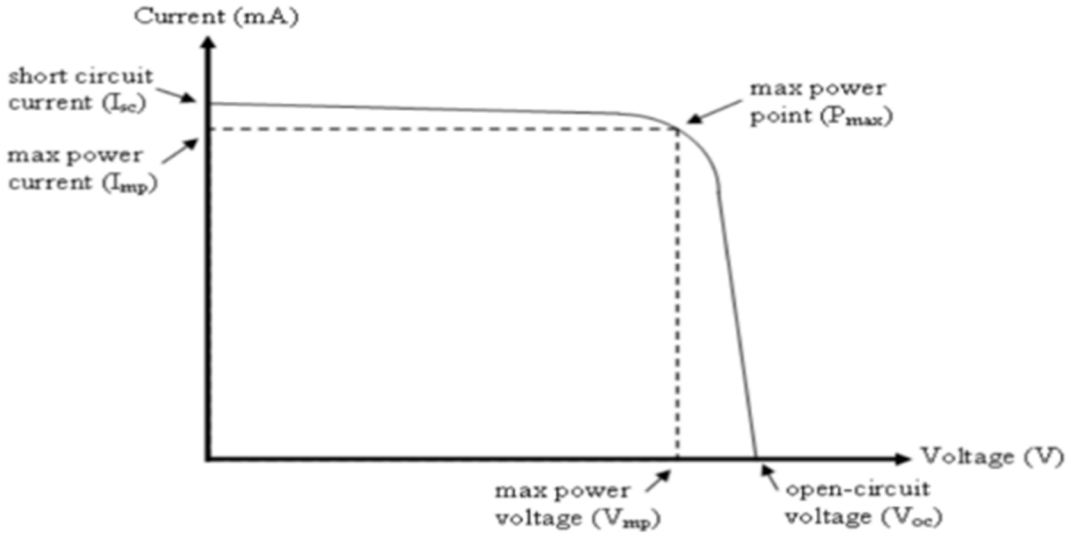

Figure 21. Generic I-V curve. Source: [19].

P_{max} is the potential output of a solar cell at its maximum. It is a measure of the quantity of the PV system.

$$P_{\max} = I_{\max} V_{\max} \tag{3}$$

I_{sc} is the current through the material when the voltage is at zero. It is a relationship between the generation rate, G, electron and hole diffusion lengths, L_n and L_p respectively, as well as the area of the cell. There is an inverse relationship between the size of the bandgap of material and the amount of I_{sc}.

$$I_{sc} = qGA(L_n + L_p) \tag{4}$$

V_{oc} is the maximum voltage of a cell, measured when the current is at zero. It is a relationship between the temperature, T, Boltzmann constant, k, intrinsic carrier concentration, n_i, as well as G. Conversely to I_{sc}, the higher the bandgap the lower V_{oc} becomes. This creates a balancing act between the two to generate the highest P_{max}.

$$V_{oc} = \frac{2kT}{q} \ln\left(\frac{G\tau_o}{n_i}\right) \tag{5}$$

FF is the measure of the squareness of an I-V curve. This translates to the V_{mp} and I_{mp} being as close as possible to V_{oc} and I_{sc}. The FF is a great measurement of the effectiveness of the solar cell and can represent low loss factors.

$$FF = \frac{P_{\max}}{I_{sc} V_{oc}} \tag{6}$$

Efficiency is often the focal point of many companies on the construction of their solar cell, as it measures the output power of the cell in relation to the input power, $P_{spectrum}$.

$$\eta = \frac{P_{\max}}{P_{spectrum}} \tag{7}$$

IV. CIGS SOLAR CELLS

As technology continues to advance, and solar charging becomes more commonplace, a solution must be found for PV technology that is versatile, lightweight, and relatively inexpensive to manufacture. The solution to this dilemma may just be thin film solar systems. As focus of this work is the construction of a copper indium gallium (di)selenide (CIGS), solar cell, that is what will be explored in this chapter.

A. THIN FILM SOLAR CELLS

Thin film solar cells are a microstructure of individual layers of material commonly deposited in a gaseous form on a substrate made of either glass metal or plastic. The completed cell will have thicknesses in the range of a few nanometers (nm) to several micrometers (μm). The structure of these cells is slightly altered from the traditional solar cell to accommodate the change in size and building design, which will be explored in the next section.

Due to the requirement of minimal thickness, many materials cannot be utilized to create thin film solar cells. Materials with high absorption coefficients, α, and direct band gap materials are required to create a truly thin film PV system. Direct band gap materials have the bottom of the conduction band and the top of the valence band aligned at the same momentum value; therefore, minimal energy is required to produce EHP. Common PV materials, such as silicon, Si, are insufficient for thin film due to these factors. CIGS has a very high absorption coefficient and is a direct bandgap material, making it a perfect choice to model the thin film solar technology with.

Beyond only being an excellent candidate for thin film technologies, CIGS has also demonstrated high radiation resistance, outstanding stability in rugged outdoor applications, and has a reported payback time of only four months [20]. Combine these findings with the fact that unlike other thin film alternatives, such as cadmium telluride, CdTe, and amorphous silicon, a-Si, CIGS is non-toxic like CdTe is, and does not degrade as a-Si does after sustained exposure to solar irradiation [4]. From cost to durability, the CIGS thin film cell is the way of the future.

B. CIGS TRADITIONAL DESIGN

The modern CIGS is a thin film, I-III-VI compound semiconductor that is traditionally created with a grid overlay. This PV system is created by intermixing two separate materials, copper gallium selenide, CGS, and copper indium selenide, CIS, together to create $CuIn_{(1-x)}Ga_{(x)}Se_2$. The 'x' represents the mole fraction of the system that is made of gallium, the higher the value of x the greater the amount of CGS in the compound. An x equivalent to one would denote a pure CGS material, Equation 8 shows the calculation of x, while Figure 22 shows the decaying crystal structure of CIGS with increased x values.

$$x = \frac{Ga}{Ga + In} \tag{8}$$

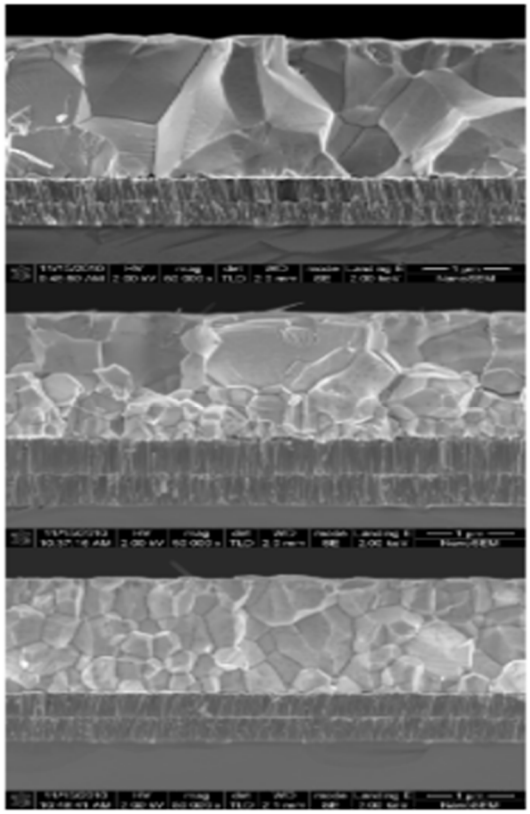

Figure 22. Changes to CIGS crystal structure with increasing x. Top: x=0.4, middle: x=0.5, bottom: x=1.0. Source: [21].

The molar ratio between Ga and In in the compound is what gives CIGS a diverse spectrum of efficiencies. As the value of x is changed between the two materials, so too is the absorption coefficient and more drastically the bandgap. Ga and In have a bandgap of 1.7 eV and 1.0 eV, respectively, meaning that theoretically CIGS' bandgap can range from 1.0 to 1.7 eV. While 1.7 eV is the ideal bandgap for a solar cell and having an x of 1 would seem logical, once an x value exceeds 0.3 and the Ga content is increased the material experiences higher defect densities that cause greater recombination rates in the absorber, all of which increase exponentially as the Ga increases [22]. For this reason, the mole fraction experimented will remain between 0.3 and 0.4, as to not exceed modeling capabilities associated with this exponential defect growth.

Figure 23 shows a traditional structure for a CIGS solar cell. Of note the cell depicted resembles the traditional cell structure depicted in section 3C, with a major difference being there is no FSF or BSF. Due to the thin nature of the material the BSF and FSF are not required to ensure proper carrier absorption and separation of EHP. The materials that make up the traditional CIGS model depicted are roughly what will be utilized in the experiment, with exception of the substrate. The substrate will consist of soda lime glass, which assists with the growth of the absorber layer due to introduction of sodium, Na, from the soda-lime glass [4]. The top layer will consist of an aluminum doped zinc oxide, ZnO:Al or AZO for short, this will act as the TCO, part of the passivation layer. The bottom part of the passivation layer consists of cadmium sulfide, CdS, which acts as a buffer and is n-type to the typical p-type CIGS material. The majority of the cell will consist of the CIGS absorber layer, which is the backbone and namesake to the solar cell. This is where the EHPs are generated and separated to their respective busbars. Below that is the molybdenum, Mo, or the ohmic contact that is required to assist in the collection of charges. The final portion of the cell is the substrate, as discussed in Section A. Figure 24 shows a side view of an experimental CIGS cell created.

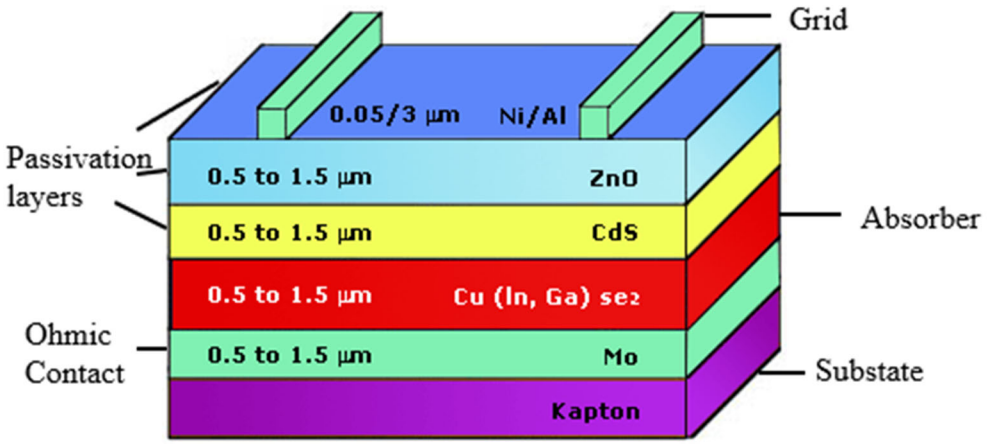

Figure 23. Traditional CIGS PV cell construction. Adapted from [23].

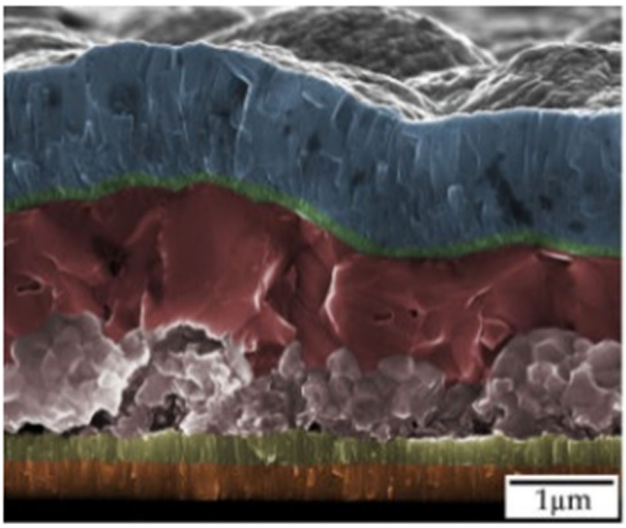

Figure 24. Experimental CIGS cell. Layers top to bottom: TCO (blue), buffer (green), absorber (red and pink), back contact (olive), substrate (orange). Source: [24].

C. EXPERIMENTAL CIGS DESIGN

The CIGS PV cell design utilized in this study is a novel design first investigated by Herrera [3] in 2017 and later by Logar [2] in 2022. This experimental design deviates from a traditional model of a BSC CIGS cell developed by SunPower [16] by adding a vertical p-n junction as the absorber layer. This additional layer theoretically can decrease the recombination loss by assisting the separation of charges in the absorber layer.

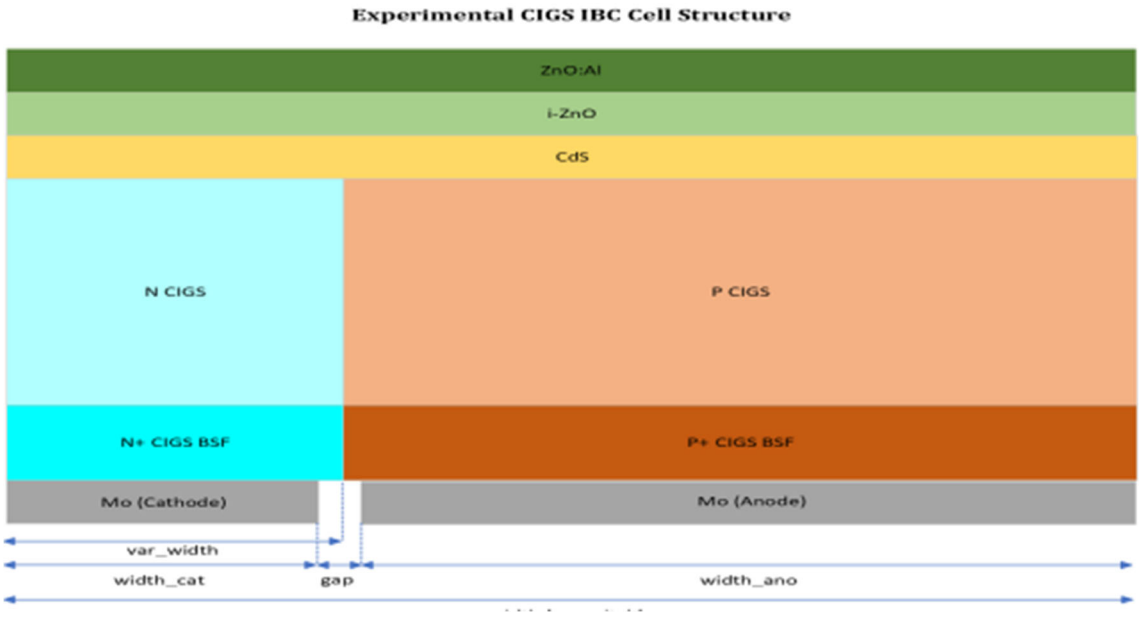

Figure 25. Novel design CIGS solar cell. Source: [2].

Figure 25 demonstrates a combination of Figure 19, the BSC cell design, and Figure 23, a traditional CIGS PV cell with the addition of the aforementioned vertical p-n junction. The highly doped n+ CIGS and p+ CIGS regions act as the contacts that assist the proper carriers to their respective busbars. The passivation layers consist of AZO, intrinsic ZnO, and CdS layers. The AZO is the TCO layer, the CdS acts as a buffer, and the i-ZnO is a highly resistive layer to reduce shunt paths between the TCO and buffer [25].

For the experimental design an ARC in modelled in Silvaco, albeit not depicted in Figure 25. Equation 9 demonstrates the optimal refractive index, n_1, of an ARC, with n_0 and n_2 representing the refractive indices of the bordering materials to the ARC. For the purposes of the modelled cell the bordering materials are air and AZO with refractive indices of 1.0 and 2.0 respectively. When inputted into Equation 9 the refractive index of 1.414 is achieved, nearly identical to the refractive index of magnesium fluoride, MgF_2, of 1.413. For that reason, MgF_2 is utilized as the material for the ARC, as it is nearly a perfect fit.

$$n_1 = \sqrt{n_0 n_2} \tag{9}$$

As there is a variety of possible bandgaps for a CIGS PV material due to the adaptability of the molar ratio between Ga and In, an equation must be used to calculate the proper bandgap at every x value. There are three sources that provided bandgap equations, with minute differences in the output, and so the equation with the smallest output will be utilized in the Silvaco model to allow room for error and demonstrate the worst possible outcome of the optimized cell. Equation 10 [26] depicts the bandgap calculation in its entirety with x, molar ratio, and T, temperature in K, as variables. For most materials Silvaco can generate a bandgap number without external sources, however an error was discovered in the Silvaco software, and an incorrect bandgap is produced. The correct bandgap given by Equation 10 must be manually entered. Silvaco software engineers have been notified and the upcoming version of Silvaco will have the correction [2].

$$\begin{aligned} Eg_{CIGS}(x,T) &= \{1.036 - 225(4.238e^{-5}) - 170(8.75e^{-5})[\coth(\frac{170}{2T}) - 1]\}(1-x) \\ &+\{1.691 + 259(8.82e^{-5}) - 189(16e^{-5})[\coth(\frac{189}{2T}) - 1]\}x - .02x(1-x) \end{aligned} \quad (10)$$

V. EXPERIMENT MODELING

This chapter covers the keystone to the success of this thesis. By employing the variable parameters in the optimal model produced by Logar [2] and defining a range of numbers for all input variables, the NOLH can produce a multitude of parameter combinations, called design points. Each design point can then be inputted into the ATLAS device simulator created by Silvaco to create a model CIGS solar cell and assess its performance. The measured outputs of the found cells are then inputted into a statistical analysis tool called JMP to analyze the data and find a subset of the parameter space associated with higher efficiency. Once this range is found, the cycle restarts with an updated test set based on the revised parameter ranges. For the case of this thesis, three cycles of test, model, and analyze were completed, with the results depicted in Chapter VI. The following sections delve into the foundation of the NOLH and Silvaco tools. The JMP software will not be explored in depth as it is an analyst tool that requires no coding.

A. NEARLY ORTHOGONAL LATIN HYPERCUBES

NOLHs are a class of space-filling experiment designs [27]. A design is a matrix with a column for each varied parameter (also called a factor). As described in the title, these predetermined columns are nearly orthogonal, meaning the columns produced is nearly independent (also called nearly uncorrelated) between each pair of columns. Another benefit of the NOLH is that it can identify synergy between parameters, since the parameters are varied simultaneously, vice keeping one parameter constant and varying others around it. This method can generate a test set of design points that very efficiently spans the given range of data, as will be seen in Chapter VI. NOLHs are often used for large-scale simulation studies where it is impractical or impossible to consider every potential parameter combination [27].

To construct NOLHs, each parameter that is adjusted must have a minimum and maximum boundary as well as a specified number of decimal places. The resulting parameter values in each column will be evenly spaced across the boundaries. The stack_nolhs.rb program, part of the data farming ruby scripts package implemented by

Sanchez [28], is a free software tool that accomplishes this task for studies involving up to 100 factors, also allowing the analyst to construct a base design or add "stacks" that expand the design and further improve its ability to fill the space of interest. Figure 26 depicts the simple input code used for the first set of data generated for testing in Silvaco. The parameters depicted are the values that are adjusted to optimize the novel CIGS cell design, and the values under the '^Z' are the output values from the NOLH. In total, each of the three iterations produced 353 design points (7 stacks of an NOLH with 17 design points) for a total of 1,059 total parameter combinations to be inputted in to the Silvaco software. Table 2 depicts the corresponding data ranges as depicted in Figure 26. Each parameter spans a large range for the initial dataset to get an overall estimate of the impact of each variable to the measured output. As will be depicted in Chapter VI, as each cycle is completed the overall average efficiency of the datasets increases as the optimal variables are modeled.

```
C:\Users\brand>stack_nolhs.rb
To terminate input enter ctrl-d (Mac/Unix/Linux) or ctrl-z (Windows).
Enter ranges for each factor on a separate line.

MIN     MAX     #DIGITS
0.04 1 2
0.2 1 2
0.2 1 2
1 8 2
1 8 2
0.05 1 2
0.04 0.2 2
0.2 0.4
^Z
1.0     0.28    0.55    2.31    7.13    0.64    0.15    0
0.91    1.0     0.3     3.63    4.28    0.23    0.16    0
0.88    0.55    0.93    2.09    1.22    0.61    0.16    0
0.58    0.9     1.0     3.84    7.56    0.2     0.17    0
0.94    0.23    0.57    2.53    5.81    0.73    0.11    0
0.97    0.95    0.45    2.97    4.06    0.26    0.07    0
```

Figure 26. NOLH example inputs and generated parameters.

Table 2. Optimization parameters ranges for dataset one.

Variable	Minimum	Maximum	Decimal places
AZO (Thickness, μm)	0.04	1	2
ZnO (Thickness, μm)	0.20	1	2
CdS (Thickness, μm)	0.20	1	2
CIGS (Thickness, μm)	1	8	2
CIGS+ (Thickness, μm)	1	8	2
Mo (Thickness, μm)	0.05	1	2
Var_Width	0.04	0.20	2
X	0.20	0.40	2

The parameters depicted in Table 2 are the only parameters of the CIGS solar cell that are adjusted in any of the trials. These are found to be the characteristics that are more controlled in the manufacturing of the solar cell and have the most human manipulation involved. All parameters shown in Table 2 have been discussed thoroughly in previous sections except for Var_width, or varying width. This variable sets the location of the anode and cathode on the cell, as well as determines the position of various mesh nodes and interfaces. Chapter 6 covers in detail the effects that each of the chosen variables has on the overall efficiency and performance of the designed cell.

B. SILVACO MODELING

The Silvaco modeling software ATLAS is a one to three dimensional, physically based simulation software that specializes in semiconductor implementation. These modeled physical systems can be solved for varying voltages, doping levels, carrier concentrations, and different thickness of materials, as well as many other material properties that are the foundation of different devices. Computer modeling allows the experimentation of novel device construction and the implementation of devices in new or radical environments without the rigorous physical processes and costly manufacturing. Silvaco and similar modeling software are not only cost effective, but also fundamental to the testing phase of new designs. In the fast paced and evolving business world, most companies utilize various forms of this modeling software to ensure manufacturing time, effort, and materials are not wasted.

ATLAS is the device simulator that is often referred to as Silvaco, the parent company. This simulator operates by text being entered into the user interface called Deckbuild. This interface is a plain text language window that a user can input the physical dimensions and properties of the simulated model and output desired measurements. As depicted in Figure 27, the code, while in plain text, does have a required structure that must be adhered to for the system to properly build the model. The structure of Silvaco ATLAS coding requirements will be quickly clarified to further the understanding of the code utilized to model the novel CIGS solar cell, as found in Appendix A.

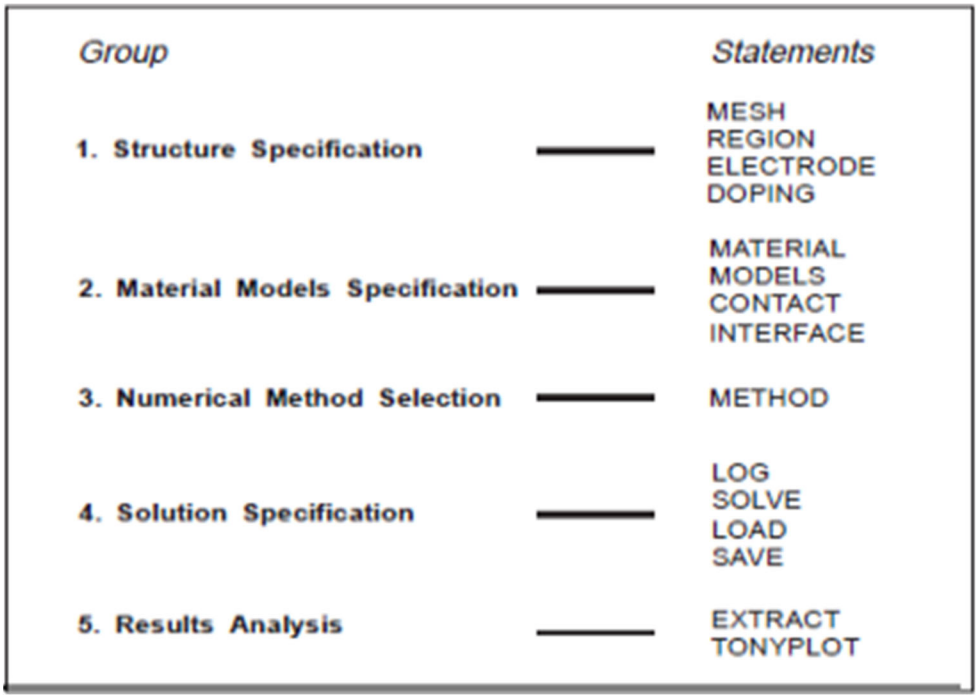

Figure 27. Command groups for ATLAS. Source: [29].

The first command group for the Deckbuild interface is structure specification, with statements in mesh, region, electrode, and doping. A mesh is made up of vertical and horizontal lines that cover the simulation domain, depicted in Figure 28 as green lines. Where these lines cross is called a node, where calculations are conducted. The finer the mesh, the higher the overall resolution of the output and potentially the longer the

simulation can take along with the increase in the possibility of convergence errors. The mesh density in certain areas can be changed to account for more precise simulation measurements in areas of interest. The black lines are the boundaries of what are called regions. Regions must align with nodes of a mesh and annotate the different material locations within the simulation. While material definitions take place when selecting regions, Figure 28 does not depict the material, only the region boundaries, Figure 29 depicts the same model with materials assigned to the regions. Electrode placement and doping come next for group one statements. The electrodes can be placed anywhere in the material. Silvaco has a library of typical default doping values for certain material, which can be adjusted to the user preference to create unique material structures.

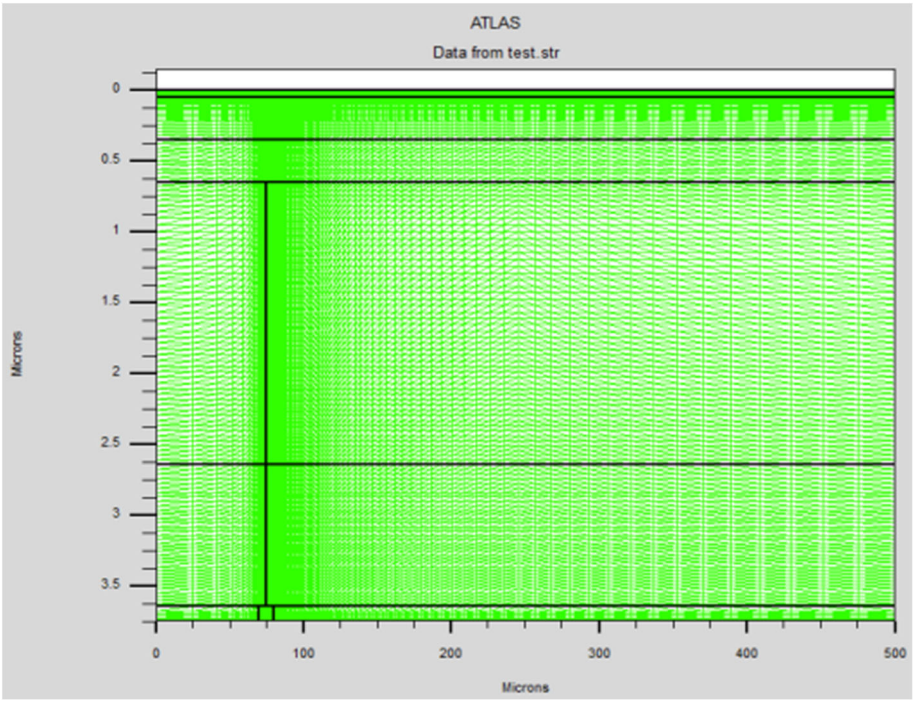

Figure 28. Tonyplot of mesh and region boundaries.

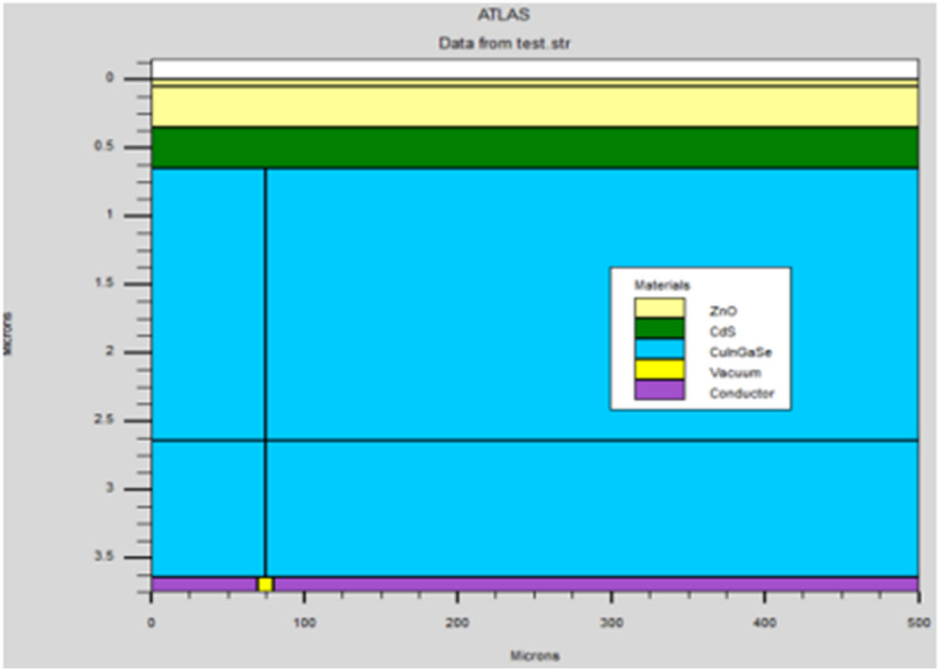

Figure 29. Tonyplot of material defined regions.

Silvaco models an ideal material, without defects, or traps, which are inevitably created during the manufacturing process. Physical defects in the material often lie in the fermi level of the material energy band and can draw charges away from both the valence and conduction band, distorting the electrical characteristics of said material and the overall device. The goal of this work is to achieve as realistic of a solar cell as possible. To account for the ideal material given as default by Silvaco, traps can be modeled into the system as depicted in the code in Appendix A.

The last set of statements that must be entered into the Deckbuild interface is focused on the solving of the relationships generated from the material created in the previous statements. Method refers to the preferred way of resolving the equations that are in the subsequent part of the code. The solution specification statements are where the output data that a user would like to view will be specified. Such data could be equations, similar to fill factor, efficiency, or max power, others could be Tonyplot requirements such as short circuit current and open circuit voltage. Finally, the last group of code will contain the results analysis, where the desired data is extracted from the file and placed into graphs called Tonyplots, as depicted in Figures 28 and 29.

VI. RESULTS

This chapter will cover the formation and analysis of both the input and output data generated through the NOLH and Silvaco ATLAS. There were three data sets generated from the NOLH, the first of which was a wide range estimation based upon a previous NPS graduate [2] as can be seen in Table 3, the second and third sets of data were generated after the output from Silvaco was analyzed through the JMP analysis software. This chapter will step through the evolution of each set of data sets from formation to implementation and finally analysis, demonstrating the outstanding optimization capability of the NOLH and the remarkable potential of a BSC CIGS thin film solar cell.

Table 3. Starting optimal parameter settings. Source: [2].

Variable Name	Parameter Setting
AZO [μm]	0.05
ZnO [μm]	0.30
CdS [μm]	0.30
CIGS [μm]	2
CIGS+ [μm]	1
Mo [μm]	0.10
Var_Width	0.05
X	0.34
Efficiency [%]	24.32

A. INITIAL DATA SET

As shown in Table 2 of Chapter 5, the initial starting values for the trials were chosen using a wider range of data points than nominally recommended. This is to ensure an extensive set of combinations could be generated across as wide of a field as practical to increase the probability of homing in on an optimal pattern of parameters. The initial set of data included 353 different trials. The total run time for all trials was 50.84 hours, divided between twelve computers running simultaneously. To focus attention on the optimization of the CIGS PV material, the emphasis on the generated data from Silvaco was efficiency. Figure 30 is a graphical representation of the mapped efficiencies found

during the first set of data. As can be seen from Figure 30, the data spans from 17.8-26.5% with an average of 21.6%. As expected from the initial run of data the output spans a wide range of efficiencies, however, what was not as expected was the outlier of the most efficient cell found was 0.66% higher than the second most efficient cell. By this revelation, it shows that the NOLH does do an effective job of spanning the majority of possible outcomes.

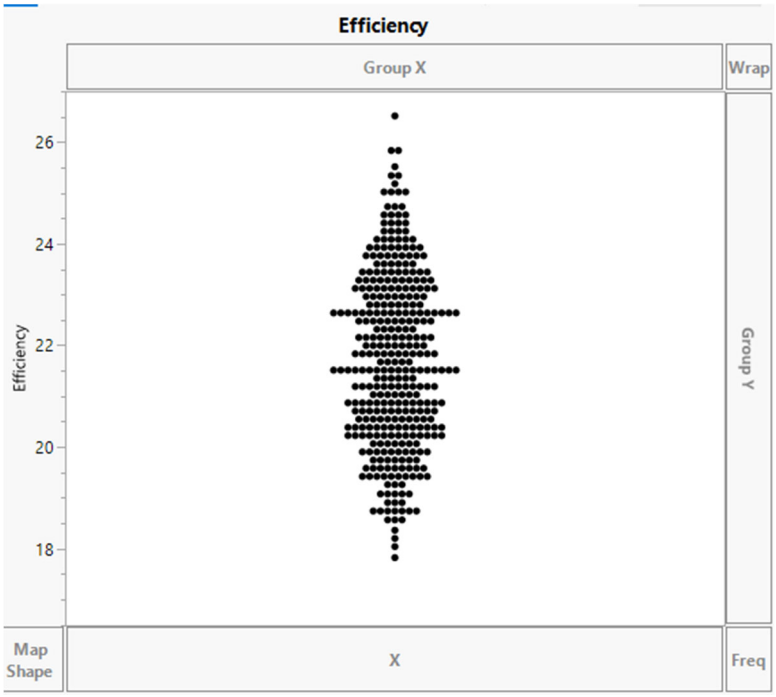

Figure 30. Efficiency range for first set of data.

The next step for analyzing the data was to verify if the JMP prediction software could generate a working set of parameters that could predict a better output. To do this, all the data was sent from an Excel file into the JMP software. Figure 31 depicts the output of the prediction software generated. Regretfully, the prediction profiler was unable to give an accurate cell model, as the highest efficiency that it represented only reached 25.44%. Due to that, optimization efforts defaulted to manual trend identification utilizing the graph build capabilities of the JMP software.

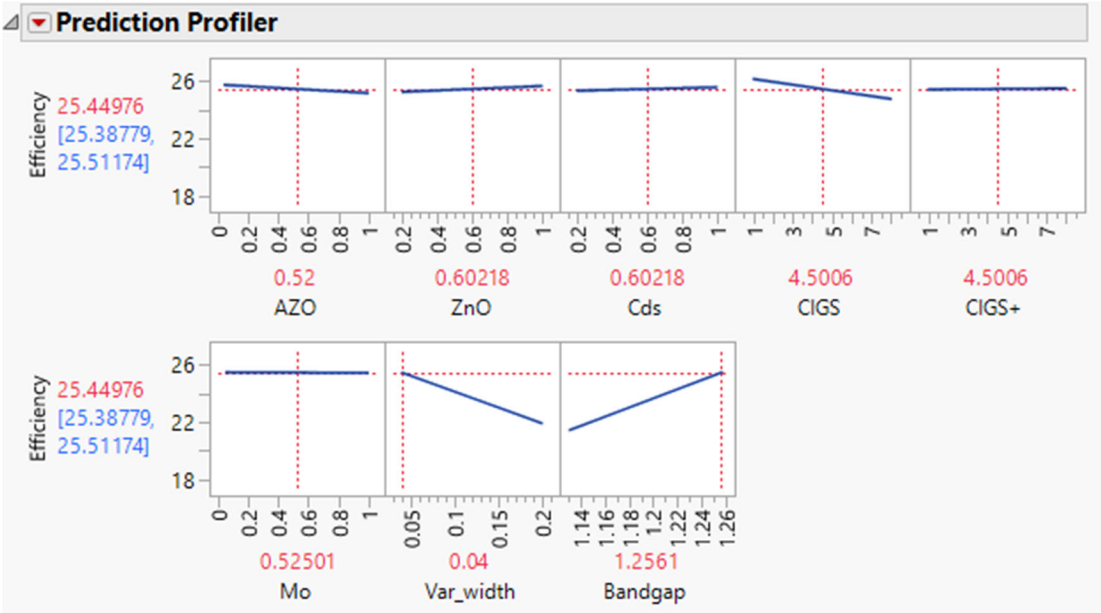

Figure 31. Prediction Profiler output from JMP for first set of data.

To manually identify trends each variable was first entered into a graph with the efficiency on the y-axis and the variable as the x-axis. Not all variables demonstrated a strong correlation between their value and efficiency output, such as AZO, ZnO, CdS, and Mo as depicted in Figure 32. The solid black line in each graph is smoothed to the data and represents the relationship between each variable and its corresponding efficiency. The blue and red dots are the 353 data points, colored by their bandgap magnitude. The highest bandgap is colored red. As can be seen from all graphs in Figure 32, bandgap magnitude has a truly relevant correlation to efficiency. However, judging by the trend line, none of the other four variables depicted have a strong correlation, and therefore had minor adjustments for the second dataset.

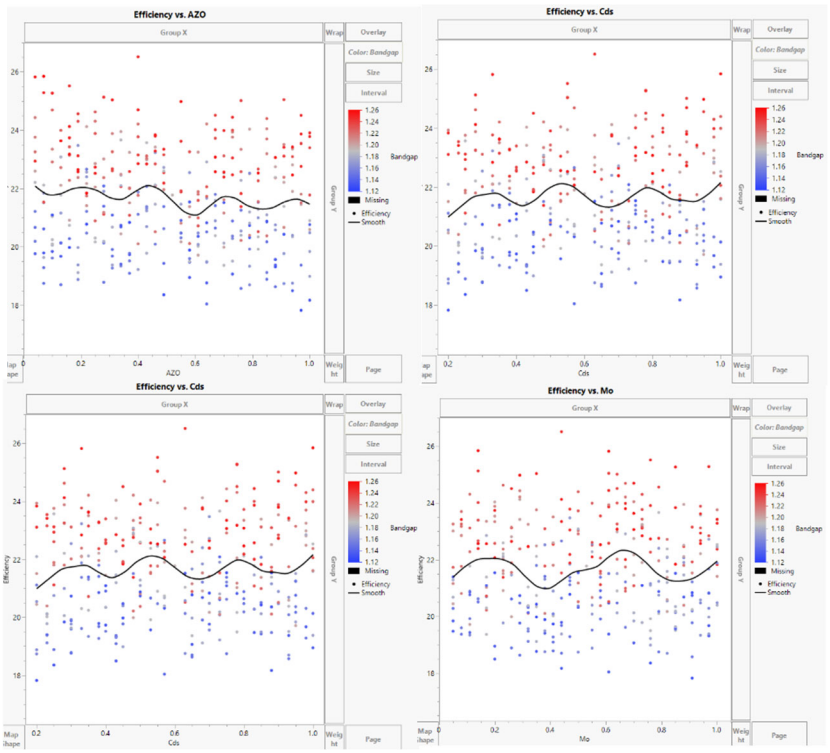

Figure 32. Efficiency vs. AZO, ZnO, CdS, and Mo graphs for dataset one.

The remaining four variables, CIGS, CIGS+, Var_width, and x, were all shown to have a substantial impact on the efficiency of the cell, as well with each other. The impact of the correlation between each variable cannot be seen on separate graphs, and so one graph was generated that depicts the four variables and efficiency. Figure 33 depicts the five-variable graph. Efficiency is placed on the y-axis and will remain so for all graphs depicted. CIGS+ is on the x-axis and has five separate iterations of its range spanning vertically on the graph, effectively breaking the image into five separate graphs. Var_width is on the top-axis, and has the range broken up between all the sub-graphs. The bandgap, or x, is represented by the color-coded data points. And finally, the CIGS variable is depicted by shapes that represent equally spaced ranges of data, as shown by the legend on the right-hand side of Figure 33. There is a clear correlation between the size of Var_width and efficiency as well as the size of the bandgap and efficiency. However, the size of CIGS and CIGS+ does not show as strong a correlation to efficiency, but to each other. As can be seen on the graph, the highest efficiency levels appear to happen when CIGS is between 1 and 2.53 while CIGS+ is mid-range between 2 and 5.

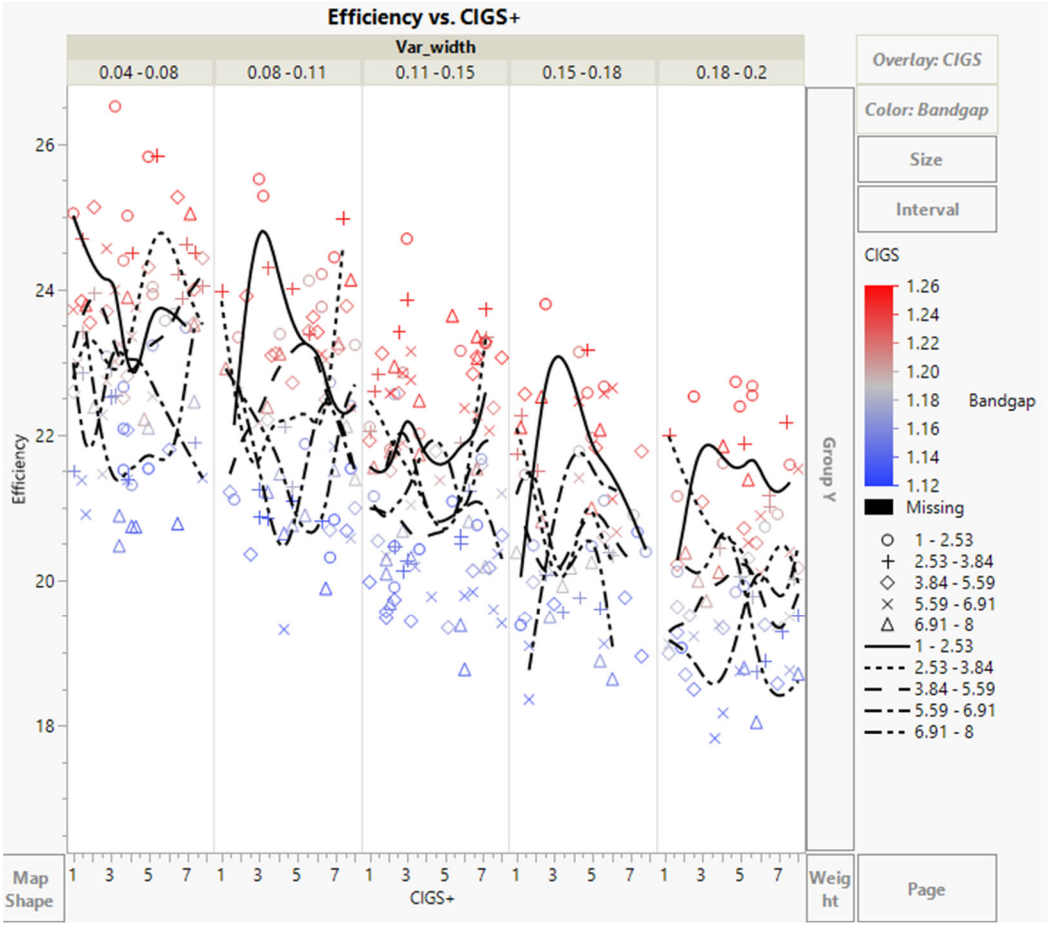

Figure 33. Efficiency vs. CIGS+, Var_width, CIGS, and Bandgap graph for first set of data.

With the analysis of Figure 33 the wide range of variables was reduced to match the newfound revelations. However, as this would only be the second iteration of Silvaco trials, the ranges were not drastically reduced, in the chance that there was an overlook on a potentially optimal cell, similar to the 26.5% found as an outlier. Therefore, most variables were adjusted slightly, as can be seen in Table 4. CIGS and CIGS+ ranges were not adjusted to gather more representation of their relationship in the second dataset run. The new ranges were placed into the NOLH algorithm, and another set of 353 data points were generated.

Table 4. First and second dataset parameters ranges.

	Dataset 1			Dataset 2		
Variable	Min	Max	Decimals	Min	Max	Decimals
AZO [µm]	0.04	1	2	0.04	0.95	2
ZnO [µm]	0.20	1	2	0.30	0.95	2
CdS [µm]	0.20	1	2	0.25	1	2
CIGS [µm]	1	8	2	1	8	2
CIGS+ [µm]	1	8	2	1	8	2
Mo [µm]	0.05	1	2	0.10	1	2
Var_width	0.04	0.20	2	0.04	0.15	2
X	0.20	0.40	2	0.30	0.40	2

B. SECOND DATA SET

The second set of data did not reveal as drastic of a range of efficiencies as the first set of data. There was an improvement once again in efficiency, and just as importantly, in average efficiency. The graph depicted in Figure 34 shows that the range has increased to 20.7 to 26.8%, with an average of 23.4%. The analysis of the increase of efficiency will be discussed in Section D of this chapter. Figure 34 depicts a tighter grouping of datapoints with, once again, a decidedly large gap between the most efficient and second most efficient runs.

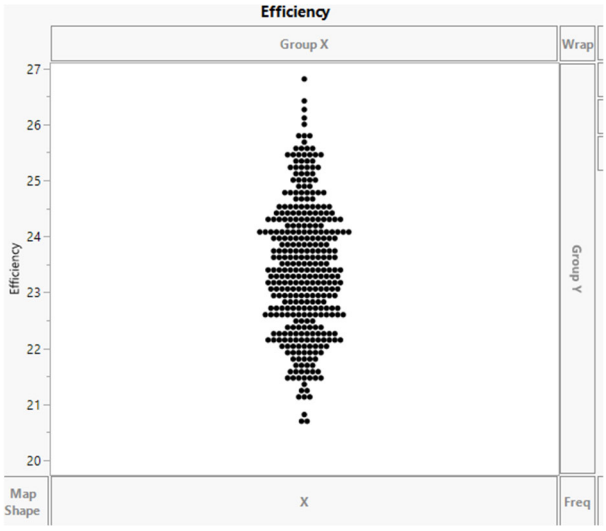

Figure 34. Efficiency range for second set of data.

The analysis of the second set of data followed the same trend as the first, beginning by evaluating the relationship between each variable and cell efficiency. Each variable was then assessed to determine if there was a pattern. Figure 35 shows the relationship between AZO, ZnO, CdS, and Mo depicted in four graphs. The downward trend for AZO persists and so the range for AZO was drastically changed for the third set of data. ZnO was adjusted for an optimal higher range, as well as CdS and Mo, as each graph depicts a lower average set of efficiencies at lower thicknesses.

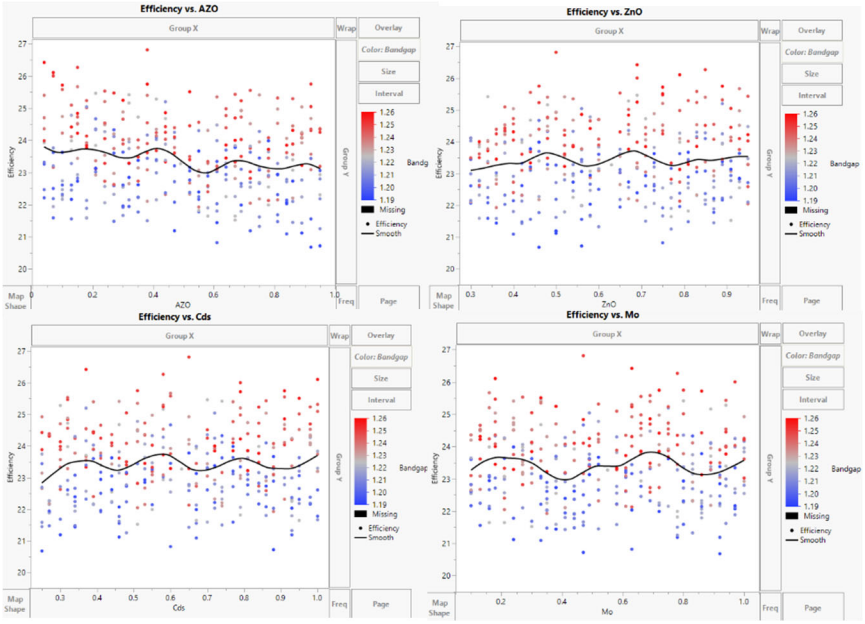

Figure 35. Efficiency vs. AZO, ZnO, CdS, and Mo graphs for second set of data.

The graph generated for the last four variables, as depicted in Figure 36, shows a decreased slope when compared to Figure 33, this is indicative of the fact that the average efficiency generated from this data set is closer to the optimal parameter. The relationships between the variables have stayed the same between this dataset and the last. Therefore, the ranges of the variables will be more drastically adjusted to fit the optimal parameters generated from the data. This adjustment includes CIGS+ and CIGS variables being adjsuted to account for the marked relationship depicted on the graph. Table 5 shows the

final set of ranges that will be implemented into the NOLH. As before, all parameter settings will be computed to two decimal places.

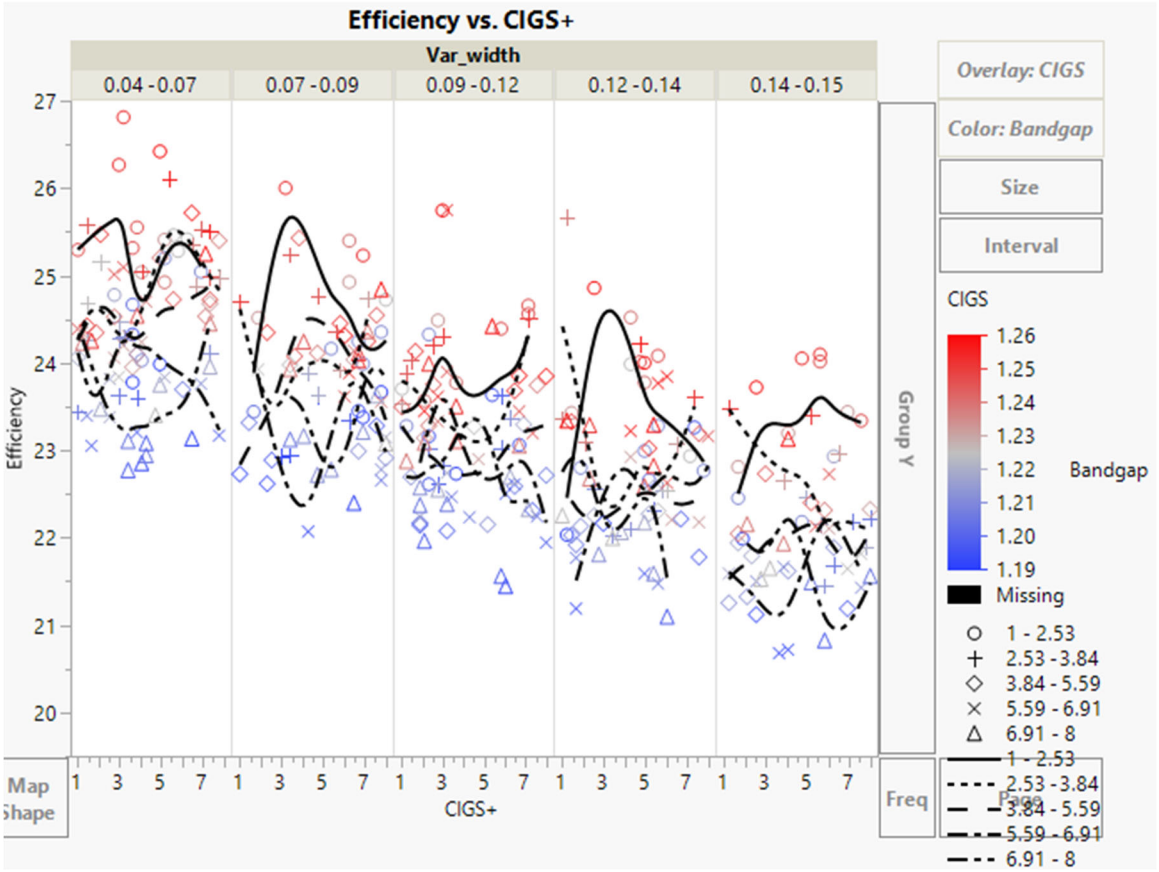

Figure 36. Efficiency vs. CIGS+, Var_width, CIGS, and Bandgap for second set of data.

Table 5. Datasets one, two, and three parameter ranges.

	Dataset 1		Dataset 2		Dataset 3	
Variable	Min	Max	Min	Max	Min	Max
AZO [µm]	0.04	1	0.04	0.95	0.04	0.40
ZnO [µm]	0.20	1	0.30	0.95	0.40	1
CdS [µm]	0.20	1	0.25	1	0.30	1
CIGS [µm]	1	8	1	8	1	5
CIGS+ [µm]	1	8	1	8	3	7
Mo [µm]	0.05	1	0.1	1	0.15	1
Var_width	0.04	0.20	0.04	0.15	0.04	0.10
X	0.20	0.40	0.30	0.40	0.33	0.40

C. FINAL DATA SET

The implementation of the final data set gave the anticipated highest efficiency of all the trials. It incidentally also took the most time, at 63.1 hours. Figure 37 depicts the range of efficiencies generated, with the new range spanning from 23.1 to 27.08%, with an average of 24.9%. All analysis of the data outcomes will be explored in the next section of this chapter.

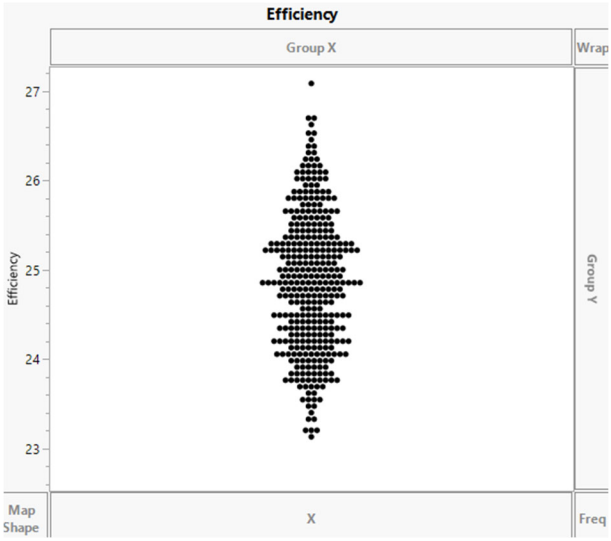

Figure 37. Efficiency range for third set of data.

D. OVERALL RESULTS

The combination of all the output datapoints generated by Silvaco can be seen in Figures 38 and 39, with the raw data given in Appendix B. The increased data points at higher efficiencies demonstrates the culmination of all three previous efficiency datasets, and that by utilization of the NOLH the results had an upward trend on average. The Silvaco generated I-V curve is depicted in Figure 39, showing the radical differences between the three datasets. The first set of data had an average efficiency of 21.6%, below the industry standard currently for CIGS solar cells, and below both previous NPS graduate works [2, 3]. The next set of data averaged a 23.4% efficiency, rivaling industry standard and exceeding the efficiency first generated by this novel cell design in 2019 [3]. Finally,

the last set of data generated averaged an output that exceeded every previously designed CIGS solar cell, BSC or not. This demonstrates that not only is the optimized cell a groundbreaking discovery, but the NOLH was so effective in optimization that it generated, on average, an efficiency that had never been seen before.

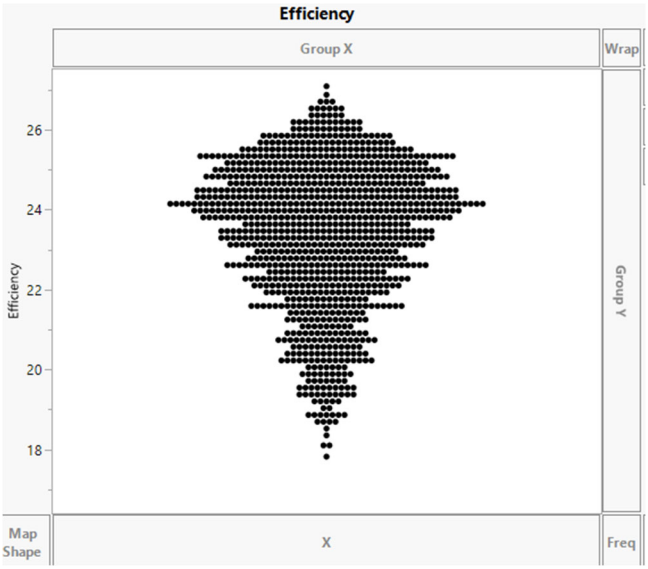

Figure 38. Efficiency plot of all datapoints.

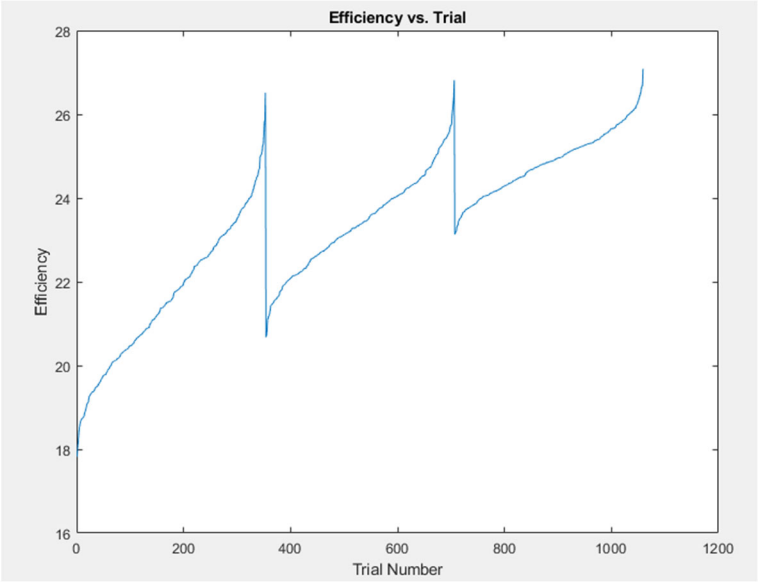

Figure 39. Efficiency vs. Trial plot

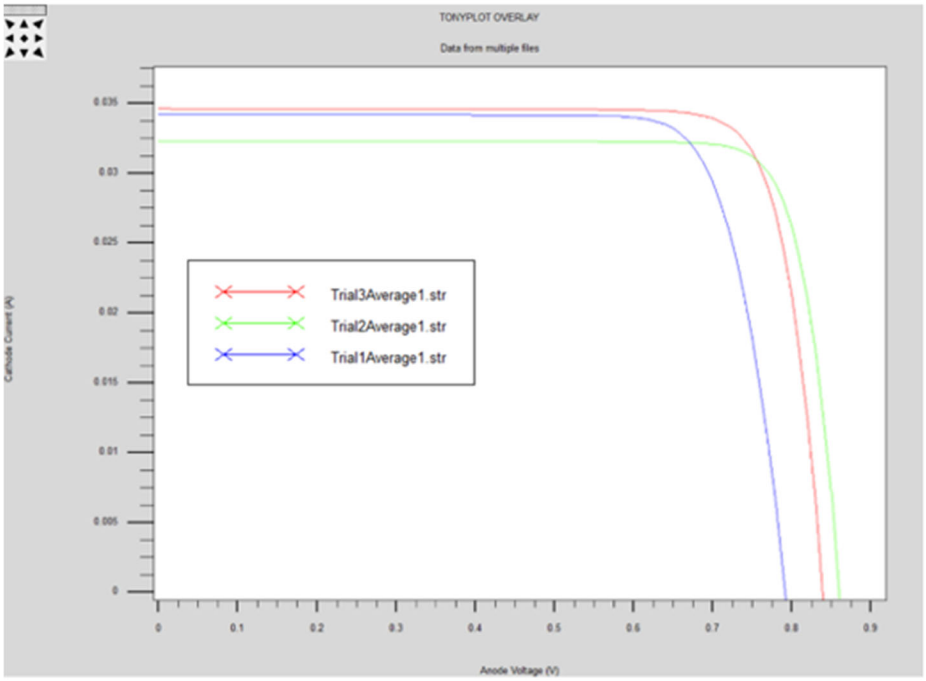

Figure 40. I-V curve of the average of all datasets.

While the average efficiency generated is a compelling argument as to the effectiveness of the NOLH, the big-ticket item of the research conducted is the cell with the highest efficiency. Overall, the best cell generated from the data points was at 27.0865% efficient. That is an increase of 2.77% from the previous work conducted, and a relative increase of 10.21%. This extreme of an increase in a brief period is unprecedented.

While the most efficient cell was slightly over half of a percent higher from the first dataset to the last, the ramifications of the final efficiency are extreme. The relative increase from the dataset one best cell to the final cell is 2.1% in both efficiency and max power output. Table 6 shows the breakdown of the each of the optimal cells found in the three datasets. As can be seen there are only minute differences between each one. The same can be stated for the I-V curves depicted in Figure 40 of all three dataset optimal outputs. The NOLH was capable of producing an output from the first set of data that nearly matched the optimal one discovered after 706 additional trials.

Table 6. Comparison of the optimal cells performance from each data set.

	Dataset 1	Dataset 2	Dataset 3
AZO [µm]	0.40	0.38	0.18
ZnO [µm]	0.45	0.50	0.59
CdS [µm]	0.63	0.65	0.67
CIGS [µm]	1	1	1
CIGS+ [µm]	3.19	3.19	4.25
Mo [µm]	0.44	0.47	0.50
Var_width	0.04	0.04	0.04
X	0.38	0.39	0.39
I_{SC} [mA]	36.90	36.90	36.90
Voc [V]	0.85	0.859	0.861
P_m [mW]	26.50	26.80	27.10
V_m [V]	0.75	0.75	0.76
I_m [mA]	35.40	35.60	35.70
FF	84.67	84.98	85.28
Efficiency [%]	26.52	26.81	27.0865

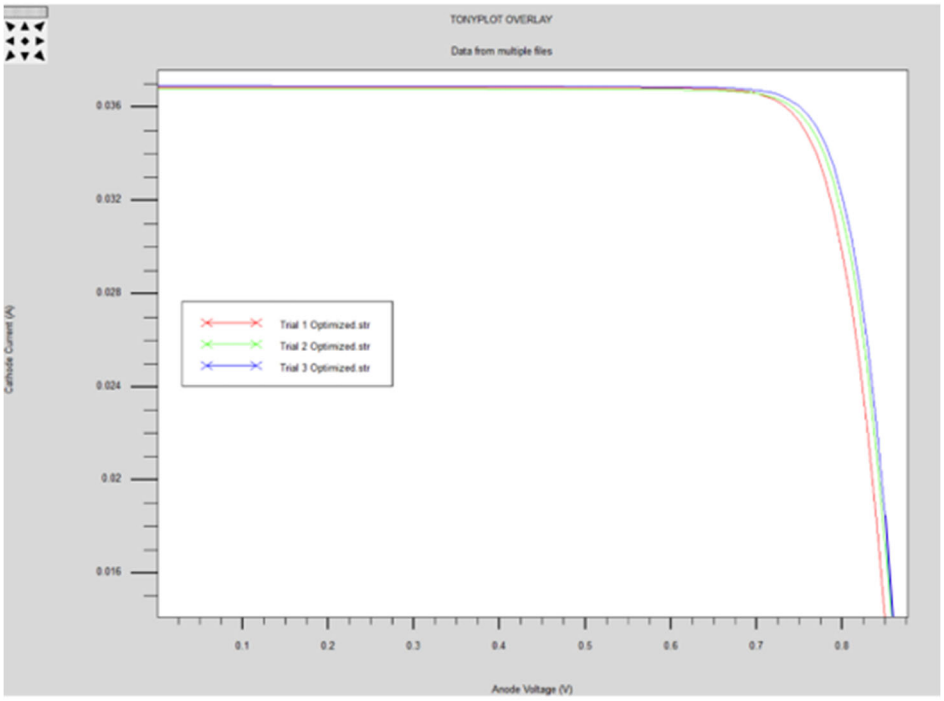

Figure 41. I-V curve of the best cell from all three datasets.

While the optimal cell discovered through the trial runs was found to be 27.0865% efficient, there was still room for improvement. Upon studying the interactions each variable had on the output of the cell, additional trials were conducted to further optimize the BSC CIGS cell. The parameters were adjusted in minute steps to maintain control and predict the output. Table 7 is a summary of the hand manipulated trials and the subsequent efficiencies found.

Table 7. Manipulated parameters and final optimal BCS CIGS PV cell.

	Trial 1	Trial 2	Trial 3	Trial 4	Trial 5	Trial 6
AZO [µm]	0.20	0.18	0.18	0.18	0.15	0.15
ZnO [µm]	0.59	0.60	0.59	0.59	0.59	0.60
CdS [µm]	0.67	0.67	0.70	0.65	0.67	0.70
CIGS [µm]	1	1	1	1	1	1
CIGS+ [µm]	4.25	4.25	4.25	4.25	4.25	4.25
Mo [µm]	0.50	0.50	0.50	0.50	0.50	0.50
Var_width	0.04	0.04	0.04	0.04	0.04	0.04
X	0.39	0.39	0.39	0.39	0.39	0.39
Efficiency [%]	27.0677	27.087	27.0926	27.0829	27.1082	27.1148

Once again, the optimal efficiency was dethroned, and an alternative set of data was found, with a 0.0283% increase overall. The minute increase may seem trivial on the surface, and with such minor differences between variables the new set of data would be hard to replicate perfectly in an industrial setting, but the implications of higher quality solar cells cannot be ignored. The marriage of optimization algorithms and analysis tools with physical manipulation was able to provide an optimal cell that far exceeded all expectations. Figure 41 demonstrates the I-V curve for trial six, the overall optimized solar cell. The minuscule difference between the I-V curve of the most optimal cell and Figure 40 would make it indistinguishable from the others, and so it is plotted separately. Table 8 shows the performance parameters of the most optimal cell, as compared to the two previously designed BSC CIGS solar cells conducted by Herrera [3] and Logar [2], as can be seen, the utilization of the NOLH for optimization has catapulted the BSC CIGS solar cell performance to unprecedented heights. Finally, Figure 41 is the Silvaco Tonyplot

output the design of the solar cell, and Figure 42 is a 3-dimensional representation of the novel BSC CIGS cell design.

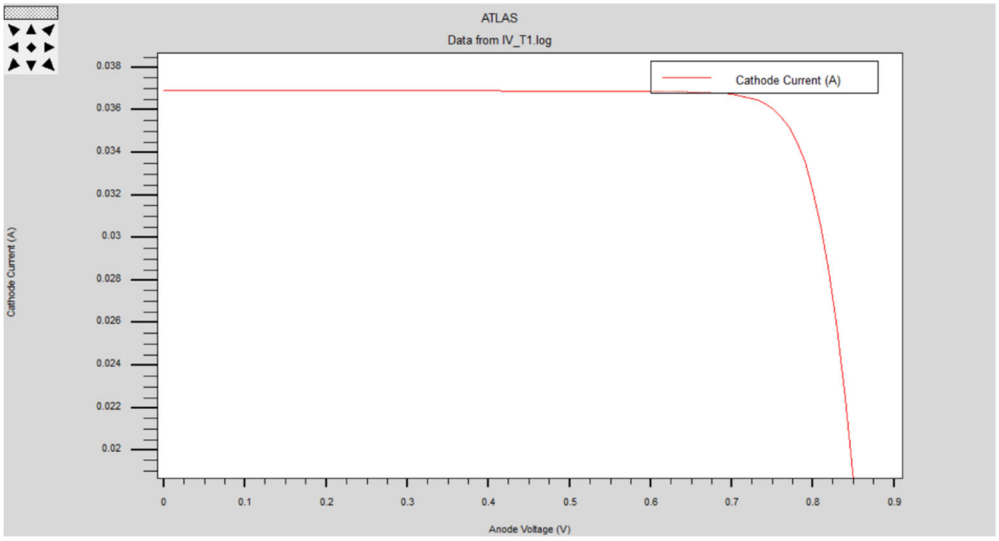

Figure 42. I-V curve of optimal cell.

Table 8. Comparison of optimal cell performances. Adapted from: [2].

	Herrera	Logar	Trial 6
AZO [µm]	-	0.05	0.15
ZnO [µm]	0.40	0.30	0.60
CdS [µm]	0.45	0.30	0.70
CIGS [µm]	11	2	1
CIGS+ [µm]	6	1	4.25
Mo [µm]	0.40	0.10	0.50
Var_width	0.15	0.05	0.04
X	0.45	0.34	0.39
I_{SC} [mA]	35.08	37.23	36.90
Voc [V]	0.845	0.84	0.862
P_m [mW]	23	24.33	27.12
V_m [V]	0.73	0.69	0.76
I_m [mA]	31.50	35.26	35.69
FF	77.60	77.80	85.20
Efficiency [%]	23.00	24.32	27.1148

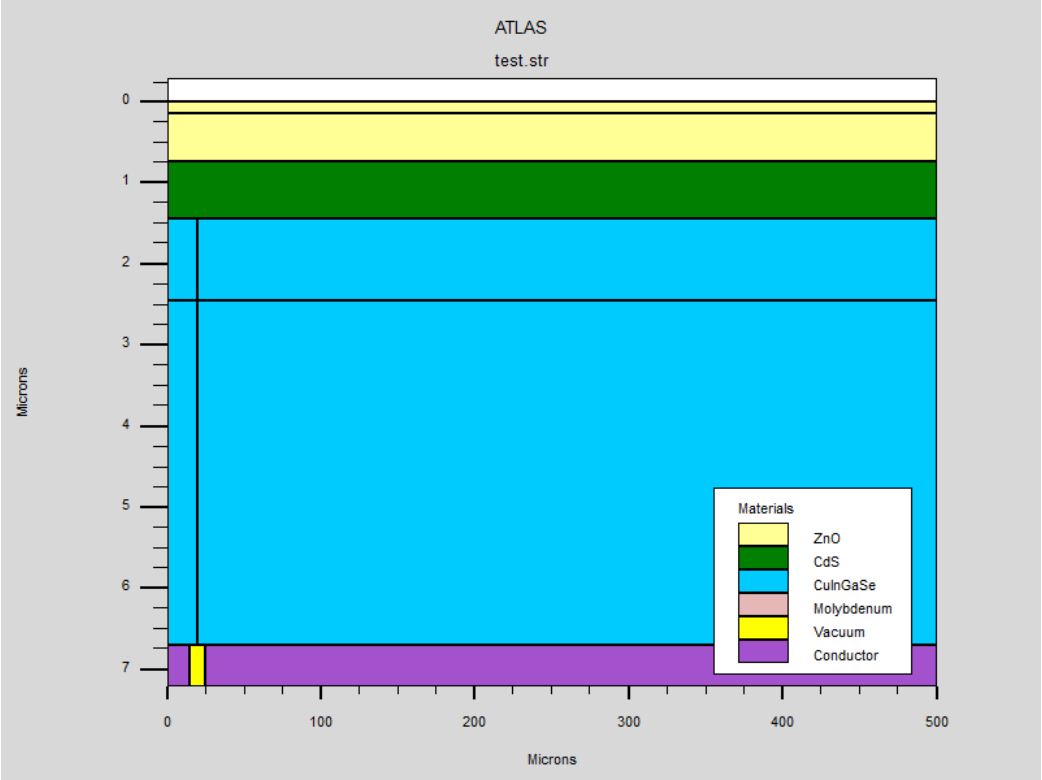

Figure 43. Tonyplot of optimal cell design.

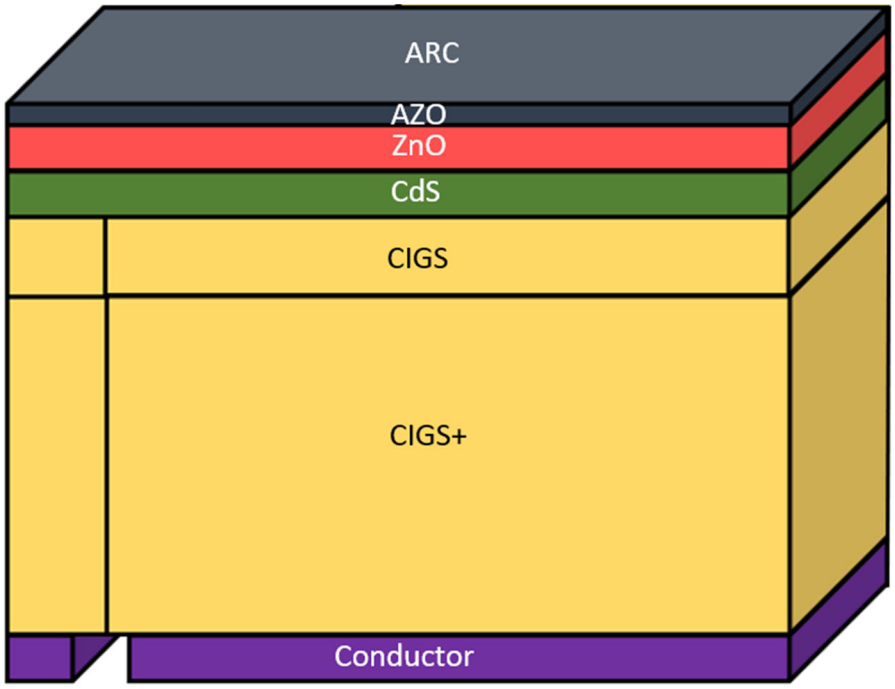

Figure 44. 3-D model of optimal cell.

THIS PAGE INTENTIONALLY LEFT BLANK

VII. CONCLUSION

The goal of this work was not only to generate an efficient model for a novel design BSC CIGS solar cell, but also to demonstrate the effectiveness and efficiency of the NOLH. Both goals have been accomplished. Over the span of 1,065 trials the overall relative efficiency of the designed solar cell was increased by 11.5% with a run time of only 168 hours. Of these 1,065, trials, over 34.6% of them yielded efficiencies greater than or equal to the starting parameters. This demonstrates that not only was an optimized solar cell produced, but that there are 368 other combinations of thickness and molar ratio that can produce a highly efficient solar cell.

The data reflects a relatively small number of trials with an extremely healthy output. That is the goal of optimization, to achieve the best possible answer in as few iterations as possible. The NOLH was critical in the foundation of this work. The algorithm is only as good as the data the user inputs into it, and so further design parameters could be utilized to further optimize the BSC CIGS PV material. The JMP software was also an invaluable tool to demonstrate the relationship between variables and the nuanced effects a variable had on the overall output. Silvaco ATLAS is a one-of-a-kind software, with its built-in material parameters and plain text coding, Silvaco made generating the novel design quick and easy, with high adaptability for future exploration in BSC CIGS solar cell designs.

The BSC CIGS PV material design is the way of the future. As a flexible, thin film solar cell with a low-cost point, CIGS has the potential to change the common perspective of solar cells. The adaptability of the material make it a perfect fit for non-flat surfaces and rugged environments, while the light weight is ideal for applications such as drones, satellites, and the warfighter. With the adaptation of the BSC there will no longer be losses due to shadowing, and the solar cell will have higher efficiency while simultaneously blending in better with surroundings. The BSC CIGS solar cell designed in this work has the efficiency to rival current cells on the market with the flexibility to make them obsolete.

A. FUTURE WORK

The design parameters that were varied in this work are not all inclusive, and many more could potentially be adapted and optimized to produce a potentially better performing solar cell. Due to the experimental nature of a BSC CIGS solar cell, and lack of industry guidance and information, several assumptions were made during the building and implementation of the Silvaco code. Future work could involve adjusting doping levels of the varied materials, experimenting with temperature effects on the solar cell, and replacing some materials for a more optimal type.

Due to the thin, aluminum foil consistency of the CIGS solar cell, a possible new area of study could be 3D printing the BSC CIGS design. The field of printed photovoltaics is currently in its infancy, but with the nature of the thin film and vertical junction, a 3D printer capability would potentially speed up production and accessibility to renewable energy. For the warfighter, access to a print-ready mobile energy source could be revolutionary.

For future work for the NOLH, optimization of rad-hard materials and multijunction solar cells would be the next logical step. Rad-hard materials are an essential part of satellites and U.S. mission readiness for forward deployed forces and home defense. As these satellites orbit around the Earth, their main source of power for years is solar cells, that must operate at certain levels to maintain charge while constantly being bombarded by radiation. If the weight of the cell were to decrease and the radiation resistance to increase, the government could save millions to billions of dollars in future work, and essential security measures would remain in place for future generations.

APPENDIX A. SILVACO CODE

The following code is modified from Logar[2]. The code presented has the optimal parameters found in the totality of this work.

```
go atlas simflag="-P 8"
##### STRUCTURE DEFINITIONS #####
#Layer thicknesses
set AZO=        0.15
set ZnO=        0.6
set CdS=        0.7
set CIGS=       1
set CIGS_plus=          4.25
set Mo=                  0.5
set gap=        10
#Y-dimensions
set L1=                 $AZO
set L2=                 $AZO+$ZnO
set L3=                 $AZO+$ZnO+$CdS
set L4=                 $AZO+$ZnO+$CdS+$CIGS
set L5=                 $AZO+$ZnO+$CdS+$CIGS+$CIGS_plus
set L6=                 $AZO+$ZnO+$CdS+$CIGS+$CIGS_plus+$Mo
#X-dimensions
set width=      500
set width3d=    100e6/$width
set div=        20
set var_width=0.04*$width
set width_cat= $var_width-($gap/2)
set width_ano=          $var_width+($gap/2)
#Miscellaneous
set x.comp=     0.39
set Eg_CIGS= 1.250718

##### MESH #####
#surface is 200 sq micron = 1/500000 sq cm
mesh width=    $width3d
x.mesh loc=0            spac=$width/$div
x.mesh loc=$width_cat           spac=$gap/($div)
x.mesh loc=$var_width           spac=$width/$div
x.mesh loc=$width_ano           spac=$gap/$div
x.mesh loc=$width       spac=$width/$div

y.mesh          loc=0           spac=$L1/($div/2)
```

```
y.mesh loc=$L1              spac=$AZO/($div/2)
y.mesh loc=$L2              spac=$ZnO/($div/2)
y.mesh loc=$L3              spac=$CdS/($div/2)
y.mesh loc=($L4-$L3)/2      spac=($L4-$L3)/(2*$div)
y.mesh loc=$L4              spac=$CIGS/(3*$div)
y.mesh loc=$L5              spac=$CIGS_plus/(2*$div)
y.mesh loc=$L6              spac=$Mo/($div/2)

##### MATERIAL DEFINITIONS #####
region num=1  material=ZnO          x.min=0                     x.max=$width
        y.min=0                 y.max=$L1
region num=2  material=ZnO          x.min=0                     x.max=$width
        y.min=$L1     y.max=$L2
region num=3  material=CdS          x.min=0                     x.max=$width
        y.min=$L2     y.max=$L3
region num=4  material=CIGS                 x.min=0
        x.max=$var_width     y.min=$L3     y.max=$L4
region num=5  material=CIGS                 x.min=$var_width     x.max=$width
        y.min=$L3     y.max=$L4
region num=6  material=CIGS                 x.min=0
        x.max=$var_width     y.min=$L4     y.max=$L5
region num=7  material=CIGS                 x.min=$var_width     x.max=$width
        y.min=$L4     y.max=$L5
region num=8  material=Molybdenum           x.min=0
        x.max=$width_cat     y.min=$L5     y.max=$L6 conductor
region num=9  material=Vacuum               x.min=$width_cat     x.max=$width_ano
        y.min=$L5     y.max=$L6
region num=10 material=Molybdenum           x.min=$width_ano     x.max=$width
        y.min=$L5     y.max=$L6 conductor

electrode name=cathode      num=1           x.min=0
        x.max=$width_cat     y.min=$L5     y.max=$L6
electrode name=anode        num=2           x.min=$width_ano     x.max=$width
        y.min=$L5     y.max=$L6

doping AL     uniform       conc=1e18     region=1          #possible change of
these
doping n.type  uniform conc=1e18    region=2
doping n.type  uniform conc=1e17    region=3
doping n.type  uniform conc=8e16    region=4
doping p.type  uniform      conc=8e16     region=5
doping n.type  uniform      conc=4e18     region=6
doping p.type  uniform conc=4e18    region=7

#from excel file. Compiled from other sources
```

```
material region=1       EG300=3.3     AFFINITY=4.5          EPSILON=9
        NC300=2.2e18          NV300=1.8e19          MUN=100      MUP=25
        index.file='ZnO_Al.txt'  #from reference 8
material region=2       EG300=3.3     AFFINITY=4.5          EPSILON=9
        NC300=2.2e18          NV300=1.8e19          MUN=100      MUP=25
        index.file='ZnO.txt'
material region=3       EG300=2.48    AFFINITY=4.18         EPSILON=10
        NC300=2.2e18          NV300=1.8e19          MUN=100      MUP=25
material material=CIGS        EG300=$Eg_CIGS    AFFINITY=4.26
        EPSILON=13.6          NC300=2.2e18          NV300=1.8e19          MUN=100
        MUP=25        COPT=5e-17  AUGN=8.3e-32   AUGP=1.8e-31  TAUN=2e-7
TAUP=2e-7
material material=Molybdenum
material material=Vacuum              real.index=1    imag.index=0

##### TRAPS #####
trap    material=ZnO donor            e.level=0       sign=1e-14     sigp=3e-13
        density=3e16  degen.fac=1   x.min=0          x.max=$width
        y.min=0       y.max=$L1
trap    material=ZnO donor            e.level=0       sign=1e-15     sigp=1e-15
        density=1e16  degen.fac=1   x.min=0                 x.max=$width
        y.min=$L1     y.max=$L2
trap    material=CdS  donor           e.level=0       sign=1e-15     sigp=1e-12
        density=1e16  degen.fac=1   x.min=0          x.max=$width
        y.min=$l2     y.max=$L3
trap    material=CIGS         donor           e.level=0       sign=4e-16     sigp=4e-14
        density=7.5e13        degen.fac=1   x.min=0          x.max=$var_width
        y.min=$L3     y.max=$L4
trap    material=CIGS         acceptor        e.level=0       sign=4e-16     sigp=4e-14
        density=7.5e13        degen.fac=1   x.min=$var_width x.max=$width
        y.min=$L3     y.max=$L4
trap    material=CIGS         donor           e.level=0       sign=4e-16     sigp=4e-14
        density=7.5e13        degen.fac=1   x.min=0          x.max=$var_width
        y.min=$L4     y.max=$L5
trap    material=CIGS         acceptor        e.level=0       sign=4e-16     sigp=4e-14
        density=7.5e13        degen.fac=1   x.min=$var_width x.max=$width
        y.min=$L4     y.max=$L5

##### INTERFACES #####
interface x.min=0             x.max=$width          y.min=0       y.max=0
        s.n=45 s.p=45 s.x #semiconductor -> insulator    #verify with manual (s.n/s.p)
interface x.min=0             x.max=$width          y.min=$L1     y.max=$L1     s.n=5
        s.p=5   s.s #semiconductor -> semiconductor
interface x.min=0             x.max=$width          y.min=$L2     y.max=$L2     s.n=5
        s.p=5   s.s
```

```
interface x.min=0               x.max=$var_width    y.min=$L3     y.max=$L3     s.n=5
        s.p=5   s.s
interface x.min=$var_width  x.max=$width                y.min=$L3     y.max=$L3
        s.n=5   s.p=5   s.s
interface x.min=0               x.max=$var_width    y.min=$L4     y.max=$L4     s.n=5
        s.p=5   s.s
interface x.min=$var_width  x.max=$width                y.min=$L4     y.max=$L4
        s.n=5   s.p=5   s.s
interface x.min=0               x.max=$width_cat    y.min=$L5     y.max=$L5     s.n=45
        s.p=45 s.m #semiconductor -> metal
interface x.min=$width_ano  x.max=$width                y.min=$L5     y.max=$L5
        s.n=45 s.p=45 s.m
interface x.min=$width_cat  x.max=$width_ano    y.min=$L5     y.max=$L5     s.n=45
        s.p=45 s.x
interface x.min=$var_width  x.max=$var_width    y.min=$L3     y.max=$L4     s.n=5
        s.p=5   s.s
interface x.min=$var_width  x.max=$var_width    y.min=$L4     y.max=$L5     s.n=45
        s.p=45 s.m

# Refractive index of MgF2 = 1.413
interface       optical         ar.index=1.413          x.min=0
        x.max=$width            y.min=0                 y.max=0                 coating=1
interface       optical         reflect=0.9     x.min=0
        x.max=$width_cat        y.min=$L5       y.max=$L5
interface       optical         reflect=0.9     x.min=$width_cat        x.max=$width
        y.min=$L5       y.max=$L5

contact num=1 name=cathode con.resist=.05e-8
contact num=2 name=anode    con.resist=.05e-8

#save out.file= "test.str"    #for seeing cell structure
#tonyplot test.str

##### Modeling the cell ##### (temp 1: 26.85 C)
models srh fermi ni.fermi bgn optr auger print temp=300 bound.trap
method gummel newton itlimit=200 maxtraps=20
        #iteration limit and maxtraps, look in manual
output photogen recomb u.auger u.srh u.trap traps u.radiative  band.param con.band
val.band gaussian.band  flowlines opt.intens j.electron j.hole j.total j.drift j.diffusion
e.mobility h.mobility qfn qfp

#Solar spectrum
beam num=1 x.origin=$width/2 y.origin=-0.5 AM1.5 wavel.start=0.3 wavel.end=1.2
wavel.num=100 front.refl back.refl reflects=1 min.power=1e-6 angle=90
solve init
```

```
solve previous
# Solving illuminated condition
# b#=# --> beam # intensity
solve b1=0.001
solve b1=0.01
solve b1=0.1
solve b1=0.5
solve b1=1.0

# change vfinal if no x-axis crossing for Voc and FF calcs
log outfile="IV_T1.log"
solve vanode=0 name=anode vstep=0.01 vfinal=0.85
log off

tonyplot IV_T1.log

extract init infile="IV_T1.log"
extract name="Isc" y.val from curve(v."anode",i."cathode") where x.val=0.0
extract name="Voc" x.val from curve(v."anode",i."cathode") where y.val=0.0
extract name="Pm" max(curve(v."anode",(v."anode"*i."cathode")))
extract name="Vm" x.val from curve(v."anode",(v."anode"*i."cathode")) where y.val=$"Pm"
extract name="Im" $"Pm"/$"Vm"
extract name="FF" $"Pm"/($"Isc"*$"Voc")
extract name="Opt Int"          max(beam."1")
extract name="Eff" (abs($"Pm")/$"Opt Int")
```

THIS PAGE INTENTIONALLY LEFT BLANK

APPENDIX B. TRIAL DATA

Th tables shown display the full range of data generated from the NOLH and the following output generated from Silvaco. The data is broken up into the three corresponding data sets.

DATASET 1

AZO	ZnO	Cds	CIGS	CIGS+	Mo	Var	X	Bandgap	Efficiency	Time
0.4	0.45	0.63	1	3.19	0.44	0.04	0.38	1.24438	26.5158	9.78
0.07	0.8	1	3.41	5.38	0.14	0.06	0.4	1.25706	25.8467	11.9
0.04	0.68	0.33	2.31	4.94	0.61	0.06	0.39	1.250718	25.8242	13.87
0.16	0.88	0.55	1.44	2.97	0.76	0.08	0.38	1.24438	25.517	14.73
0.07	0.68	0.78	1.22	3.19	0.97	0.1	0.38	1.24438	25.2845	11.6
0.1	0.75	0.78	4.94	6.47	0.85	0.06	0.39	1.250718	25.2695	12.8
0.28	0.75	0.28	4.94	2.09	0.14	0.04	0.38	1.24438	25.1312	8.59
0.91	0.83	0.55	1.88	1	0.61	0.05	0.37	1.238046	25.0463	13.08
0.31	0.68	0.55	7.56	7.13	0.35	0.05	0.39	1.250718	25.0379	12.89
0.76	0.38	0.9	2.09	3.84	0.64	0.06	0.37	1.238046	25.0137	11.21
0.55	0.75	0.95	3.41	7.34	0.29	0.08	0.4	1.25706	24.9805	8.59
0.4	0.93	0.9	1	2.97	0.7	0.12	0.39	1.250718	24.697	7.1
0.1	0.85	0.57	3.19	1.44	0.67	0.06	0.35	1.22539	24.6923	10.16
0.25	0.63	0.28	3.63	6.91	0.23	0.05	0.35	1.22539	24.6264	12.08
0.19	0.65	0.95	6.03	2.75	0.79	0.06	0.37	1.238046	24.5609	9.96
0.67	0.8	0.78	3.41	7.34	0.64	0.07	0.37	1.238046	24.5123	7.61
0.97	0.95	0.45	2.97	4.06	0.26	0.07	0.38	1.24438	24.5082	
0.73	0.4	0.83	1.88	6.91	0.61	0.1	0.38	1.24438	24.4417	8.51
0.04	0.43	0.75	4.28	7.78	0.29	0.04	0.33	1.21275	24.4313	15.43
0.85	0.93	1	1.88	3.63	0.5	0.07	0.35	1.22539	24.3977	7.53
0.25	0.75	0.78	3.84	4.94	0.11	0.06	0.34	1.219068	24.3074	11.36
0.19	0.85	0.98	2.75	3.41	0.73	0.09	0.36	1.231716	24.3029	9.48
0.64	0.5	0.48	2.97	6.47	0.29	0.05	0.33	1.21275	24.2134	11.81
0.4	0.88	0.35	1.22	6.25	0.67	0.09	0.34	1.219068	24.2104	9.38
0.16	0.65	0.28	6.91	7.78	0.44	0.09	0.39	1.250718	24.1257	9.15
0.22	0.68	0.68	1.44	5.59	0.29	0.08	0.31	1.200126	24.1219	9.6
0.85	0.98	0.53	2.97	7.78	0.7	0.05	0.33	1.21275	24.0464	13.48
0.79	0.48	0.43	1	5.16	0.2	0.07	0.31	1.200126	24.0352	8.93
0.67	0.43	0.75	2.53	4.72	0.14	0.1	0.37	1.238046	24.0146	7.62
0.73	0.45	0.83	4.28	7.34	0.64	0.07	0.36	1.231716	23.999	8.46
0.13	0.3	1	6.03	3.19	0.55	0.05	0.35	1.22539	23.9933	9.23
0.7	0.57	0.98	2.75	1	0.67	0.1	0.38	1.24438	23.9857	
0.34	0.43	0.55	2.53	2.09	0.88	0.05	0.31	1.200126	23.9506	10.84
0.73	0.45	0.2	2.31	5.16	0.61	0.05	0.33	1.21275	23.9337	14.38
1	0.3	0.5	4.28	2.31	0.76	0.09	0.38	1.24438	23.9083	7.28
0.25	0.65	0.9	8	3.84	0.94	0.07	0.36	1.231716	23.8854	7.31
0.31	0.73	0.28	3.63	6.69	0.2	0.06	0.33	1.21275	23.883	11.65
0.97	0.63	0.83	3.19	2.97	0.61	0.11	0.39	1.250718	23.8673	6.84
0.46	0.3	0.2	5.16	1.44	0.85	0.07	0.39	1.250718	23.8376	8.03

0.46	0.53	0.9	1.22	2.53	0.67	0.16	0.4	1.25706	23.7988	7.15
1	0.75	0.68	8	1.66	0.47	0.07	0.38	1.24438	23.783	5.47
0.4	0.9	0.33	4.94	7.56	0.73	0.08	0.36	1.231716	23.7715	7.19
0.73	0.45	0.63	1.22	6.25	1	0.1	0.33	1.21275	23.7604	8.44
0.04	0.57	0.25	6.69	4.28	0.35	0.05	0.33	1.21275	23.7588	11.06
0.16	0.88	0.68	3.63	7.13	0.2	0.13	0.39	1.250718	23.7373	9.89
0.67	0.28	0.8	6.47	1	0.5	0.05	0.36	1.231716	23.722	7.99
0.85	0.3	0.98	4.28	2.75	0.08	0.05	0.34	1.219068	23.6987	10.07
0.34	0.25	0.73	1.66	6.25	0.79	0.04	0.29	1.187518	23.6649	17.3
0.13	0.55	0.35	7.13	5.38	0.7	0.12	0.4	1.25706	23.634	8.72
0.55	0.95	0.35	4.72	5.81	0.94	0.1	0.38	1.24438	23.62	8.1
0.43	0.65	0.25	1.88	5.81	0.94	0.05	0.29	1.187518	23.5707	14.34
0.97	0.75	0.23	5.38	1.88	0.58	0.06	0.37	1.238046	23.5439	8.59
0.97	0.5	0.9	4.06	7.34	0.2	0.05	0.32	1.206436	23.5377	12.66
0.91	0.7	0.35	6.91	7.34	0.41	0.04	0.33	1.21275	23.5074	8.66
0.19	0.53	0.7	1.88	6.91	0.47	0.05	0.26	1.168636	23.4747	12.82
0.16	0.33	0.5	5.38	5.59	0.73	0.08	0.35	1.22539	23.4288	7.38
0.94	0.48	0.93	2.75	2.53	1	0.13	0.39	1.250718	23.4217	6.18
0.46	0.38	0.43	3.41	1.44	0.29	0.05	0.31	1.200126	23.4191	8.2
0.91	0.33	0.23	5.16	6.03	0.08	0.09	0.39	1.250718	23.4149	7.14
1	0.48	0.4	2.97	5.59	0.14	0.1	0.36	1.231716	23.3968	8.07
0.94	0.33	0.85	1.44	4.06	0.14	0.08	0.31	1.200126	23.3868	7.91
0.94	0.65	0.93	6.47	4.06	0.17	0.04	0.32	1.206436	23.3529	8.47
0.1	0.43	0.8	2.53	7.13	0.2	0.11	0.33	1.21275	23.348	10.66
0.49	0.43	0.75	8	6.69	0.44	0.11	0.39	1.250718	23.3468	7.48
0.76	0.98	0.48	1.44	1.88	0.2	0.1	0.33	1.21275	23.3425	7.76
0.46	0.28	0.38	4.94	7.13	1	0.11	0.39	1.250718	23.285	12.82
0.31	0.55	0.38	2.09	7.13	0.08	0.13	0.35	1.22539	23.2602	8.61
0.58	0.33	0.28	1	7.13	0.64	0.13	0.36	1.231716	23.2588	9.78
0.04	0.73	0.5	7.34	7.13	0.05	0.09	0.34	1.219068	23.2573	7.8
0.61	0.3	0.98	6.47	3.41	0.32	0.04	0.32	1.206436	23.2467	8.1
0.37	0.7	0.28	1.88	8	0.73	0.09	0.31	1.200126	23.238	12.91
0.46	0.93	0.33	1.22	5.16	0.73	0.05	0.26	1.168636	23.2306	14.54
0.85	0.85	0.55	3.84	7.13	0.08	0.08	0.33	1.21275	23.1929	8.52
0.16	1	0.78	3.19	4.72	0.08	0.16	0.4	1.25706	23.1751	11
0.49	0.4	0.23	1.44	5.81	0.73	0.13	0.36	1.231716	23.1562	10.29
0.4	0.57	0.35	6.25	3.19	0.91	0.11	0.37	1.238046	23.15	13.5
0.16	0.75	0.95	1.22	4.28	0.26	0.15	0.34	1.219068	23.1407	14.74
0.19	0.85	0.25	4.06	1.66	0.26	0.13	0.38	1.24438	23.1205	6.85
0.7	1	0.85	3.84	3.84	0.94	0.1	0.35	1.22539	23.1183	7.53
0.43	0.7	0.3	6.91	4.06	0.11	0.09	0.35	1.22539	23.1157	6.89
0.91	0.5	0.2	5.59	6.25	0.73	0.1	0.38	1.24438	23.1093	7.54
0.94	0.9	0.88	5.38	3.63	0.38	0.09	0.36	1.231716	23.092	10.38
0.13	0.55	0.48	2.31	2.75	0.5	0.07	0.28	1.18122	23.0804	7.29
0.67	0.85	0.8	4.72	6.69	0.64	0.14	0.4	1.25706	23.0754	7.07
0.88	0.7	0.75	4.28	8	0.7	0.14	0.4	1.25706	23.0622	8.16
0.73	1	0.53	6.91	6.69	0.47	0.11	0.38	1.24438	23.0482	7.08
0.43	0.95	0.48	6.25	6.47	0.5	0.09	0.34	1.219068	23.029	6.93
0.28	0.38	0.63	6.03	3.19	0.05	0.07	0.32	1.206436	23.0124	7.19

0.43	0.43	0.98	5.81	1.22	0.64	0.06	0.31	1.200126	22.983	8.89
0.04	0.68	0.25	6.91	2.31	0.94	0.13	0.38	1.24438	22.938	12.77
0.64	1	0.48	2.75	2.97	0.67	0.06	0.28	1.18122	22.9104	12.02
0.1	0.3	0.75	7.56	1.22	0.5	0.08	0.34	1.219068	22.91	7.01
0.25	0.43	0.48	1.44	2.75	0.08	0.13	0.32	1.206436	22.8566	12.89
0.25	0.8	0.98	3.41	1.44	0.17	0.07	0.28	1.18122	22.8524	13.42
0.4	0.48	0.43	6.47	2.75	0.08	0.14	0.39	1.250718	22.851	8.12
0.46	0.95	0.9	3.19	1.44	0.97	0.13	0.36	1.231716	22.8429	6.27
0.43	0.38	0.33	4.94	6.47	0.73	0.14	0.39	1.250718	22.8416	7.84
0.94	0.8	0.98	4.28	3.84	0.26	0.07	0.31	1.200126	22.8102	9.16
0.97	0.4	0.48	6.03	3.19	0.79	0.12	0.38	1.24438	22.7569	5.87
0.88	0.7	0.63	6.69	2.75	0.7	0.06	0.31	1.200126	22.7454	9.02
0.25	0.33	0.9	1.22	4.72	0.76	0.2	0.39	1.250718	22.731	12.58
0.49	0.93	0.7	2.09	6.69	0.97	0.08	0.27	1.174926	22.7205	8.59
0.13	0.2	0.9	5.38	4.72	0.82	0.08	0.34	1.219068	22.7171	11.89
0.31	0.83	0.4	1.22	5.59	0.94	0.18	0.37	1.238046	22.6738	12.88
0.82	0.57	0.45	1.44	5.59	0.14	0.16	0.36	1.231716	22.6664	8.5
0.22	0.4	0.57	2.31	3.63	0.44	0.04	0.24	1.156068	22.6599	16.49
0.19	0.5	0.7	5.59	6.03	0.26	0.16	0.39	1.250718	22.6455	9.82
0.31	0.48	0.25	2.75	1.22	0.55	0.14	0.36	1.231716	22.6079	7.67
0.04	0.93	0.65	6.69	1.88	0.41	0.09	0.31	1.200126	22.5963	7.04
0.49	0.35	0.5	3.84	1	0.23	0.06	0.29	1.187518	22.5937	8.34
0.37	0.25	0.4	1.22	4.72	0.61	0.17	0.37	1.238046	22.5803	11.61
0.76	0.98	0.57	3.84	2.53	0.2	0.13	0.36	1.231716	22.5752	7.08
0.67	0.28	0.5	6.69	2.09	0.14	0.14	0.4	1.25706	22.5732	6.5
0.19	0.65	0.83	6.03	5.59	0.94	0.16	0.39	1.250718	22.5701	7.46
0.7	0.78	0.53	4.94	1.44	0.17	0.15	0.39	1.250718	22.562	5.85
0.22	0.5	0.53	1	2.31	0.14	0.11	0.27	1.174926	22.561	7.92
0.58	0.85	0.3	3.63	3.19	0.55	0.04	0.26	1.168636	22.5444	9.95
0.49	0.98	0.4	1	5.59	0.41	0.19	0.38	1.24438	22.5441	9.53
0.7	0.57	1	5.81	5.16	1	0.06	0.29	1.187518	22.5298	13.5
0.82	0.25	0.55	1.66	2.53	0.58	0.18	0.4	1.25706	22.5289	12.41
0.79	0.88	0.55	2.53	2.97	0.38	0.05	0.25	1.16235	22.5252	9.81
0.25	1	0.63	7.56	2.31	0.55	0.15	0.39	1.250718	22.5187	6.27
0.79	0.3	0.88	5.16	3.63	0.88	0.07	0.31	1.200126	22.5081	6.47
0.34	0.25	0.98	4.72	6.47	0.35	0.09	0.32	1.206436	22.4855	7.84
0.73	0.23	0.45	7.78	3.63	0.88	0.11	0.38	1.24438	22.4681	6.58
0.94	0.48	0.8	6.47	4.28	0.32	0.15	0.4	1.25706	22.4626	6.71
0.34	0.93	0.55	6.91	7.34	1	0.06	0.28	1.18122	22.4538	11.51
0.22	0.65	0.68	1.88	7.78	0.79	0.1	0.26	1.168636	22.4009	9.41
0.7	0.23	0.7	1.88	4.94	0.14	0.18	0.39	1.250718	22.3926	12.4
0.91	0.7	0.33	6.69	7.78	0.29	0.1	0.34	1.219068	22.3851	7.46
0.88	1	0.53	7.56	2.09	0.82	0.05	0.29	1.187518	22.3801	7.57
0.19	0.28	0.7	8	3.41	0.29	0.09	0.33	1.21275	22.3775	8.91
0.28	0.38	1	4.72	7.56	0.23	0.13	0.34	1.219068	22.373	10.59
0.88	0.23	0.38	5.59	6.03	1	0.11	0.37	1.238046	22.3688	10.12
0.16	0.98	0.57	2.75	1.22	0.11	0.15	0.34	1.219068	22.279	6.69
0.76	0.73	0.43	5.81	2.53	0.55	0.06	0.28	1.18122	22.278	9.21
0.82	0.93	0.65	5.59	6.69	0.76	0.13	0.36	1.231716	22.2658	6.85

0.91	0.4	0.38	8	4.72	0.94	0.07	0.31	1.200126	22.2117	6.43
0.04	0.35	0.28	4.06	3.41	0.23	0.08	0.29	1.187518	22.2085	11.62
0.49	0.35	0.8	3.19	7.34	0.47	0.18	0.38	1.24438	22.1833	8.66
0.22	0.23	0.8	5.59	2.97	0.7	0.08	0.31	1.200126	22.1702	7.85
0.46	0.48	0.35	2.75	4.28	0.23	0.1	0.28	1.18122	22.1179	7.24
0.07	0.63	0.8	7.78	7.56	0.35	0.09	0.29	1.187518	22.1158	13
0.13	0.65	0.33	1.66	1	0.88	0.14	0.31	1.200126	22.1102	7.72
0.46	0.38	0.33	7.13	1.22	0.55	0.16	0.39	1.250718	22.0991	7.36
0.34	0.53	0.2	7.34	4.94	0.82	0.06	0.28	1.18122	22.0959	11.16
0.28	0.43	0.73	1.66	3.63	0.82	0.07	0.22	1.143516	22.0859	8.61
0.43	0.88	0.85	4.06	3.84	0.88	0.05	0.24	1.156068	22.0709	10.98
0.34	0.83	0.57	7.34	5.38	0.2	0.17	0.39	1.250718	22.0676	7.02
0.64	0.68	1	6.69	7.34	0.58	0.14	0.36	1.231716	22.0586	11.18
0.25	0.63	0.78	3.19	1	0.23	0.14	0.32	1.206436	22.0483	6.46
0.37	0.25	0.3	2.09	3.63	0.64	0.14	0.34	1.219068	22.0153	7.26
0.37	0.43	0.83	2.75	1.22	0.67	0.19	0.38	1.24438	22.0032	6.29
0.49	0.53	0.38	2.09	4.94	0.79	0.16	0.33	1.21275	21.9621	8.54
0.55	0.2	0.45	3.84	1	0.91	0.13	0.36	1.231716	21.922	7.7
0.28	0.2	0.73	3.63	7.34	0.88	0.04	0.26	1.168636	21.9021	25.58
0.94	0.23	0.57	2.53	5.81	0.73	0.11	0.31	1.200126	21.9003	
0.61	0.68	0.25	5.59	2.75	0.26	0.13	0.34	1.219068	21.8894	6.49
0.55	0.83	0.45	2.97	5.16	0.47	0.19	0.38	1.24438	21.8847	7.97
0.4	0.85	0.33	1.66	5.38	1	0.1	0.25	1.16235	21.8769	7.78
0.07	0.63	0.68	6.47	6.91	0.47	0.08	0.26	1.168636	21.8422	10.81
0.22	0.8	0.45	7.34	4.06	0.85	0.19	0.4	1.25706	21.8406	6.91
0.76	0.63	0.85	5.38	5.16	1	0.17	0.38	1.24438	21.8258	6.96
0.97	0.48	0.25	1.88	2.09	0.41	0.14	0.33	1.21275	21.8047	8.05
0.61	1	0.28	4.06	2.31	0.88	0.14	0.34	1.219068	21.8005	7.04
0.67	0.4	0.38	4.72	6.03	0.35	0.04	0.24	1.156068	21.7966	9.56
0.13	0.8	0.83	1	4.28	0.11	0.17	0.29	1.187518	21.7772	9.59
1	0.85	0.53	3.84	7.56	0.38	0.16	0.36	1.231716	21.7763	8.47
0.52	0.6	0.6	4.5	4.5	0.53	0.12	0.3	1.19382	21.7749	9.13
0.4	0.9	0.55	7.34	2.09	0.08	0.14	0.34	1.219068	21.7665	5.94
0.22	0.88	0.93	3.63	1	0.67	0.16	0.34	1.219068	21.7434	8.66
0.64	0.35	0.88	7.34	3.63	0.05	0.14	0.35	1.22539	21.7279	6.66
0.64	0.3	0.65	1.66	6.91	0.97	0.11	0.26	1.168636	21.6691	8.35
0.7	0.68	1	1.66	4.06	0.23	0.18	0.33	1.21275	21.6136	11.53
0.61	0.25	0.88	2.31	7.56	0.58	0.19	0.36	1.231716	21.5919	9.92
0.67	0.78	1	3.84	6.91	0.82	0.11	0.28	1.18122	21.5881	7.24
0.82	0.55	0.53	7.13	1.22	0.26	0.14	0.34	1.219068	21.5503	5.21
0.82	0.4	0.75	1.66	4.94	0.2	0.06	0.2	1.13098	21.5382	15.68
0.58	0.83	0.88	1.88	7.78	0.5	0.08	0.21	1.137246	21.5377	8.75
0.07	0.38	0.73	6.03	8	0.44	0.18	0.36	1.231716	21.5319	8.17
0.82	0.7	0.68	8	6.69	0.91	0.13	0.33	1.21275	21.5308	7.62
0.7	0.38	0.63	1.66	3.63	0.85	0.07	0.21	1.137246	21.5188	11.19
0.97	0.57	0.53	2.53	2.09	0.58	0.17	0.34	1.219068	21.5105	7.07
0.07	0.73	0.95	7.13	6.91	0.64	0.1	0.27	1.174926	21.5105	7.92
0.97	0.83	0.48	2.97	1	0.61	0.07	0.24	1.156068	21.5099	6.16
0.37	0.43	0.2	5.16	2.09	0.23	0.13	0.32	1.206436	21.5091	11.75

0.55	0.68	0.83	6.91	4.06	0.26	0.09	0.27	1.174926	21.4618	6.37
0.46	0.25	0.43	6.25	2.53	0.88	0.07	0.28	1.18122	21.4614	13.28
0.97	0.57	0.4	1.22	1.44	0.7	0.16	0.31	1.200126	21.4529	6.89
0.22	0.9	0.7	5.81	4.28	1	0.15	0.32	1.206436	21.4107	6.85
0.67	0.78	0.38	6.25	7.78	0.38	0.05	0.23	1.14979	21.4103	10.39
0.28	0.57	0.35	3.63	3.84	0.05	0.07	0.22	1.143516	21.3922	9.15
0.91	0.55	0.88	7.34	8	0.17	0.1	0.29	1.187518	21.3872	10.95
0.49	0.38	0.75	6.03	3.84	0.58	0.05	0.23	1.14979	21.3801	9.65
0.76	0.78	0.48	7.34	5.38	0.23	0.18	0.38	1.24438	21.3791	6.6
0.58	0.73	0.85	6.25	4.72	0.82	0.14	0.32	1.206436	21.3776	6.82
0.43	0.95	0.33	6.69	1.44	0.47	0.06	0.24	1.156068	21.3773	9.14
0.43	0.2	0.35	1.66	4.06	0.38	0.07	0.25	1.16235	21.3116	14.4
0.82	0.3	0.5	3.19	4.72	0.05	0.09	0.28	1.18122	21.2839	7.88
0.76	0.98	0.95	3.19	2.97	0.47	0.08	0.23	1.14979	21.2536	6.37
0.43	0.53	0.95	3.41	6.25	0.79	0.12	0.26	1.168636	21.2357	8.05
0.22	0.63	0.75	7.56	3.41	0.91	0.08	0.24	1.156068	21.2156	6.53
0.04	0.35	0.68	5.16	1.44	0.67	0.08	0.24	1.156068	21.2144	6.47
0.79	0.57	0.43	5.81	8	0.82	0.11	0.28	1.18122	21.1957	9.65
0.28	0.48	0.78	3.19	6.47	0.5	0.19	0.33	1.21275	21.1775	10.38
0.7	0.28	0.65	2.09	1.66	0.05	0.18	0.33	1.21275	21.1574	5.81
0.13	0.5	0.88	2.31	1.22	0.76	0.14	0.26	1.168636	21.1572	6.43
0.28	0.23	0.25	5.81	6.03	0.58	0.17	0.37	1.238046	21.1179	8.45
0.4	0.53	0.2	2.31	1.66	0.47	0.1	0.24	1.156068	21.11296	6.24
0.85	0.93	0.5	1	5.59	0.76	0.16	0.27	1.174926	21.0976	9.64
0.1	0.73	0.4	2.53	4.72	0.73	0.09	0.2	1.13098	21.0916	8.48
0.31	0.98	0.75	1.22	5.38	0.17	0.13	0.22	1.143516	21.088	9.45
0.37	0.8	0.83	4.28	2.97	0.7	0.2	0.36	1.231716	21.0814	7.56
0.1	0.98	0.63	6.47	3.19	0.32	0.14	0.29	1.187518	21.0373	8.37
0.58	0.95	0.78	2.75	6.47	0.17	0.18	0.32	1.206436	21.0259	8.28
0.82	0.33	0.28	5.38	8	0.38	0.08	0.26	1.168636	20.9952	7.77
0.61	1	0.85	7.34	4.94	0.67	0.17	0.35	1.22539	20.9911	6.84
0.16	0.2	0.68	1.44	6.91	0.23	0.19	0.31	1.200126	20.9119	9.26
0.55	0.85	0.4	5.81	1.66	0.58	0.07	0.22	1.143516	20.9064	5.46
1	0.28	0.55	2.31	7.13	0.64	0.15	0.29	1.187518	20.8982	
0.67	0.95	0.9	6.91	5.38	0.41	0.1	0.26	1.168636	20.8919	6.29
0.25	0.33	0.65	6.47	6.03	0.67	0.19	0.35	1.22539	20.8904	15.04
0.73	0.38	0.8	7.78	3.41	0.11	0.06	0.23	1.14979	20.8855	9.61
0.85	0.7	0.5	3.41	2.97	0.79	0.08	0.21	1.137246	20.8778	7.85
0.85	0.55	0.38	2.97	3.41	0.11	0.08	0.21	1.137246	20.8553	7.87
0.37	0.93	0.7	2.31	6.91	0.91	0.1	0.2	1.13098	20.8358	8.65
0.64	0.73	0.78	2.53	6.25	0.97	0.1	0.21	1.137246	20.8241	7.65
0.79	0.78	0.73	7.56	6.25	0.97	0.12	0.28	1.18122	20.809	7.3
0.55	0.28	0.5	6.91	2.31	0.08	0.16	0.33	1.21275	20.8085	6.2
0.22	0.95	0.65	7.34	6.47	0.47	0.06	0.2	1.13098	20.776	12.06
1	0.53	0.95	2.09	6.69	0.11	0.11	0.22	1.143516	20.7613	7.48
0.88	0.45	0.25	7.78	4.72	0.79	0.09	0.26	1.168636	20.7514	6.83
0.34	0.98	0.5	7.13	4.06	0.91	0.07	0.21	1.137246	20.7376	6.8
0.16	0.5	0.57	2.31	6.25	0.35	0.19	0.29	1.187518	20.7374	8.23
0.79	0.88	0.3	7.78	4.28	0.29	0.05	0.21	1.137246	20.7329	10.23

0.61	0.33	0.35	4.94	5.16	0.17	0.2	0.36	1.231716	20.7173	6.93
0.43	0.2	0.93	4.94	6.69	0.17	0.1	0.26	1.168636	20.6918	8.17
0.34	0.43	0.68	4.06	7.56	0.88	0.09	0.21	1.137246	20.6821	7.88
0.31	0.75	0.57	7.78	2.75	0.05	0.14	0.28	1.18122	20.6755	7.38
0.91	0.65	0.73	6.69	6.25	0.55	0.17	0.33	1.21275	20.6654	6.69
0.04	0.45	0.53	1	7.34	0.58	0.17	0.23	1.14979	20.665	10.91
0.67	0.95	0.8	7.78	4.28	0.44	0.08	0.23	1.14979	20.6427	5.83
0.49	1	0.75	5.16	8	0.14	0.11	0.24	1.156068	20.6217	7.33
0.07	0.8	0.73	2.97	5.81	0.26	0.13	0.22	1.143516	20.6139	9.13
1	0.85	0.93	4.94	5.59	0.82	0.16	0.31	1.200126	20.5927	7.49
0.88	0.23	0.63	6.25	7.78	0.94	0.09	0.26	1.168636	20.5782	7.28
0.76	0.83	0.2	4.28	1.44	0.82	0.12	0.26	1.168636	20.5425	6.27
0.82	0.8	0.63	6.69	5.38	0.61	0.2	0.36	1.231716	20.519	7.5
0.46	0.35	0.9	5.38	5.81	0.5	0.2	0.34	1.219068	20.5158	6.92
0.64	0.63	0.85	2.75	5.81	0.14	0.13	0.23	1.14979	20.5101	7.98
1	0.48	0.7	1.66	1.88	1	0.16	0.26	1.168636	20.4827	6.37
0.55	0.23	0.8	8	3.41	0.64	0.06	0.23	1.14979	20.4734	9.69
0.61	0.5	0.9	2.09	4.94	0.94	0.16	0.25	1.16235	20.473	7.58
0.22	0.28	0.55	3.41	2.31	0.29	0.12	0.24	1.156068	20.4708	8.27
0.55	0.78	0.45	1	2.31	0.61	0.14	0.21	1.137246	20.4699	7.87
0.34	0.63	0.2	3.19	3.84	0.05	0.19	0.31	1.200126	20.4446	7.2
0.91	0.65	0.85	1.88	3.63	0.35	0.13	0.2	1.13098	20.4298	12.66
0.76	0.83	0.57	2.97	5.81	1	0.17	0.28	1.18122	20.3955	8.06
0.94	0.9	0.45	1.44	7.78	0.55	0.17	0.26	1.168636	20.3948	8.78
0.79	0.4	0.23	5.59	7.56	0.88	0.18	0.33	1.21275	20.3925	7.06
0.67	0.5	0.93	7.13	1	0.32	0.15	0.29	1.187518	20.3811	5.95
0.85	0.68	0.5	7.13	2.09	0.58	0.19	0.34	1.219068	20.3762	6.17
0.73	0.73	0.95	6.25	7.78	0.5	0.11	0.24	1.156068	20.3662	7.4
0.61	0.83	0.88	4.06	2.53	0.32	0.1	0.21	1.137246	20.3591	6.39
0.94	0.78	0.4	6.47	1.88	0.85	0.14	0.28	1.18122	20.345	5.61
0.82	0.98	0.4	3.41	6.03	0.35	0.17	0.29	1.187518	20.3423	8.21
0.79	0.2	0.57	1.44	6.69	0.5	0.09	0.21	1.137246	20.3161	15.03
0.55	0.8	0.98	7.56	3.19	0.32	0.11	0.24	1.156068	20.309	7.02
0.25	0.9	0.33	3.84	5.38	0.17	0.18	0.29	1.187518	20.3007	9.85
0.73	0.65	0.83	6.91	1.88	0.97	0.12	0.25	1.16235	20.2847	6.28
0.16	0.98	0.83	3.41	2.97	0.05	0.14	0.23	1.14979	20.2797	7.99
0.1	0.88	0.35	7.56	4.94	0.91	0.17	0.29	1.187518	20.2439	7.41
0.76	1	0.48	5.38	1.66	0.17	0.2	0.34	1.219068	20.2192	5.41
0.04	0.73	0.8	6.03	3.41	0.91	0.14	0.24	1.156068	20.1884	7.39
0.28	0.23	0.73	7.56	7.13	0.85	0.14	0.28	1.18122	20.1864	7.86
0.85	0.35	0.95	4.94	7.34	0.79	0.11	0.23	1.14979	20.1718	7.99
0.55	0.85	0.7	5.16	8	0.82	0.19	0.31	1.200126	20.171	7.64
0.25	0.73	0.78	8	3.84	0.85	0.17	0.29	1.187518	20.1677	8.7
0.13	0.7	1	3.41	2.75	0.32	0.14	0.22	1.143516	20.1359	10.51
0.28	0.23	0.63	5.16	6.47	0.85	0.11	0.24	1.156068	20.1335	7.52
0.7	0.95	0.23	4.28	2.53	0.7	0.16	0.28	1.18122	20.1251	5.78
0.13	0.5	0.85	2.09	1.66	0.64	0.2	0.27	1.174926	20.1246	6.45
0.58	0.28	0.88	7.78	3.84	0.32	0.2	0.34	1.219068	20.1122	6.5
0.4	0.2	0.73	6.25	6.03	0.38	0.19	0.33	1.21275	20.1027	8.94

0.1	0.4	0.23	4.72	5.16	0.79	0.18	0.29	1.187518	20.1001	7.81
0.46	0.88	0.93	8	1.88	0.41	0.12	0.24	1.156068	20.0892	6.34
0.61	0.25	0.73	2.75	2.53	0.55	0.16	0.26	1.168636	20.0813	8.72
0.1	0.55	0.28	2.53	4.94	0.88	0.2	0.28	1.18122	20.0575	9.82
0.61	0.78	0.23	3.19	7.78	0.41	0.18	0.29	1.187518	20.02	10.24
0.7	0.95	0.48	7.34	2.75	0.26	0.2	0.31	1.200126	19.9875	5.92
0.16	0.5	0.45	4.72	1	0.35	0.11	0.2	1.13098	19.9776	6.86
0.19	0.35	0.65	5.16	1.88	0.97	0.17	0.27	1.174926	19.9756	8.84
0.79	0.55	0.3	1	5.16	0.11	0.18	0.24	1.156068	19.9213	9.31
0.82	0.53	0.53	7.56	3.41	0.76	0.17	0.29	1.187518	19.9178	6.45
0.31	0.2	0.68	2.09	2.31	0.58	0.14	0.23	1.14979	19.9074	10.92
0.58	0.68	0.3	7.78	6.47	0.38	0.09	0.2	1.13098	19.887	7.01
1	0.63	0.95	2.31	4.72	0.7	0.19	0.27	1.174926	19.8398	8.42
0.1	0.73	0.28	6.25	6.47	0.05	0.12	0.21	1.137246	19.8394	7.99
0.07	0.57	0.38	5.81	6.03	0.44	0.13	0.21	1.137246	19.7886	8.02
0.97	0.53	0.43	7.78	5.81	0.08	0.14	0.23	1.14979	19.781	6.44
0.43	0.9	0.23	2.53	5.59	0.73	0.2	0.28	1.18122	19.7807	11.22
0.37	0.78	0.45	6.47	4.28	0.91	0.14	0.23	1.14979	19.7737	7.84
0.91	1	0.3	3.63	4.28	0.23	0.16	0.26	1.168636	19.7689	
0.04	0.9	0.7	4.72	6.69	0.29	0.15	0.22	1.143516	19.7635	11.6
0.37	0.35	0.4	4.28	2.31	0.41	0.11	0.2	1.13098	19.7316	6.69
0.61	0.55	0.95	7.13	3.19	0.11	0.2	0.31	1.200126	19.7145	8.27
0.31	0.8	0.38	7.13	2.09	0.44	0.14	0.23	1.14979	19.682	6.11
0.13	0.88	0.98	3.84	2.97	0.97	0.15	0.21	1.137246	19.6746	7.16
0.07	0.7	0.3	4.94	1.66	0.85	0.2	0.28	1.18122	19.634	7.22
0.1	0.3	0.33	3.63	5.38	0.67	0.16	0.24	1.156068	19.6149	12.74
0.58	0.25	0.3	5.81	7.56	0.08	0.12	0.24	1.156068	19.5957	7.58
0.88	0.33	0.53	5.38	1.88	0.85	0.11	0.21	1.137246	19.5665	5.99
0.88	0.88	0.7	3.63	3.41	0.32	0.17	0.25	1.16235	19.5631	7.39
0.37	0.93	0.4	2.53	8	0.55	0.19	0.24	1.156068	19.5177	9.91
0.73	0.48	0.93	5.38	2.31	0.85	0.19	0.28	1.18122	19.5095	6.41
0.58	0.83	0.78	5.59	7.56	0.76	0.2	0.29	1.187518	19.4958	7.56
0.64	0.33	0.85	7.78	2.75	0.38	0.16	0.26	1.168636	19.4898	6.07
0.64	0.3	0.88	4.06	1.44	0.32	0.16	0.24	1.156068	19.475	6.01
0.58	0.93	0.83	4.06	1.88	0.05	0.14	0.21	1.137246	19.475	10.01
0.49	0.25	0.85	4.28	3.19	0.11	0.14	0.22	1.143516	19.4322	7.65
0.34	0.63	0.23	6.25	8	0.38	0.14	0.22	1.143516	19.4038	11.42
0.19	0.9	0.23	4.72	6.25	0.97	0.19	0.26	1.168636	19.3789	7.93
0.31	0.75	1	6.69	3.84	0.44	0.19	0.27	1.174926	19.378	6.57
0.88	0.55	0.93	2.09	1.22	0.61	0.16	0.21	1.137246	19.3746	
0.7	0.78	0.65	6.47	6.91	0.17	0.2	0.29	1.187518	19.3644	7.76
0.34	0.2	0.35	5.16	5.16	0.11	0.14	0.25	1.16235	19.3421	15.2
0.79	0.45	0.43	5.16	4.06	0.94	0.18	0.26	1.168636	19.3346	6.6
0.88	0.2	0.43	5.81	4.28	0.97	0.08	0.2	1.13098	19.3133	14.3
0.07	0.45	0.98	3.63	7.13	0.47	0.19	0.23	1.14979	19.2855	7.69
0.31	0.75	0.38	4.72	1.66	0.41	0.18	0.24	1.156068	19.2725	10.3
0.4	0.7	0.73	6.03	2.53	0.76	0.2	0.27	1.174926	19.2203	6.07
0.85	0.35	0.23	6.25	5.59	0.32	0.15	0.24	1.156068	19.119	11.7
0.19	0.23	0.68	6.03	1.22	0.35	0.2	0.28	1.18122	19.115	11.24

0.37	0.4	0.43	5.59	1.66	0.41	0.17	0.23	1.14979	19.0914	5.95
0.73	0.53	0.65	1.44	1.88	0.7	0.19	0.21	1.137246	19.0652	7.79
1	0.78	0.45	4.72	1.22	0.76	0.2	0.27	1.174926	18.9863	5.54
0.58	0.9	1	3.84	7.56	0.2	0.17	0.21	1.137246	18.9489	
0.85	0.55	0.25	2.97	6.25	0.26	0.18	0.23	1.14979	18.8866	9.49
0.19	0.28	0.2	7.13	5.38	0.55	0.17	0.25	1.16235	18.8798	8.36
0.28	0.83	0.3	6.91	5.16	0.41	0.18	0.23	1.14979	18.7844	9.63
0.64	0.28	0.3	8	6.03	0.35	0.13	0.21	1.137246	18.7626	8.95
0.94	0.35	0.63	5.81	7.56	0.38	0.19	0.25	1.16235	18.7525	10.89
0.07	0.25	0.75	6.03	4.94	0.79	0.18	0.23	1.14979	18.7465	7.25
0.91	0.9	0.2	2.97	5.81	0.5	0.2	0.25	1.16235	18.7382	10.48
0.13	0.38	0.65	7.13	8	0.44	0.19	0.23	1.14979	18.7006	8.09
0.79	0.57	0.93	5.38	2.09	0.82	0.2	0.25	1.16235	18.6965	6.65
0.88	0.33	0.65	7.56	6.03	0.29	0.17	0.23	1.14979	18.6314	6.26
0.76	0.45	0.93	4.06	6.91	0.91	0.2	0.23	1.14979	18.5729	7.48
0.94	0.45	0.43	4.06	2.53	0.2	0.18	0.21	1.137246	18.4942	9.11
0.49	0.45	0.25	5.59	1.66	0.76	0.17	0.2	1.13098	18.3546	10.67
1	0.53	0.88	6.69	4.06	0.44	0.18	0.21	1.137246	18.1688	5.98
0.64	0.75	0.57	8	5.81	0.61	0.2	0.22	1.143516	18.04	6.82
0.97	0.4	0.2	5.59	3.63	0.91	0.18	0.2	1.13098	17.8227	6.18

DATASET 2

AZO	ZNO	Cds	CIGS	CIGS+	MO	VAR	X	Band	Efficiency	Time
0.38	0.5	0.65	1	3.19	0.47	0.04	0.39	1.250718	26.8124	2.07
0.04	0.69	0.37	2.31	4.94	0.63	0.05	0.4	1.25706	26.4214	5.31
0.15	0.85	0.58	1.44	2.97	0.78	0.06	0.39	1.250718	26.2667	5.46
0.07	0.79	1	3.41	5.38	0.18	0.05	0.4	1.25706	26.1065	5.5
0.07	0.69	0.79	1.22	3.19	0.97	0.08	0.39	1.250718	26.003	5.58
0.92	0.46	0.51	6.03	3.19	0.8	0.09	0.39	1.250718	25.7489	5.73
0.38	0.89	0.91	1	2.97	0.72	0.09	0.4	1.25706	25.7458	5.74
0.1	0.75	0.79	4.94	6.47	0.86	0.05	0.4	1.25706	25.717	5.82
0.15	0.93	0.6	2.75	1.22	0.16	0.12	0.37	1.238046	25.667	5.83
0.1	0.83	0.6	3.19	1.44	0.69	0.05	0.38	1.24438	25.5812	5.89
0.72	0.44	0.91	2.09	3.84	0.66	0.05	0.38	1.24438	25.5513	5.95
0.24	0.65	0.32	3.63	6.91	0.27	0.04	0.38	1.24438	25.5311	5.96
0.52	0.75	0.95	3.41	7.34	0.33	0.06	0.4	1.25706	25.5098	6.06
0.27	0.75	0.32	4.94	2.09	0.18	0.04	0.39	1.250718	25.4696	6.09
0.21	0.69	0.7	1.44	5.59	0.33	0.06	0.35	1.22539	25.462	6.09
0.67	0.95	0.86	3.84	3.84	0.94	0.08	0.38	1.24438	25.4301	6.09
0.32	0.34	0.74	1.66	6.25	0.8	0.04	0.35	1.22539	25.4161	6.14
0.75	0.52	0.46	1	5.16	0.24	0.06	0.36	1.231716	25.4108	6.16
0.04	0.48	0.77	4.28	7.78	0.33	0.04	0.37	1.238046	25.3995	6.17
0.38	0.85	0.39	1.22	6.25	0.69	0.07	0.37	1.238046	25.3985	6.3
0.61	0.54	0.51	2.97	6.47	0.33	0.04	0.37	1.238046	25.3489	6.32
0.81	0.89	1	1.88	3.63	0.52	0.06	0.38	1.24438	25.3166	6.35
0.86	0.81	0.58	1.88	1	0.63	0.05	0.38	1.24438	25.2939	6.43
0.41	0.67	0.3	1.88	5.81	0.94	0.04	0.35	1.22539	25.2816	6.45
0.3	0.69	0.58	7.56	7.13	0.38	0.05	0.4	1.25706	25.2463	6.45

0.18	0.83	0.98	2.75	3.41	0.75	0.07	0.38	1.24438	25.2357	6.48
0.69	0.46	0.84	1.88	6.91	0.63	0.08	0.39	1.250718	25.2307	6.52
0.24	0.75	0.79	3.84	4.94	0.16	0.05	0.37	1.238046	25.2037	6.53
0.44	0.89	0.37	1.22	5.16	0.75	0.04	0.33	1.21275	25.1984	6.6
0.32	0.48	0.58	2.53	2.09	0.89	0.04	0.35	1.22539	25.1611	6.61
0.13	0.38	1	6.03	3.19	0.58	0.04	0.38	1.24438	25.0952	6.61
0.92	0.91	0.48	2.97	4.06	0.3	0.06	0.39	1.250718	25.0477	6.62
0.18	0.56	0.72	1.88	6.91	0.49	0.05	0.33	1.21275	25.0433	6.62
0.89	0.4	0.86	1.44	4.06	0.18	0.06	0.36	1.231716	25.039	6.67
0.18	0.67	0.95	6.03	2.75	0.8	0.05	0.38	1.24438	25.0136	6.69
0.64	0.79	0.79	3.41	7.34	0.66	0.06	0.38	1.24438	24.9818	6.7
0.81	0.93	0.55	2.97	7.78	0.72	0.04	0.36	1.231716	24.9738	6.73
0.69	0.5	0.65	1.22	6.25	1	0.08	0.36	1.231716	24.926	6.75
0.69	0.5	0.25	2.31	5.16	0.63	0.05	0.37	1.238046	24.924	6.84
0.3	0.73	0.32	3.63	6.69	0.24	0.05	0.36	1.231716	24.8814	6.84
0.44	0.56	0.91	1.22	2.53	0.69	0.12	0.4	1.25706	24.858	6.85
0.15	0.67	0.32	6.91	7.78	0.47	0.07	0.4	1.25706	24.8373	6.85
0.13	0.58	0.51	2.31	2.75	0.52	0.06	0.34	1.219068	24.7791	6.86
0.64	0.48	0.77	2.53	4.72	0.18	0.08	0.38	1.24438	24.7706	6.9
0.1	0.48	0.81	2.53	7.13	0.24	0.08	0.36	1.231716	24.7394	6.91
0.15	0.4	0.53	5.38	5.59	0.75	0.06	0.38	1.24438	24.7261	6.91
0.69	0.5	0.84	4.28	7.34	0.66	0.06	0.38	1.24438	24.7232	6.93
0.35	0.71	0.32	1.88	8	0.75	0.07	0.35	1.22539	24.723	6.96
0.04	0.6	0.3	6.69	4.28	0.38	0.05	0.37	1.238046	24.7024	6.96
0.67	0.6	0.98	2.75	1	0.69	0.08	0.39	1.250718	24.6955	6.98
0.92	0.54	0.91	4.06	7.34	0.24	0.04	0.36	1.231716	24.6784	6.98
0.44	0.44	0.46	3.41	1.44	0.33	0.04	0.35	1.22539	24.6766	7.06
0.21	0.46	0.6	2.31	3.63	0.47	0.04	0.32	1.206436	24.6685	7.09
0.3	0.58	0.41	2.09	7.13	0.13	0.1	0.38	1.24438	24.6573	7.09
0.55	0.4	0.32	1	7.13	0.66	0.1	0.38	1.24438	24.5607	7.1
0.38	0.87	0.37	4.94	7.56	0.75	0.07	0.38	1.24438	24.5454	7.12
0.24	0.67	0.91	8	3.84	0.94	0.06	0.38	1.24438	24.5383	7.15
0.81	0.83	0.58	3.84	7.13	0.13	0.06	0.37	1.238046	24.5339	7.17
0.81	0.38	0.98	4.28	2.75	0.13	0.05	0.37	1.238046	24.5284	7.22
0.15	0.75	0.95	1.22	4.28	0.3	0.12	0.37	1.238046	24.521	7.23
0.72	0.93	0.51	1.44	1.88	0.24	0.08	0.36	1.231716	24.5161	7.24
0.15	0.85	0.7	3.63	7.13	0.24	0.1	0.39	1.250718	24.5131	7.24
0.24	0.48	0.51	1.44	2.75	0.13	0.1	0.36	1.231716	24.4879	7.25
0.61	0.95	0.51	2.75	2.97	0.69	0.05	0.34	1.219068	24.476	7.28
0.52	0.91	0.39	4.72	5.81	0.94	0.08	0.39	1.250718	24.4519	7.28
0.86	0.71	0.39	6.91	7.34	0.44	0.04	0.37	1.238046	24.4475	7.29
0.44	0.38	0.25	5.16	1.44	0.86	0.06	0.39	1.250718	24.4256	7.32
0.13	0.58	0.39	7.13	5.38	0.72	0.09	0.4	1.25706	24.4154	7.32
0.47	0.46	0.27	1.44	5.81	0.75	0.1	0.38	1.24438	24.392	7.33
0.64	0.36	0.81	6.47	1	0.52	0.05	0.38	1.24438	24.3896	7.33
0.95	0.52	0.44	2.97	5.59	0.18	0.08	0.38	1.24438	24.3606	7.34
0.04	0.73	0.53	7.34	7.13	0.1	0.07	0.37	1.238046	24.3602	7.34
0.21	0.67	0.7	1.88	7.78	0.8	0.08	0.33	1.21275	24.3549	7.37
0.92	0.75	0.27	5.38	1.88	0.61	0.05	0.38	1.24438	24.3488	7.41

0.95	0.38	0.53	4.28	2.31	0.78	0.07	0.39	1.250718	24.3477	7.41
0.41	0.48	0.98	5.81	1.22	0.66	0.05	0.36	1.231716	24.3449	7.44
0.27	0.48	0.74	1.66	3.63	0.83	0.06	0.31	1.200126	24.3266	7.46
0.21	0.54	0.55	1	2.31	0.18	0.09	0.33	1.21275	24.3264	7.48
0.86	0.4	0.27	5.16	6.03	0.13	0.07	0.4	1.25706	24.3114	7.48
0.92	0.65	0.84	3.19	2.97	0.63	0.09	0.39	1.250718	24.3079	7.48
0.58	0.38	0.98	6.47	3.41	0.35	0.04	0.36	1.231716	24.3078	7.51
0.55	0.83	0.34	3.63	3.19	0.58	0.04	0.33	1.21275	24.3003	7.55
0.75	0.85	0.58	2.53	2.97	0.41	0.05	0.33	1.21275	24.2781	7.59
0.24	0.79	0.98	3.41	1.44	0.21	0.06	0.34	1.219068	24.2698	7.61
0.95	0.75	0.7	8	1.66	0.49	0.06	0.39	1.250718	24.2485	7.63
0.44	0.36	0.41	4.94	7.13	1	0.08	0.39	1.250718	24.2479	7.65
0.47	0.89	0.72	2.09	6.69	0.97	0.07	0.33	1.21275	24.2479	7.65
0.89	0.67	0.93	6.47	4.06	0.21	0.04	0.36	1.231716	24.2391	7.66
0.41	0.71	0.34	6.91	4.06	0.16	0.07	0.38	1.24438	24.2388	7.7
0.1	0.38	0.77	7.56	1.22	0.52	0.06	0.37	1.238046	24.2256	7.72
0.15	0.95	0.79	3.19	4.72	0.13	0.12	0.4	1.25706	24.2219	7.73
0.89	0.52	0.93	2.75	2.53	1	0.1	0.39	1.250718	24.2069	7.73
0.27	0.44	0.65	6.03	3.19	0.1	0.06	0.36	1.231716	24.2006	7.82
0.38	0.83	0.37	1.66	5.38	1	0.08	0.33	1.21275	24.1632	7.86
0.41	0.91	0.51	6.25	6.47	0.52	0.07	0.37	1.238046	24.1405	7.87
0.18	0.83	0.3	4.06	1.66	0.3	0.1	0.39	1.250718	24.134	7.92
0.27	0.3	0.74	3.63	7.34	0.89	0.04	0.33	1.21275	24.1166	7.93
0.13	0.3	0.91	5.38	4.72	0.83	0.07	0.37	1.238046	24.1127	7.94
0.47	0.48	0.77	8	6.69	0.47	0.08	0.39	1.250718	24.1038	7.94
0.89	0.79	0.98	4.28	3.84	0.3	0.06	0.36	1.231716	24.0992	7.95
0.41	0.85	0.86	4.06	3.84	0.89	0.04	0.32	1.206436	24.0991	7.97
0.47	0.93	0.44	1	5.59	0.44	0.14	0.39	1.250718	24.0985	7.98
0.78	0.6	0.48	1.44	5.59	0.18	0.12	0.38	1.24438	24.0822	8.04
0.89	0.87	0.88	5.38	3.63	0.41	0.07	0.38	1.24438	24.0764	8.08
0.47	0.42	0.53	3.84	1	0.27	0.05	0.34	1.219068	24.0625	8.09
0.84	0.71	0.65	6.69	2.75	0.72	0.05	0.36	1.231716	24.0598	8.11
0.24	0.4	0.91	1.22	4.72	0.78	0.15	0.39	1.250718	24.0521	8.14
0.32	0.34	0.98	4.72	6.47	0.38	0.07	0.36	1.231716	24.0389	8.18
0.44	0.91	0.91	3.19	1.44	0.97	0.1	0.38	1.24438	24.0325	8.23
0.41	0.3	0.39	1.66	4.06	0.41	0.06	0.33	1.21275	24.0285	8.25
0.69	0.95	0.55	6.91	6.69	0.49	0.08	0.39	1.250718	24.0247	8.28
0.3	0.81	0.44	1.22	5.59	0.94	0.14	0.38	1.24438	24.0165	8.3
0.35	0.34	0.44	1.22	4.72	0.63	0.13	0.38	1.24438	24.0122	8.3
0.67	0.32	0.72	1.88	4.94	0.18	0.13	0.4	1.25706	24.0017	8.3
0.61	0.38	0.67	1.66	6.91	0.97	0.08	0.33	1.21275	23.9902	8.37
0.04	0.69	0.3	6.91	2.31	0.94	0.1	0.39	1.250718	23.9862	8.39
0.13	0.79	0.84	1	4.28	0.16	0.13	0.35	1.22539	23.9862	8.39
0.78	0.46	0.77	1.66	4.94	0.24	0.05	0.3	1.19382	23.9858	8.4
0.04	0.42	0.32	4.06	3.41	0.27	0.07	0.35	1.22539	23.9789	8.47
0.32	0.89	0.58	6.91	7.34	1	0.05	0.34	1.219068	23.954	8.47
0.75	0.38	0.88	5.16	3.63	0.89	0.06	0.36	1.231716	23.9524	8.48
0.04	0.89	0.67	6.69	1.88	0.44	0.07	0.35	1.22539	23.9247	8.51
0.18	0.36	0.72	8	3.41	0.33	0.07	0.37	1.238046	23.924	8.53

0.89	0.32	0.6	2.53	5.81	0.75	0.08	0.36	1.231716	23.9233	8.55
0.38	0.6	0.39	6.25	3.19	0.92	0.09	0.38	1.24438	23.8985	8.56
0.3	0.52	0.3	2.75	1.22	0.58	0.11	0.38	1.24438	23.8873	8.57
0.86	0.54	0.25	5.59	6.25	0.75	0.08	0.39	1.250718	23.8845	8.58
0.44	0.52	0.39	2.75	4.28	0.27	0.08	0.34	1.219068	23.88	8.61
0.64	0.83	0.81	4.72	6.69	0.66	0.11	0.4	1.25706	23.8539	8.61
0.84	0.71	0.77	4.28	8	0.72	0.11	0.4	1.25706	23.8485	8.64
0.18	0.54	0.72	5.59	6.03	0.3	0.12	0.4	1.25706	23.8442	8.67
0.21	0.32	0.81	5.59	2.97	0.72	0.06	0.35	1.22539	23.8406	8.69
0.67	0.6	1	5.81	5.16	1	0.05	0.34	1.219068	23.8348	8.69
0.72	0.73	0.46	5.81	2.53	0.58	0.05	0.34	1.219068	23.8171	8.7
0.67	0.44	0.65	1.66	3.63	0.86	0.06	0.3	1.19382	23.7782	8.7
0.47	0.56	0.41	2.09	4.94	0.8	0.12	0.37	1.238046	23.7764	8.73
0.35	0.34	0.34	2.09	3.63	0.66	0.11	0.37	1.238046	23.7738	8.74
0.18	0.67	0.84	6.03	5.59	0.94	0.12	0.4	1.25706	23.7676	8.74
0.07	0.65	0.7	6.47	6.91	0.49	0.06	0.33	1.21275	23.7625	8.77
0.72	0.93	0.6	3.84	2.53	0.24	0.1	0.38	1.24438	23.7539	8.79
0.32	0.56	0.25	7.34	4.94	0.83	0.05	0.34	1.219068	23.7458	8.83
0.27	0.44	1	4.72	7.56	0.27	0.1	0.37	1.238046	23.7446	8.89
0.78	0.34	0.58	1.66	2.53	0.61	0.14	0.4	1.25706	23.7209	8.89
0.13	0.67	0.37	1.66	1	0.89	0.11	0.35	1.22539	23.7037	8.92
0.64	0.46	0.41	4.72	6.03	0.38	0.04	0.32	1.206436	23.6965	8.93
0.41	0.44	0.37	4.94	6.47	0.75	0.11	0.39	1.250718	23.6811	8.93
0.55	0.81	0.88	1.88	7.78	0.52	0.07	0.3	1.19382	23.6672	8.95
0.78	0.38	0.53	3.19	4.72	0.1	0.07	0.34	1.219068	23.6414	8.97
0.3	0.93	0.77	1.22	5.38	0.21	0.1	0.31	1.200126	23.6329	8.97
0.72	0.93	0.95	3.19	2.97	0.49	0.06	0.32	1.206436	23.6301	8.97
0.07	0.79	0.74	2.97	5.81	0.3	0.1	0.31	1.200126	23.6254	9.01
0.1	0.73	0.44	2.53	4.72	0.75	0.07	0.3	1.19382	23.6254	9
0.07	0.65	0.81	7.78	7.56	0.38	0.07	0.34	1.219068	23.6229	9.03
0.84	0.32	0.41	5.59	6.03	1	0.08	0.38	1.24438	23.6161	9.05
0.38	0.52	0.46	6.47	2.75	0.13	0.11	0.39	1.250718	23.6148	9.13
0.47	0.42	0.81	3.19	7.34	0.49	0.13	0.39	1.250718	23.6055	9.17
0.27	0.6	0.39	3.63	3.84	0.1	0.06	0.31	1.200126	23.6029	9.18
0.92	0.52	0.3	1.88	2.09	0.44	0.11	0.37	1.238046	23.5683	9.18
0.86	0.71	0.37	6.69	7.78	0.33	0.08	0.37	1.238046	23.5575	9.2
0.24	0.65	0.79	3.19	1	0.27	0.11	0.36	1.231716	23.5366	9.21
0.69	0.32	0.48	7.78	3.63	0.89	0.09	0.39	1.250718	23.4997	9.22
0.52	0.3	0.48	3.84	1	0.92	0.1	0.38	1.24438	23.4955	9.23
0.35	0.48	0.84	2.75	1.22	0.69	0.14	0.39	1.250718	23.4827	9.27
0.84	0.95	0.55	7.56	2.09	0.83	0.05	0.34	1.219068	23.4676	9.34
0.75	0.3	0.6	1.44	6.69	0.52	0.07	0.31	1.200126	23.4507	9.35
0.64	0.36	0.53	6.69	2.09	0.18	0.11	0.4	1.25706	23.4498	9.37
0.78	0.89	0.67	5.59	6.69	0.78	0.1	0.38	1.24438	23.4472	9.5
0.38	0.56	0.25	2.31	1.66	0.49	0.08	0.32	1.206436	23.4413	9.54
0.15	0.3	0.7	1.44	6.91	0.27	0.14	0.36	1.231716	23.4394	9.61
0.92	0.81	0.51	2.97	1	0.63	0.06	0.32	1.206436	23.4393	9.65
0.92	0.6	0.44	1.22	1.44	0.72	0.12	0.36	1.231716	23.429	9.69
0.52	0.81	0.48	2.97	5.16	0.49	0.14	0.39	1.250718	23.3998	9.73

0.41	0.91	0.37	6.69	1.44	0.49	0.05	0.32	1.206436	23.3973	9.73
0.86	0.46	0.41	8	4.72	0.94	0.06	0.35	1.22539	23.3961	9.75
0.44	0.34	0.46	6.25	2.53	0.89	0.06	0.34	1.219068	23.3793	9.79
0.35	0.89	0.72	2.31	6.91	0.92	0.08	0.3	1.19382	23.3774	9.8
0.41	0.56	0.95	3.41	6.25	0.8	0.09	0.33	1.21275	23.3682	9.83
0.21	0.85	0.93	3.63	1	0.69	0.12	0.37	1.238046	23.3649	9.86
0.61	0.73	0.79	2.53	6.25	0.97	0.08	0.31	1.200126	23.3422	9.87
0.58	0.34	0.88	2.31	7.56	0.61	0.14	0.38	1.24438	23.34	9.88
0.44	0.44	0.37	7.13	1.22	0.58	0.12	0.4	1.25706	23.3345	9.88
0.58	0.69	0.3	5.59	2.75	0.3	0.1	0.37	1.238046	23.3314	9.92
0.67	0.77	0.55	4.94	1.44	0.21	0.12	0.39	1.250718	23.3273	9.94
0.04	0.42	0.7	5.16	1.44	0.69	0.07	0.32	1.206436	23.3168	10.08
0.64	0.77	1	3.84	6.91	0.83	0.09	0.34	1.219068	23.2951	10.17
0.32	0.81	0.6	7.34	5.38	0.24	0.13	0.4	1.25706	23.2881	10.2
0.58	0.95	0.32	4.06	2.31	0.89	0.11	0.37	1.238046	23.2841	10.23
0.24	0.95	0.65	7.56	2.31	0.58	0.12	0.39	1.250718	23.2831	10.36
0.32	0.48	0.7	4.06	7.56	0.89	0.07	0.31	1.200126	23.282	10.37
0.81	0.89	0.53	1	5.59	0.78	0.12	0.33	1.21275	23.2798	10.4
0.13	0.54	0.88	2.31	1.22	0.78	0.11	0.33	1.21275	23.2786	10.45
0.49	0.63	0.63	4.5	4.5	0.55	0.1	0.35	1.22539	23.273	10.5
0.04	0.5	0.55	1	7.34	0.61	0.13	0.31	1.200126	23.263	10.52
0.89	0.52	0.81	6.47	4.28	0.35	0.12	0.4	1.25706	23.2217	10.53
0.47	0.44	0.77	6.03	3.84	0.61	0.05	0.31	1.200126	23.2065	10.58
0.07	0.73	0.95	7.13	6.91	0.66	0.08	0.33	1.21275	23.2042	10.63
0.67	0.69	1	1.66	4.06	0.27	0.14	0.36	1.231716	23.1972	10.64
0.61	0.69	1	6.69	7.34	0.61	0.11	0.38	1.24438	23.1959	10.73
0.95	0.83	0.55	3.84	7.56	0.41	0.12	0.38	1.24438	23.1919	10.81
0.64	0.77	0.41	6.25	7.78	0.41	0.05	0.31	1.200126	23.1691	10.84
0.07	0.44	0.74	6.03	8	0.47	0.13	0.38	1.24438	23.1618	10.86
0.52	0.77	0.48	1	2.31	0.63	0.11	0.31	1.200126	23.1616	10.9
0.52	0.69	0.84	6.91	4.06	0.3	0.07	0.33	1.21275	23.1583	10.95
0.75	0.6	0.46	5.81	8	0.83	0.08	0.34	1.219068	23.1493	10.96
0.35	0.48	0.25	5.16	2.09	0.27	0.1	0.36	1.231716	23.1424	11.08
0.21	0.91	0.67	7.34	6.47	0.49	0.05	0.3	1.19382	23.1309	11.34
0.21	0.79	0.48	7.34	4.06	0.86	0.14	0.4	1.25706	23.1264	11.37
0.21	0.65	0.77	7.56	3.41	0.92	0.07	0.32	1.206436	23.1185	11.37
0.69	0.44	0.81	7.78	3.41	0.16	0.05	0.32	1.206436	23.1016	11.38
0.61	0.42	0.88	7.34	3.63	0.1	0.11	0.38	1.24438	23.1002	11.4
0.92	0.6	0.55	2.53	2.09	0.61	0.13	0.37	1.238046	23.0885	11.42
0.38	0.87	0.58	7.34	2.09	0.13	0.11	0.37	1.238046	23.0821	11.45
0.75	0.85	0.34	7.78	4.28	0.33	0.04	0.31	1.200126	23.0772	11.46
0.86	0.58	0.88	7.34	8	0.21	0.08	0.35	1.22539	23.0714	11.47
0.55	0.91	0.79	2.75	6.47	0.21	0.13	0.36	1.231716	23.0689	11.52
0.95	0.56	0.95	2.09	6.69	0.16	0.09	0.31	1.200126	23.0619	11.59
0.52	0.83	0.44	5.81	1.66	0.61	0.06	0.31	1.200126	23.052	11.83
0.78	0.71	0.7	8	6.69	0.92	0.1	0.37	1.238046	23.0474	11.96
0.61	0.65	0.86	2.75	5.81	0.18	0.1	0.32	1.206436	23.0249	12.02
0.72	0.65	0.86	5.38	5.16	1	0.13	0.39	1.250718	23.0236	12.03
0.21	0.36	0.58	3.41	2.31	0.33	0.09	0.32	1.206436	23.0209	12.09

0.58	0.54	0.91	2.09	4.94	0.94	0.12	0.33	1.21275	22.9933	12.14
0.41	0.3	0.93	4.94	6.69	0.21	0.08	0.33	1.21275	22.9903	12.38
0.27	0.52	0.79	3.19	6.47	0.52	0.14	0.36	1.231716	22.9724	12.39
0.81	0.58	0.41	2.97	3.41	0.16	0.07	0.3	1.19382	22.9438	12.46
0.64	0.91	0.81	7.78	4.28	0.47	0.06	0.32	1.206436	22.9368	12.52
0.95	0.36	0.58	2.31	7.13	0.66	0.12	0.35	1.22539	22.9344	12.61
0.81	0.71	0.53	3.41	2.97	0.8	0.07	0.3	1.19382	22.9313	12.68
0.15	0.54	0.6	2.31	6.25	0.38	0.14	0.34	1.219068	22.9307	12.88
0.21	0.87	0.72	5.81	4.28	1	0.12	0.36	1.231716	22.9252	12.95
0.78	0.4	0.32	5.38	8	0.41	0.07	0.33	1.21275	22.9115	13.12
0.55	0.73	0.86	6.25	4.72	0.83	0.11	0.36	1.231716	22.8978	13.18
0.58	0.81	0.88	4.06	2.53	0.35	0.08	0.31	1.200126	22.8886	13.25
0.78	0.58	0.55	7.13	1.22	0.3	0.11	0.37	1.238046	22.872	13.4
0.32	0.93	0.53	7.13	4.06	0.92	0.06	0.3	1.19382	22.8485	13.64
0.15	0.93	0.84	3.41	2.97	0.1	0.11	0.32	1.206436	22.8244	13.98
0.72	0.77	0.51	7.34	5.38	0.27	0.13	0.39	1.250718	22.8187	14
0.67	0.36	0.67	2.09	1.66	0.1	0.14	0.36	1.231716	22.8112	14.03
0.95	0.52	0.72	1.66	1.88	1	0.12	0.33	1.21275	22.8003	14.25
0.84	0.32	0.65	6.25	7.78	0.94	0.07	0.33	1.21275	22.7812	14.36
0.64	0.91	0.91	6.91	5.38	0.44	0.08	0.33	1.21275	22.777	15.26
0.52	0.32	0.81	8	3.41	0.66	0.05	0.31	1.200126	22.768	15.9
0.89	0.87	0.48	1.44	7.78	0.58	0.13	0.33	1.21275	22.7667	15.96
0.1	0.93	0.65	6.47	3.19	0.35	0.11	0.34	1.219068	22.7416	15.97
0.86	0.67	0.86	1.88	3.63	0.38	0.1	0.3	1.19382	22.7324	16.03
0.35	0.79	0.84	4.28	2.97	0.72	0.15	0.38	1.24438	22.7311	16.34
0.15	0.54	0.48	4.72	1	0.38	0.08	0.3	1.19382	22.7288	17.44
0.24	0.4	0.67	6.47	6.03	0.69	0.14	0.38	1.24438	22.7272	17.5
0.84	0.5	0.3	7.78	4.72	0.8	0.07	0.33	1.21275	22.7156	17.85
0.47	0.95	0.77	5.16	8	0.18	0.09	0.32	1.206436	22.714	18.76
0.72	0.81	0.25	4.28	1.44	0.83	0.09	0.33	1.21275	22.6937	18.82
0.75	0.77	0.74	7.56	6.25	0.97	0.09	0.34	1.219068	22.6932	24.78
0.52	0.36	0.53	6.91	2.31	0.13	0.12	0.37	1.238046	22.6719	7.24
0.75	0.58	0.34	1	5.16	0.16	0.13	0.32	1.206436	22.6622	7.98
0.69	0.73	0.95	6.25	7.78	0.52	0.08	0.32	1.206436	22.6554	7.69
0.32	0.65	0.25	3.19	3.84	0.1	0.14	0.36	1.231716	22.6527	17.93
0.27	0.32	0.3	5.81	6.03	0.61	0.13	0.38	1.24438	22.628	9.66
0.35	0.42	0.44	4.28	2.31	0.44	0.08	0.3	1.19382	22.6185	14.55
0.3	0.3	0.7	2.09	2.31	0.61	0.11	0.31	1.200126	22.6113	7.29
0.1	0.73	0.32	6.25	6.47	0.1	0.09	0.31	1.200126	22.6112	7.32
0.13	0.71	1	3.41	2.75	0.35	0.11	0.31	1.200126	22.6106	12.22
0.27	0.32	0.65	5.16	6.47	0.86	0.09	0.32	1.206436	22.5888	7.53
0.58	0.95	0.86	7.34	4.94	0.69	0.13	0.38	1.24438	22.5867	8.63
0.24	0.87	0.37	3.84	5.38	0.21	0.13	0.34	1.219068	22.5683	8.21
0.69	0.67	0.84	6.91	1.88	0.97	0.09	0.33	1.21275	22.568	13.67
0.58	0.34	0.74	2.75	2.53	0.58	0.12	0.33	1.21275	22.5577	14.23
0.78	0.93	0.44	3.41	6.03	0.38	0.13	0.35	1.22539	22.5495	9.49
0.72	0.81	0.6	2.97	5.81	1	0.13	0.34	1.219068	22.5469	6.81
0.3	0.75	0.6	7.78	2.75	0.1	0.11	0.34	1.219068	22.5456	14.65
0.07	0.6	0.41	5.81	6.03	0.47	0.1	0.31	1.200126	22.5033	8.26

0.1	0.58	0.32	2.53	4.94	0.89	0.15	0.34	1.219068	22.4679	6.96
0.04	0.73	0.81	6.03	3.41	0.92	0.11	0.32	1.206436	22.4673	6.82
0.13	0.54	0.86	2.09	1.66	0.66	0.15	0.33	1.21275	22.4542	9.92
0.58	0.4	0.39	4.94	5.16	0.21	0.15	0.38	1.24438	22.4005	17.16
0.55	0.69	0.34	7.78	6.47	0.41	0.07	0.3	1.19382	22.3924	10.45
0.52	0.79	0.98	7.56	3.19	0.35	0.09	0.32	1.206436	22.38	6.24
0.44	0.85	0.93	8	1.88	0.44	0.09	0.32	1.206436	22.3689	6.81
0.52	0.83	0.72	5.16	8	0.83	0.14	0.36	1.231716	22.324	8.48
0.27	0.32	0.74	7.56	7.13	0.86	0.11	0.34	1.219068	22.3203	8.16
0.1	0.38	0.37	3.63	5.38	0.69	0.12	0.32	1.206436	22.3198	8.33
0.44	0.42	0.91	5.38	5.81	0.52	0.15	0.37	1.238046	22.3159	11.48
0.81	0.42	0.95	4.94	7.34	0.8	0.09	0.31	1.200126	22.31133	5.89
0.95	0.83	0.93	4.94	5.59	0.83	0.12	0.35	1.22539	22.3063	7.37
0.1	0.46	0.27	4.72	5.16	0.8	0.13	0.34	1.219068	22.2724	9.8
0.67	0.91	0.27	4.28	2.53	0.72	0.12	0.34	1.219068	22.2526	7.93
0.64	0.54	0.93	7.13	1	0.35	0.12	0.35	1.22539	22.2492	6.57
0.55	0.34	0.34	5.81	7.56	0.13	0.09	0.32	1.206436	22.2443	9.14
0.89	0.77	0.44	6.47	1.88	0.86	0.11	0.34	1.219068	22.2399	8.02
0.35	0.77	0.48	6.47	4.28	0.92	0.11	0.32	1.206436	22.2348	6.04
0.35	0.89	0.44	2.53	8	0.58	0.14	0.32	1.206436	22.2241	6.99
0.04	0.87	0.72	4.72	6.69	0.33	0.12	0.31	1.200126	22.2141	6.73
0.86	0.67	0.74	6.69	6.25	0.58	0.13	0.36	1.231716	22.2054	7.77
0.07	0.5	0.98	3.63	7.13	0.49	0.14	0.32	1.206436	22.1873	12.57
0.95	0.65	0.95	2.31	4.72	0.72	0.14	0.33	1.21275	22.1814	5.59
0.75	0.46	0.27	5.59	7.56	0.89	0.13	0.36	1.231716	22.1779	6.24
0.55	0.89	0.84	4.06	1.88	0.1	0.11	0.31	1.200126	22.1672	7.67
0.1	0.85	0.39	7.56	4.94	0.92	0.13	0.34	1.219068	22.1671	7.51
0.13	0.85	0.98	3.84	2.97	0.97	0.12	0.3	1.19382	22.1649	14.27
0.41	0.87	0.27	2.53	5.59	0.75	0.15	0.34	1.219068	22.1518	11.97
0.81	0.69	0.53	7.13	2.09	0.61	0.14	0.37	1.238046	22.1513	6.1
0.32	0.3	0.39	5.16	5.16	0.16	0.11	0.33	1.21275	22.151	6.74
0.84	0.4	0.55	5.38	1.88	0.86	0.09	0.31	1.200126	22.143	6.28
0.18	0.42	0.67	5.16	1.88	0.97	0.13	0.33	1.21275	22.1325	6.53
0.78	0.79	0.65	6.69	5.38	0.63	0.15	0.38	1.24438	22.1291	6.07
0.38	0.3	0.74	6.25	6.03	0.41	0.14	0.36	1.231716	22.1057	9.1
0.86	0.95	0.34	3.63	4.28	0.27	0.12	0.33	1.21275	22.1012	6.14
0.47	0.34	0.86	4.28	3.19	0.16	0.11	0.31	1.200126	22.0781	11.96
0.84	0.3	0.46	5.81	4.28	0.97	0.07	0.3	1.19382	22.0713	8.37
0.24	0.73	0.79	8	3.84	0.86	0.13	0.34	1.219068	22.0595	5.94
0.72	0.95	0.51	5.38	1.66	0.21	0.15	0.37	1.238046	22.046	8.11
0.84	0.58	0.93	2.09	1.22	0.63	0.12	0.3	1.19382	22.0341	10.89
0.84	0.85	0.72	3.63	3.41	0.35	0.13	0.33	1.21275	22.0333	7.51
0.61	0.38	0.88	4.06	1.44	0.35	0.12	0.32	1.206436	22.0289	7.39
0.78	0.56	0.55	7.56	3.41	0.78	0.13	0.35	1.22539	21.9907	5.95
0.69	0.56	0.67	1.44	1.88	0.72	0.14	0.3	1.19382	21.9883	6.98
0.3	0.79	0.41	7.13	2.09	0.47	0.11	0.31	1.200126	21.9598	10.99
0.32	0.65	0.27	6.25	8	0.41	0.11	0.31	1.200126	21.9446	7.98
0.07	0.71	0.34	4.94	1.66	0.86	0.15	0.34	1.219068	21.941	10.97
0.55	0.36	0.88	7.78	3.84	0.35	0.15	0.37	1.238046	21.9276	6.32

0.3	0.75	0.41	4.72	1.66	0.44	0.13	0.32	1.206436	21.9187	12.25
0.58	0.77	0.27	3.19	7.78	0.44	0.14	0.34	1.219068	21.8996	10.57
0.18	0.87	0.27	4.72	6.25	0.97	0.14	0.33	1.21275	21.8882	7.13
0.55	0.81	0.79	5.59	7.56	0.78	0.15	0.35	1.22539	21.8184	8.64
0.61	0.4	0.86	7.78	2.75	0.41	0.12	0.33	1.21275	21.8025	9.42
0.69	0.52	0.93	5.38	2.31	0.86	0.14	0.34	1.219068	21.792	16.15
0.55	0.87	1	3.84	7.56	0.24	0.13	0.31	1.200126	21.778	15.03
0.35	0.46	0.46	5.59	1.66	0.44	0.13	0.32	1.206436	21.7708	9.21
0.81	0.58	0.3	2.97	6.25	0.3	0.14	0.32	1.206436	21.685	10.5
0.3	0.75	1	6.69	3.84	0.47	0.14	0.33	1.21275	21.6664	5.79
0.58	0.58	0.95	7.13	3.19	0.16	0.15	0.35	1.22539	21.6451	9.03
0.67	0.77	0.67	6.47	6.91	0.21	0.15	0.35	1.22539	21.6446	6.81
0.75	0.5	0.46	5.16	4.06	0.94	0.14	0.33	1.21275	21.6189	12.69
0.18	0.32	0.7	6.03	1.22	0.38	0.15	0.34	1.219068	21.5917	7.5
0.07	0.34	0.77	6.03	4.94	0.8	0.13	0.31	1.200126	21.5905	7.08
0.18	0.36	0.25	7.13	5.38	0.58	0.13	0.33	1.21275	21.5853	6.67
0.13	0.44	0.67	7.13	8	0.47	0.14	0.32	1.206436	21.5578	11.78
0.92	0.56	0.46	7.78	5.81	0.13	0.11	0.31	1.200126	21.5568	6.07
0.67	0.91	0.51	7.34	2.75	0.3	0.15	0.35	1.22539	21.5237	5.96
0.38	0.71	0.74	6.03	2.53	0.78	0.15	0.33	1.21275	21.501	6.62
0.27	0.81	0.34	6.91	5.16	0.44	0.14	0.32	1.206436	21.4829	9.86
0.81	0.42	0.27	6.25	5.59	0.35	0.12	0.32	1.206436	21.4754	8.64
0.86	0.87	0.25	2.97	5.81	0.52	0.15	0.33	1.21275	21.4505	8.84
0.61	0.36	0.34	8	6.03	0.38	0.1	0.3	1.19382	21.4412	6.94
0.89	0.42	0.65	5.81	7.56	0.41	0.14	0.33	1.21275	21.4284	6.1
0.75	0.6	0.93	5.38	2.09	0.83	0.15	0.33	1.21275	21.3258	8.68
0.95	0.77	0.48	4.72	1.22	0.78	0.15	0.33	1.21275	21.254	9.16
0.47	0.5	0.3	5.59	1.66	0.78	0.13	0.3	1.19382	21.19	6.42
0.72	0.5	0.93	4.06	6.91	0.92	0.15	0.31	1.200126	21.189	10.21
0.89	0.5	0.46	4.06	2.53	0.24	0.14	0.3	1.19382	21.1207	6.71
0.84	0.4	0.67	7.56	6.03	0.33	0.13	0.31	1.200126	21.0913	8.83
0.61	0.75	0.6	8	5.81	0.63	0.15	0.31	1.200126	20.8189	5.88
0.95	0.56	0.88	6.69	4.06	0.47	0.14	0.3	1.19382	20.7199	8.49
0.92	0.46	0.25	5.59	3.63	0.92	0.14	0.3	1.19382	20.6792	5.43

DATASET 3

AZO	ZNO	Cds	CIGS	CIGS+	MO	VAR	X	Bandgap	Efficiency	Time
0.18	0.59	0.67	1	4.25	0.5	0.04	0.39	1.250718	27.0865	12.04
0.09	0.91	0.61	1.25	4.13	0.79	0.05	0.39	1.250718	26.6987	12.75
0.04	0.76	0.41	1.75	5.25	0.65	0.05	0.4	1.25706	26.6632	14.33
0.05	0.76	0.8	1.13	4.25	0.97	0.06	0.39	1.250718	26.6259	15.27
0.37	0.87	0.61	1.5	3	0.65	0.04	0.39	1.250718	26.5428	12.74
0.18	0.94	0.91	1	4.13	0.73	0.07	0.4	1.25706	26.4895	7.94
0.05	0.85	1	2.38	5.5	0.23	0.05	0.4	1.25706	26.4485	11.43
0.31	0.53	0.91	1.63	4.63	0.68	0.05	0.39	1.250718	26.4034	10.78
0.11	0.76	0.72	1.25	5.63	0.36	0.05	0.37	1.238046	26.3411	13.53
0.23	0.81	0.96	2.38	6.63	0.36	0.05	0.4	1.25706	26.3297	15.59
0.32	0.61	0.5	1	5.38	0.28	0.05	0.37	1.238046	26.2657	13.75
0.3	0.55	0.85	1.5	6.38	0.65	0.06	0.39	1.250718	26.2424	14.61

0.2	0.64	0.91	1.13	3.88	0.71	0.08	0.4	1.25706	26.2197	11
0.06	0.81	0.8	3.25	6.13	0.87	0.05	0.4	1.25706	26.1984	17.73
0.34	0.94	1	1.5	4.5	0.55	0.05	0.38	1.24438	26.1373	11.75
0.18	0.91	0.43	1.13	6	0.71	0.06	0.38	1.24438	26.133	17.2
0.15	0.44	0.76	1.38	6	0.81	0.04	0.36	1.231716	26.1293	12.01
0.15	0.57	0.61	1.88	3.63	0.89	0.04	0.37	1.238046	26.124	10.75
0.04	0.57	0.78	2.88	6.88	0.36	0.04	0.38	1.24438	26.0884	11.35
0.3	0.59	0.3	1.75	5.38	0.65	0.04	0.38	1.24438	26.0876	12.37
0.38	0.49	0.87	1.25	4.75	0.23	0.05	0.37	1.238046	26.0759	12.49
0.28	0.57	0.78	1.88	5.13	0.23	0.06	0.39	1.250718	26.0539	12.65
0.12	0.72	0.37	2.5	6.38	0.31	0.04	0.38	1.24438	26.0514	14.89
0.28	0.85	0.8	2.38	6.63	0.68	0.05	0.39	1.250718	26.0479	12.97
0.3	0.59	0.67	1.13	6	1	0.06	0.37	1.238046	26.0238	13.89
0.06	0.89	0.63	2.25	3.25	0.71	0.05	0.38	1.24438	26.0106	12.51
0.1	0.64	0.74	1.5	6.38	0.52	0.04	0.35	1.22539	26.007	11.95
0.24	0.49	0.37	1	6.5	0.68	0.07	0.39	1.250718	25.9903	9.27
0.14	0.87	0.48	1.13	5.63	0.95	0.09	0.39	1.250718	25.9832	12.17
0.14	0.76	0.61	4.75	6.5	0.42	0.04	0.4	1.25706	25.9803	12.68
0.2	0.94	0.41	1.13	5.38	0.76	0.04	0.35	1.22539	25.955	12.83
0.29	0.68	0.98	2	3	0.71	0.06	0.39	1.250718	25.9318	11.19
0.13	0.81	0.37	3.25	3.63	0.23	0.04	0.39	1.250718	25.9159	12.24
0.3	0.59	0.85	2.88	6.63	0.68	0.05	0.39	1.250718	25.8909	14.15
0.38	0.61	0.93	2	3.88	1	0.07	0.4	1.25706	25.8848	7.29
0.09	0.91	0.72	2.5	6.5	0.28	0.07	0.4	1.25706	25.868	8.59
0.12	0.81	0.8	2.63	5.25	0.2	0.05	0.38	1.24438	25.8645	12.67
0.09	0.81	0.96	1.13	4.88	0.34	0.08	0.38	1.24438	25.8625	9.48
0.1	0.89	0.98	2	4.38	0.76	0.06	0.38	1.24438	25.8528	13.44
0.34	0.98	0.58	2.13	6.88	0.73	0.04	0.37	1.238046	25.8273	11.32
0.4	0.61	0.48	2.13	5.63	0.23	0.06	0.39	1.250718	25.816	12.88
0.07	0.66	0.54	1.75	4	0.55	0.05	0.36	1.231716	25.8083	12.01
0.06	0.57	0.83	1.88	6.5	0.28	0.06	0.37	1.238046	25.8004	13.27
0.34	0.48	0.98	2.88	4	0.18	0.04	0.38	1.24438	25.7985	9.77
0.27	0.63	0.54	2.13	6.13	0.36	0.04	0.38	1.24438	25.7874	12.82
0.14	0.66	0.45	1.63	6.5	0.18	0.07	0.38	1.24438	25.7732	8.37
0.39	0.72	0.85	2.25	4.13	0.65	0.07	0.4	1.25706	25.7624	8.61
0.2	0.53	0.5	2.38	3.25	0.36	0.04	0.37	1.238046	25.7621	10.66
0.19	0.74	0.34	1.5	5.75	0.95	0.04	0.36	1.231716	25.75999	15.04
0.31	0.98	0.54	1.25	3.5	0.28	0.06	0.37	1.238046	25.7528	13.47
0.12	0.57	0.54	1.25	4	0.18	0.07	0.37	1.238046	25.7263	9.51
0.1	0.74	0.96	3.88	4	0.81	0.05	0.39	1.250718	25.7064	12.38
0.07	0.48	1	3.88	4.25	0.6	0.04	0.38	1.24438	25.6897	9.25
0.28	0.46	0.83	4.13	3	0.55	0.04	0.39	1.250718	25.674	9.55
0.34	0.89	0.61	2.63	6.5	0.18	0.05	0.38	1.24438	25.6683	12.81
0.2	0.46	0.45	3.25	6.5	1	0.06	0.4	1.25706	25.6675	14.61
0.16	0.78	0.37	1.5	7	0.76	0.06	0.37	1.238046	25.6635	20.49
0.39	0.63	0.91	2.75	6.63	0.28	0.04	0.37	1.238046	25.6614	10.43
0.21	0.98	0.48	1	5.63	0.47	0.09	0.39	1.250718	25.6589	14.45
0.2	0.48	0.3	3.38	3.25	0.87	0.05	0.4	1.25706	25.6578	11.28
0.12	0.49	0.91	1.13	5.13	0.79	0.1	0.4	1.25706	25.6502	9.24

0.14	0.79	0.37	2.5	6.25	0.28	0.05	0.37	1.238046	25.6476	16.75
0.16	0.44	0.48	1.13	5.13	0.65	0.09	0.39	1.250718	25.6139	11.48
0.29	0.42	0.74	1.5	5.25	0.23	0.09	0.4	1.25706	25.6028	8.13
0.33	0.44	0.61	1.38	3.88	0.63	0.09	0.4	1.25706	25.5997	7.62
0.04	0.68	0.34	4.25	4.88	0.42	0.04	0.38	1.24438	25.5691	10.7
0.11	0.55	0.63	1.75	4.5	0.5	0.04	0.34	1.219068	25.5643	12.07
0.21	0.55	0.32	1.25	5.75	0.76	0.07	0.38	1.24438	25.5627	21.74
0.13	0.57	0.76	1.38	4.5	0.84	0.05	0.34	1.219068	25.5572	12.09
0.09	0.74	0.37	4.38	6.88	0.5	0.06	0.4	1.25706	25.5386	13.11
0.32	0.91	0.61	1.88	4.13	0.44	0.04	0.35	1.22539	25.534	10.93
0.09	0.49	0.56	3.5	5.63	0.76	0.05	0.38	1.24438	25.5328	12.47
0.23	0.96	0.43	3.13	5.75	0.95	0.06	0.39	1.250718	25.529	16.74
0.11	0.74	0.72	1.5	6.88	0.81	0.06	0.35	1.22539	25.5244	14.19
0.21	0.64	0.45	1.63	5.25	0.81	0.08	0.38	1.24438	25.488	9.36
0.11	0.63	0.58	1	3.75	0.23	0.07	0.35	1.22539	25.4868	9.11
0.27	1	0.54	2	4.13	0.71	0.05	0.36	1.231716	25.4733	12.46
0.4	0.48	0.56	2.88	3.75	0.79	0.06	0.39	1.250718	25.4684	11.84
0.12	0.85	0.98	2.38	3.25	0.26	0.05	0.36	1.231716	25.4631	10.43
0.12	0.74	0.91	5	4.63	0.95	0.05	0.39	1.250718	25.4583	10.78
0.39	0.81	0.32	3.5	3.5	0.63	0.05	0.39	1.250718	25.426	9.81
0.37	0.78	0.43	4.38	6.63	0.47	0.04	0.38	1.24438	25.4126	11.09
0.38	0.42	0.63	1.88	5.75	0.76	0.06	0.37	1.238046	25.4051	12.31
0.21	0.57	0.78	5	6.25	0.5	0.06	0.4	1.25706	25.3989	12.9
0.29	1	0.87	2.63	4.63	0.95	0.06	0.38	1.24438	25.3987	20.55
0.2	0.96	0.91	2.25	3.25	0.97	0.07	0.38	1.24438	25.3954	9.34
0.37	0.49	0.32	3.38	5.88	0.18	0.06	0.4	1.25706	25.39	15.84
0.27	0.48	0.69	1.38	6.38	0.97	0.06	0.35	1.22539	25.38	15.17
0.09	1	0.8	2.25	5.13	0.18	0.09	0.4	1.25706	25.3783	9.84
0.1	0.89	0.34	2.75	3.38	0.34	0.07	0.39	1.250718	25.3761	7.46
0.07	0.74	0.41	1.38	3	0.89	0.08	0.37	1.238046	25.3704	4.6
0.07	0.66	0.43	4.5	5.5	0.73	0.07	0.4	1.25706	25.3528	7.43
0.33	0.68	0.52	1.25	5.63	0.23	0.09	0.38	1.24438	25.3434	9.16
0.38	0.85	0.98	2.88	4.63	0.34	0.05	0.37	1.238046	25.3254	10.37
0.39	0.68	0.48	1.13	3.25	0.73	0.08	0.37	1.238046	25.322	7.69
0.2	0.61	0.43	2	4.88	0.31	0.06	0.36	1.231716	25.3211	14.33
0.18	0.93	0.41	3.25	6.75	0.76	0.06	0.38	1.24438	25.3143	13.54
0.21	0.94	0.74	1.63	6.25	0.97	0.06	0.35	1.22539	25.3094	17.38
0.09	0.98	0.63	2	3.13	0.2	0.08	0.38	1.24438	25.3063	11.16
0.18	0.89	0.41	1.38	5.5	1	0.06	0.35	1.22539	25.3059	17.95
0.19	0.91	0.87	2.75	4.63	0.89	0.04	0.35	1.22539	25.2989	11.36
0.36	0.78	0.78	2.88	7	0.73	0.08	0.4	1.25706	25.2979	9.35
0.13	0.4	0.76	2.5	6.63	0.89	0.04	0.35	1.22539	25.2967	10.92
0.25	0.48	0.98	4.13	4.38	0.39	0.04	0.37	1.238046	25.2941	12.33
0.23	0.4	0.52	2.63	3	0.92	0.07	0.39	1.250718	25.2885	16.39
0.16	0.44	0.39	1.63	4.5	0.68	0.08	0.38	1.24438	25.2844	10
0.24	0.89	0.39	2.5	4.25	0.6	0.04	0.35	1.22539	25.2758	11.29
0.19	0.4	0.43	1.38	4.75	0.44	0.05	0.35	1.22539	25.2732	13.54
0.06	0.48	0.78	4.75	3.13	0.55	0.05	0.38	1.24438	25.267	11.03
0.21	0.51	0.56	2.63	3	0.31	0.05	0.36	1.231716	25.2667	11.17

0.07	0.85	0.85	1	4.88	0.2	0.09	0.36	1.231716	25.258	8.93
0.07	0.4	0.91	3.5	5.13	0.84	0.06	0.38	1.24438	25.2423	11.97
0.38	0.74	0.93	4.13	4.75	0.26	0.04	0.37	1.238046	25.241	9.86
0.4	0.81	0.72	5	3.38	0.52	0.05	0.39	1.250718	25.2342	9.83
0.19	0.53	0.41	3.25	6.13	0.76	0.08	0.4	1.25706	25.2332	8.1
0.13	0.53	0.67	3.88	4.25	0.15	0.05	0.37	1.238046	25.2332	13.13
0.28	0.89	0.83	3.13	6.25	0.68	0.08	0.4	1.25706	25.2289	10.93
0.13	0.53	1	3.13	6.75	0.31	0.07	0.38	1.24438	25.2163	8.03
0.32	0.48	0.89	3.38	4.5	0.89	0.05	0.37	1.238046	25.2147	12.75
0.19	0.57	0.98	3.75	3.13	0.68	0.05	0.37	1.238046	25.2144	14.88
0.39	0.61	0.34	1.5	3.63	0.47	0.08	0.38	1.24438	25.2018	8.94
0.11	0.42	0.83	3.63	4.13	0.73	0.05	0.37	1.238046	25.1967	12.95
0.33	0.55	0.78	1.38	5.25	0.28	0.05	0.33	1.21275	25.1933	12.49
0.21	0.51	0.83	2.25	6.63	0.52	0.09	0.39	1.250718	25.1903	17.51
0.36	0.42	0.45	3.63	5.88	1	0.06	0.39	1.250718	25.179	16.59
0.29	0.53	0.67	1.38	4.5	0.87	0.05	0.33	1.21275	25.1787	13.85
0.29	0.83	0.58	3.25	3.25	0.26	0.08	0.4	1.25706	25.1752	9.15
0.14	0.61	0.34	2	3.13	0.6	0.08	0.38	1.24438	25.1736	10.45
0.14	0.98	0.78	1.13	5.5	0.26	0.07	0.34	1.219068	25.1675	8.31
0.04	0.79	0.56	4.63	6.5	0.15	0.06	0.38	1.24438	25.1661	13.46
0.31	0.98	0.63	2.63	3.88	0.28	0.07	0.38	1.24438	25.1562	7.76
0.18	0.68	0.43	4	4.25	0.92	0.07	0.39	1.250718	25.1502	7.63
0.3	1	0.58	4.38	6.25	0.52	0.06	0.39	1.250718	25.1368	12.05
0.37	0.63	0.3	3.63	6	0.76	0.06	0.39	1.250718	25.1342	12.22
0.19	0.96	0.54	4	6.13	0.55	0.06	0.38	1.24438	25.1292	12.33
0.25	0.44	0.89	1.75	6.75	0.63	0.09	0.38	1.24438	25.129	14.78
0.04	0.76	0.34	4.38	3.75	0.95	0.07	0.39	1.250718	25.1164	7.62
0.33	0.94	0.69	3.63	6.25	0.79	0.07	0.39	1.250718	25.1037	8.81
0.18	0.61	0.5	4.13	4	0.18	0.08	0.4	1.25706	25.101	8.93
0.33	0.48	0.56	2.25	5.13	0.15	0.06	0.36	1.231716	25.0962	12.87
0.29	0.76	1	1.38	4.75	0.31	0.09	0.37	1.238046	25.0942	7.81
0.38	0.93	0.89	3.5	4.5	0.44	0.06	0.38	1.24438	25.0745	16.04
0.39	0.55	0.54	3.88	4.25	0.81	0.07	0.39	1.250718	25.0711	7.03
0.12	0.72	0.8	2.25	3	0.31	0.08	0.37	1.238046	25.0544	8.38
0.1	0.63	0.74	3.63	5.88	0.34	0.09	0.4	1.25706	25.0515	7.99
0.16	0.57	0.85	2	3.13	0.71	0.1	0.39	1.250718	25.0491	7.33
0.34	0.94	0.56	1	5.63	0.79	0.08	0.35	1.22539	25.0406	9.98
0.19	0.78	0.39	4.38	4.75	0.2	0.06	0.38	1.24438	25.0397	12.11
0.04	0.51	0.37	2.75	4.38	0.31	0.06	0.36	1.231716	25.0221	11.73
0.36	0.78	0.67	4.25	4	0.73	0.05	0.37	1.238046	25.0044	9.98
0.39	0.96	0.52	2.13	4.75	0.34	0.05	0.39	1.250718	24.9917	11.79
0.22	0.7	0.65	3	5	0.57	0.07	0.37	1.238046	24.9809	13.09
0.1	0.74	0.85	3.88	5.63	0.95	0.09	0.4	1.25706	24.975	8.25
0.09	0.4	0.72	1.25	6.38	0.31	0.1	0.37	1.238046	24.9749	12.67
0.39	0.68	0.58	1.88	3.63	0.63	0.09	0.38	1.24438	24.9698	8.09
0.29	0.68	1	3.75	5.38	1	0.05	0.36	1.231716	24.9663	11.05
0.04	0.94	0.69	4.25	3.5	0.47	0.06	0.37	1.238046	24.9661	11.52
0.38	0.61	0.83	4.13	4.88	0.39	0.08	0.4	1.25706	24.9581	7.91
0.37	0.78	0.41	4.25	6.88	0.36	0.06	0.38	1.24438	24.9576	11.5

0.24	0.87	0.89	1.5	6.88	0.55	0.06	0.33	1.21275	24.957	15.16
0.1	0.46	0.74	5	4.38	0.36	0.06	0.38	1.24438	24.952	11.92
0.13	0.68	0.43	2.5	4.63	0.15	0.05	0.34	1.219068	24.9515	12.14
0.23	0.87	0.52	2.13	5.38	0.52	0.1	0.39	1.250718	24.9362	10.83
0.31	0.79	0.5	3.75	3.88	0.6	0.05	0.36	1.231716	24.9288	10.74
0.12	1	0.67	4.75	3.75	0.6	0.08	0.4	1.25706	24.9248	7.36
0.28	0.46	0.56	4.25	3.63	0.23	0.08	0.4	1.25706	24.9182	7.06
0.39	0.87	0.54	2.13	3	0.65	0.05	0.34	1.219068	24.9004	10.98
0.31	0.98	0.96	2.25	4.13	0.52	0.05	0.34	1.219068	24.8981	11.69
0.25	0.76	0.34	3.63	4	0.34	0.07	0.38	1.24438	24.8903	7.13
0.29	0.46	0.69	1.63	3.38	0.15	0.09	0.37	1.238046	24.8852	9.53
0.07	0.63	0.89	1.75	3.13	0.79	0.08	0.35	1.22539	24.8842	8.11
0.04	0.59	0.58	1	6.63	0.63	0.09	0.34	1.219068	24.8797	9.97
0.09	0.63	0.63	1.75	6	0.42	0.09	0.36	1.231716	24.8781	17.92
0.15	0.94	0.61	4.38	6.63	1	0.05	0.36	1.231716	24.8769	13.03
0.32	0.4	0.63	1.25	6.25	0.55	0.06	0.33	1.21275	24.8693	15.3
0.06	0.79	0.48	1.88	5.13	0.76	0.06	0.33	1.21275	24.8689	14.82
0.29	0.96	0.32	2.88	3.88	0.73	0.08	0.36	1.231716	24.8582	9.11
0.28	0.55	0.45	3.13	5.88	0.42	0.04	0.34	1.219068	24.853	12.09
0.11	0.91	0.93	2.5	3	0.71	0.09	0.38	1.24438	24.8506	10.52
0.25	0.63	0.91	1.63	5.25	0.95	0.08	0.35	1.22539	24.8503	17.07
0.13	0.61	0.8	2.25	6.13	0.55	0.09	0.37	1.238046	24.848	11.03
0.05	0.72	0.72	4.13	6.38	0.52	0.05	0.35	1.22539	24.8413	15.83
0.16	0.94	0.74	1.75	6.38	0.92	0.06	0.33	1.21275	24.8412	16.79
0.4	0.61	0.74	1.38	3.5	1	0.08	0.35	1.22539	24.8205	7.91
0.37	0.55	0.45	5	5.13	0.95	0.05	0.37	1.238046	24.8175	10.84
0.36	1	0.58	4.75	3.63	0.84	0.04	0.36	1.231716	24.8163	10.72
0.4	0.46	0.61	1.75	6.5	0.68	0.08	0.36	1.231716	24.8156	9.25
0.28	0.83	1	2.63	6.38	0.84	0.07	0.36	1.231716	24.8134	8.18
0.19	0.64	0.96	2.38	6	0.81	0.07	0.35	1.22539	24.8128	11.75
0.2	0.44	0.5	4	3.88	0.89	0.05	0.36	1.231716	24.7931	10.98
0.11	0.85	0.52	4.63	4.75	0.87	0.09	0.4	1.25706	24.793	7.78
0.05	0.53	0.76	3.88	7	0.5	0.09	0.39	1.250718	24.7925	8.16
0.4	0.64	0.96	1.63	6.25	0.2	0.07	0.34	1.219068	24.7895	7.91
0.24	0.96	0.8	2	6.13	0.26	0.09	0.37	1.238046	24.7788	9.72
0.05	0.85	0.76	2.13	5.75	0.34	0.07	0.34	1.219068	24.7694	8.68
0.27	0.79	0.8	1.88	6	0.97	0.06	0.33	1.21275	24.7562	12.73
0.25	1	0.37	2.75	3.75	0.89	0.08	0.38	1.24438	24.753	9.09
0.3	0.42	0.52	4.88	4.5	0.89	0.07	0.39	1.250718	24.7521	8.14
0.15	0.87	0.63	4.63	5.5	0.28	0.09	0.4	1.25706	24.7423	7.32
0.21	0.53	0.78	3.88	4.63	0.63	0.04	0.34	1.219068	24.7406	13.53
0.04	0.51	0.72	3.38	3.25	0.71	0.06	0.35	1.22539	24.734	12.68
0.32	0.68	0.5	3.75	7	0.84	0.06	0.36	1.231716	24.7278	13.33
0.19	0.93	0.32	1.88	5.63	0.76	0.1	0.36	1.231716	24.725	11.94
0.18	0.64	0.3	1.75	3.38	0.52	0.06	0.34	1.219068	24.722	13.82
0.31	0.72	0.87	3.5	5.38	1	0.09	0.39	1.250718	24.7134	7.44
0.27	0.72	0.87	2	5.75	0.23	0.07	0.34	1.219068	24.6895	8.52
0.16	0.57	0.3	3.38	3.63	0.31	0.07	0.37	1.238046	24.6857	8.5
0.28	0.83	0.45	4	6.88	0.44	0.04	0.34	1.219068	24.6812	10.18

0.16	0.85	0.85	2.88	4.13	0.73	0.1	0.39	1.250718	24.6799	7.32
0.05	0.72	0.83	4.88	6.75	0.42	0.06	0.36	1.231716	24.6777	12.79
0.2	0.53	0.41	4.5	3.13	0.6	0.09	0.4	1.25706	24.6763	11.09
0.15	0.64	0.3	4.63	5.25	0.84	0.05	0.36	1.231716	24.6761	11
0.23	0.83	0.52	1	3.75	0.65	0.08	0.33	1.21275	24.6624	11.73
0.15	0.44	0.98	3.13	6.13	0.42	0.06	0.37	1.238046	24.6533	12.32
0.4	0.89	0.58	2.63	6.75	0.44	0.09	0.38	1.24438	24.6515	8.3
0.33	0.78	0.72	5	6.25	0.92	0.07	0.38	1.24438	24.6367	7.29
0.37	0.74	0.87	1.5	4.5	0.42	0.07	0.33	1.21275	24.6271	14.54
0.38	0.93	0.52	1.25	6.88	0.6	0.09	0.35	1.22539	24.6202	9.58
0.19	0.96	0.41	4.25	3.25	0.52	0.05	0.35	1.22539	24.6065	9.71
0.19	0.4	0.93	3.25	6.25	0.26	0.06	0.35	1.22539	24.5899	12.24
0.25	0.44	0.76	2	3.88	0.6	0.08	0.35	1.22539	24.5608	8.76
0.11	0.93	0.74	3.75	4.88	1	0.08	0.37	1.238046	24.5406	7.67
0.23	0.89	0.48	3.75	3.38	0.63	0.05	0.34	1.219068	24.5187	10.85
0.18	0.93	0.61	4.63	3.63	0.18	0.08	0.38	1.24438	24.5175	7.02
0.34	0.66	0.45	2.13	4.38	0.2	0.06	0.33	1.21275	24.516	14.13
0.3	0.79	0.96	4	6.88	0.55	0.06	0.35	1.22539	24.514	13.23
0.11	0.46	0.61	2.38	3.75	0.36	0.07	0.34	1.219068	24.5058	8.34
0.14	0.4	0.72	1.63	3.75	0.63	0.08	0.34	1.219068	24.5033	7.77
0.31	0.87	0.63	2.13	5.75	1	0.09	0.36	1.231716	24.4993	8.37
0.05	0.79	0.96	4.5	6.38	0.68	0.06	0.35	1.22539	24.497	12.5
0.33	0.66	0.58	4.5	3.13	0.34	0.08	0.38	1.24438	24.4924	6.99
0.37	0.66	0.89	4.63	7	0.26	0.06	0.36	1.231716	24.4897	11.85
0.15	0.57	0.72	2.75	6.75	0.89	0.06	0.33	1.21275	24.4897	12.48
0.27	0.51	0.89	4.63	4.5	0.15	0.08	0.38	1.24438	24.4748	10.33
0.32	0.66	0.39	1	5.38	0.2	0.09	0.34	1.219068	24.4615	9.88
0.13	0.42	0.34	3.75	5.88	0.63	0.09	0.39	1.250718	24.4607	7.6
0.34	0.78	0.56	2.38	4.13	0.81	0.06	0.33	1.21275	24.4506	12.81
0.07	0.63	0.87	1.63	3.38	0.68	0.1	0.35	1.22539	24.4459	8.81
0.31	0.83	0.54	4.63	5.5	0.31	0.09	0.39	1.250718	24.4382	9.86
0.27	0.76	1	4.25	6.63	0.63	0.08	0.39	1.250718	24.4211	16.44
0.06	0.48	0.41	2.5	5.5	0.71	0.08	0.35	1.22539	24.4209	8.05
0.24	0.79	0.87	4	5.13	0.84	0.08	0.37	1.238046	24.4179	9.18
0.11	0.72	0.78	4.75	4.38	0.92	0.06	0.35	1.22539	24.4173	12.83
0.23	0.76	0.85	4.38	4.75	0.34	0.06	0.35	1.22539	24.4076	12.32
0.07	0.78	1	2.38	4	0.39	0.08	0.34	1.219068	24.3861	7.33
0.15	0.72	0.3	2.25	4.63	0.15	0.09	0.37	1.238046	24.384	10.21
0.33	0.49	0.37	3.5	7	0.44	0.06	0.35	1.22539	24.3634	12.12
0.06	0.66	0.37	1.88	5.25	0.89	0.1	0.36	1.231716	24.3614	8.91
0.09	0.63	0.52	3.13	3	0.42	0.06	0.33	1.21275	24.3571	11.63
0.13	0.42	0.67	3.38	6.13	0.87	0.07	0.35	1.22539	24.3535	9.35
0.25	0.87	0.89	2.75	3.88	0.39	0.06	0.33	1.21275	24.3516	12.49
0.31	0.87	0.3	2.88	3.25	0.84	0.07	0.35	1.22539	24.3501	11.23
0.25	0.83	0.32	2.25	6.88	0.47	0.09	0.36	1.231716	24.3357	13.71
0.23	0.89	0.74	3.38	7	0.84	0.09	0.37	1.238046	24.3256	10.27
0.16	0.51	0.48	2.88	3.75	0.47	0.06	0.33	1.21275	24.3162	11.28
0.09	0.98	0.85	2.38	4.13	0.15	0.08	0.34	1.219068	24.3145	9.3
0.2	0.51	0.91	3.5	5.75	0.55	0.1	0.38	1.24438	24.3039	10.48

0.12	0.93	0.41	2.63	5.5	0.26	0.09	0.36	1.231716	24.2988	9.26
0.33	0.98	0.48	2.38	5.88	0.42	0.09	0.36	1.231716	24.2981	10.27
0.36	0.66	0.93	1.63	3.13	0.65	0.08	0.33	1.21275	24.2963	8.3
0.25	0.49	0.43	3.25	5.38	0.26	0.1	0.38	1.24438	24.2746	8.51
0.36	0.42	0.67	4	6.88	0.95	0.06	0.35	1.22539	24.2735	13.34
0.06	0.98	0.67	4.13	4.25	0.39	0.08	0.36	1.231716	24.2662	7.54
0.23	0.46	0.56	4.38	3.75	0.18	0.09	0.38	1.24438	24.2613	7.57
0.32	0.83	0.76	4.75	6	0.97	0.07	0.36	1.231716	24.2449	6.83
0.3	0.53	0.83	4.88	4.38	0.2	0.05	0.34	1.219068	24.2415	10.37
0.33	0.85	0.67	4.25	5.5	0.65	0.1	0.39	1.250718	24.2217	7.17
0.4	0.89	0.93	3.25	5.63	0.84	0.09	0.37	1.238046	24.2201	7.75
0.28	0.96	0.83	4.88	4.88	0.5	0.05	0.34	1.219068	24.2045	11.12
0.12	0.49	0.69	4.13	5.88	0.71	0.1	0.38	1.24438	24.2028	7.42
0.28	0.96	0.91	4.38	5.5	0.47	0.06	0.35	1.22539	24.2019	11.23
0.32	0.91	0.39	4.88	4.88	0.36	0.04	0.33	1.21275	24.1936	15
0.05	0.59	0.98	2.5	6.5	0.52	0.09	0.34	1.219068	24.1789	8.96
0.11	0.96	0.69	4.63	6.13	0.52	0.05	0.33	1.21275	24.1769	11.02
0.15	0.98	0.56	4.5	4.75	0.92	0.05	0.33	1.21275	24.1725	12.67
0.4	0.72	0.96	1.75	5.13	0.73	0.1	0.35	1.22539	24.1683	8.8
0.21	1	0.78	3.38	7	0.23	0.07	0.34	1.219068	24.1663	11.27
0.23	0.42	0.83	5	4.38	0.68	0.05	0.34	1.219068	24.1573	14.66
0.04	0.93	0.74	3.13	6.25	0.36	0.08	0.34	1.219068	24.1571	13.63
0.34	0.51	0.96	3.25	6.63	0.81	0.07	0.34	1.219068	24.1568	11.19
0.25	1	0.87	4.63	5.25	0.71	0.09	0.38	1.24438	24.1522	12.14
0.36	0.59	0.34	4.88	5.13	0.81	0.06	0.35	1.22539	24.1304	14.87
0.14	0.81	0.63	4.88	4	0.15	0.08	0.36	1.231716	24.1295	6.72
0.18	0.4	0.76	4	5.88	0.44	0.09	0.37	1.238046	24.1225	9.52
0.24	0.44	0.39	3.75	6.75	0.18	0.07	0.35	1.22539	24.1205	11.72
0.3	0.74	0.85	4.38	3.5	0.97	0.07	0.35	1.22539	24.1176	7.36
0.06	0.55	0.32	3.13	5.38	0.81	0.09	0.36	1.231716	24.1142	8.77
0.36	0.91	0.74	2.5	4.38	0.39	0.09	0.35	1.22539	24.0958	8.33
0.28	0.63	0.93	4.5	3	0.39	0.08	0.36	1.231716	24.0796	6.97
0.38	0.83	0.48	4.13	3.5	0.87	0.08	0.36	1.231716	24.0679	7.09
0.21	0.44	0.87	2.88	4.25	0.2	0.08	0.34	1.219068	24.0672	9.43
0.37	0.74	0.76	4.25	6	0.6	0.09	0.37	1.238046	24.0615	7.9
0.3	0.61	0.93	3.5	3.75	0.87	0.09	0.36	1.231716	24.0608	7.11
0.31	1	0.54	3.5	3.38	0.26	0.1	0.38	1.24438	24.055	8.07
0.23	0.85	0.98	4.75	4.25	0.39	0.07	0.35	1.22539	24.0546	16.21
0.3	0.64	0.69	1.25	3.5	0.73	0.1	0.33	1.21275	24.0517	9.39
0.07	0.91	0.98	2.63	4.13	0.97	0.08	0.33	1.21275	24.0511	9.01
0.27	0.48	0.89	2.75	3.25	0.39	0.09	0.35	1.22539	24.0443	8.63
0.32	0.55	0.32	3.63	6.75	0.89	0.09	0.37	1.238046	24.0428	8.63
0.13	0.42	0.76	4.75	6.5	0.87	0.08	0.36	1.231716	24.0404	8.31
0.05	0.68	0.45	3.75	5.88	0.5	0.07	0.33	1.21275	24.0268	8.31
0.16	0.94	0.48	1.88	7	0.6	0.1	0.34	1.219068	23.9976	10.52
0.1	0.51	0.69	3.38	3.5	0.97	0.09	0.35	1.22539	23.9957	12.69
0.05	0.78	0.39	3.25	3.38	0.87	0.1	0.36	1.231716	23.9876	8.36
0.15	0.4	0.43	3.38	5.38	0.2	0.08	0.35	1.22539	23.987	10
0.34	0.76	0.56	4.5	3.63	0.63	0.1	0.38	1.24438	23.9864	6.67

0.04	0.79	0.83	3.88	4.38	0.92	0.08	0.34	1.219068	23.9599	7.66
0.34	0.66	0.34	2.13	6	0.34	0.09	0.34	1.219068	23.9533	9.34
0.24	0.46	0.89	4.88	4.63	0.39	0.1	0.38	1.24438	23.9373	7.85
0.37	1	0.39	2.5	4.88	0.31	0.09	0.35	1.22539	23.9321	8.34
0.06	0.91	0.43	4.75	5.25	0.92	0.09	0.36	1.231716	23.9111	7.42
0.32	0.59	0.5	3.38	4.75	0.95	0.09	0.35	1.22539	23.8752	7.68
0.24	0.94	0.85	2.75	3.5	0.15	0.08	0.33	1.21275	23.8701	9.01
0.06	0.79	0.37	4	6.13	0.15	0.07	0.33	1.21275	23.8665	8.16
0.12	0.79	0.8	5	4.63	0.87	0.09	0.36	1.231716	23.8622	7.66
0.24	0.76	0.39	4.88	6.13	0.44	0.06	0.33	1.21275	23.8525	11.71
0.16	0.83	0.52	4.13	4.88	0.92	0.08	0.34	1.219068	23.8383	7.34
0.25	0.66	0.96	4.5	4.25	0.2	0.1	0.37	1.238046	23.8371	7.21
0.14	0.81	0.45	3.13	3.38	0.47	0.09	0.34	1.219068	23.8265	8.34
0.36	0.4	0.5	3.75	4.88	0.97	0.06	0.33	1.21275	23.8229	11.35
0.36	0.49	0.58	3.5	3.5	0.87	0.07	0.33	1.21275	23.8083	7.05
0.33	0.64	0.58	4.75	4.38	0.79	0.09	0.36	1.231716	23.8061	7.45
0.15	0.72	0.32	4	7	0.44	0.08	0.34	1.219068	23.7944	8
0.2	0.91	0.93	5	3.5	0.47	0.07	0.34	1.219068	23.7873	7.41
0.24	0.87	0.8	3.63	6.75	0.79	0.1	0.36	1.231716	23.7831	9.07
0.27	0.49	0.87	4.88	4	0.44	0.08	0.35	1.22539	23.7731	7.13
0.1	0.42	0.72	3.88	3.13	0.42	0.1	0.36	1.231716	23.7567	7.77
0.37	0.93	0.3	2.13	5.75	0.55	0.1	0.35	1.22539	23.7543	9.54
0.14	0.85	0.45	4.5	3.63	0.5	0.08	0.34	1.219068	23.7526	9.63
0.34	0.51	0.32	4	5.63	0.39	0.08	0.35	1.22539	23.7404	8.17
0.38	0.51	0.67	3.75	6.75	0.44	0.09	0.35	1.22539	23.7317	7.57
0.29	0.96	0.54	4.63	4	0.34	0.1	0.37	1.238046	23.7264	8.94
0.1	0.93	0.32	3.13	6	0.97	0.1	0.35	1.22539	23.7222	8.35
0.24	0.93	1	2.63	6.75	0.28	0.09	0.33	1.21275	23.6875	10.93
0.29	0.83	0.69	4.13	6.38	0.26	0.1	0.36	1.231716	23.6739	9.75
0.16	0.55	0.5	3.63	3.38	0.47	0.09	0.34	1.219068	23.671	9.86
0.31	0.59	0.93	2.75	6.38	0.92	0.1	0.34	1.219068	23.6582	8.72
0.05	0.44	0.78	3.88	5.25	0.81	0.09	0.34	1.219068	23.6486	8.19
0.32	0.68	0.93	3.5	3.63	0.84	0.1	0.35	1.22539	23.5965	7.74
0.4	0.83	0.52	3.13	3.13	0.79	0.1	0.35	1.22539	23.5952	7.81
0.39	0.64	0.5	4.88	5.75	0.18	0.08	0.34	1.219068	23.5412	7.13
0.13	0.87	0.39	4.38	5.38	0.47	0.09	0.34	1.219068	23.5306	8.25
0.14	0.81	1	4.25	4.63	0.5	0.1	0.35	1.22539	23.5142	7.92
0.1	0.46	0.3	4.5	5.5	0.6	0.09	0.35	1.22539	23.4985	8.15
0.38	0.59	0.5	2.75	3.88	0.28	0.09	0.33	1.21275	23.4641	8.66
0.27	0.46	0.39	5	5.88	0.42	0.07	0.33	1.21275	23.4547	8.18
0.21	0.59	0.34	3.63	3.38	0.79	0.09	0.33	1.21275	23.3618	7.67
0.07	0.53	0.69	4.5	7	0.5	0.1	0.34	1.219068	23.3365	9.57
0.36	0.49	0.69	4.75	5.88	0.36	0.09	0.34	1.219068	23.316	9.73
0.18	0.78	0.76	3.88	3.88	0.79	0.1	0.35	1.22539	23.2028	7.27
0.4	0.64	0.89	4.25	4.75	0.5	0.09	0.33	1.21275	23.1946	7.75
0.39	0.55	0.3	3.63	4.5	0.92	0.09	0.33	1.21275	23.1641	8.18
0.27	0.81	0.63	5	5.75	0.65	0.1	0.34	1.219068	23.1289	8.2

LIST OF REFERENCES

[1] C. Thompson, "Paying for wight in blood: An analysis of weight and protection level of a combat load during tactical operations," M.S thesis, Dept. of Operations Research, NPS, Monterey, CA, USA, 2019. [Online]. Available: https://calhoun.nps.edu/handle/10945/62831

[2] K. Logar, "Advanced hybrid solar cell design," M.S. thesis, Dept. of Elec. & Comp. Eng., NPS, Monterey, CA, 2022.

[3] J. Herrera, "Novel design of copper indium gallium diselenide (CIGS) solar cell with application on UAS puma 3 AE," M.S. thesis, Dept. of Elec. & Comp. Eng., NPS, Monterey, CA, USA, 2015. [Online]. Available: https://calhoun.nps.edu/handle/10945/67203

[4] K. Fotis, "Modeling and simulation of dual-junction CIGS solar cell using Silvaco ATLAS," M.S. thesis, Dept. of Elec. & Comp. Eng., NPS, Monterey, CA, 2012.

[5] D. Columbus, "Design and optimization of copper indium gallium selenide solar cells for lightweight battlefield application," M.S. thesis, Dept. of Elec. & Comp. Eng., NPS, Monterey, CA, 2014. [Online]. Available: https://calhoun.nps.edu/handle/10945/42600

[6] J. O'Connor, "Design and simulation of novel, high-efficiency, back-contact solar cells" Ph. D dissertation, Dept. of Elec. & Comp. Eng., NPS, Monterey, CA, USA, 2015.

[7] S. Green, "Interdigitated back-surface-contact solar cell modeling using Silvaco ATLAS," M.S. thesis, Dept. of Elec. & Comp. Eng., NPS, Monterey, CA, USA, 2015. [Online]. Available: https://calhoun.nps.edu/handle/10945/45861

[8] P. Michalopoulous, "A novel approach for the development and optimization of state-of-the-art photovoltaic devices using Silvaco," M.S. thesis, Dept. of Elec. & Comp. Eng., NPS, Monterey, CA, USA, 2002. [Online]. Available: https://calhoun.nps.edu/handle/10945/5609

[9] R. Hazen, "Light-matter interactions at the atomic level." Accessed October 7, 2021 [Online]. Available: https://www.thegreatcoursesdaily.com/light-matter-interactions-at-the-atomic-level/

[10] Wikipedia, "Electronic band structure." Accessed September 12, 2021 [Online]. Available: https://en.wikipedia.org/wiki/Electronic_band_structure

[11] PVeducation, "Semiconductor Materials." Accessed April 28, 2022 [Online]. Available: https://www.pveducation.org/pvcdrom/pn-junctions/semiconductor-materials

[12] K. Jager, O. Isabella, A. Smets, R. A. van Swaaij, and M. Zeman, *Solar Energy: Fundamentals, Technology, and Systems*, Delft University of Technology, 2014. [Online]. Available: https://courses.edx.org/c4x/DelftX/ET.3034TU/asset/solar_energy_v1.1.pdf

[13] B. Zeghbroech, "P-N Junctions." Accessed March 19, 2022 [Online]. Available: http://truenano.com/PSD20/contents/toc4.htm

[14] J. Nelson, "Air mass," Engineering LibreTexts, June 05, 2019. [Online]. Available: https://eng.libretexts.org/Bookshelves/Materials_Science/Supplemental_Modules_(Materials_Science)/The_Science_of_Solar/Solar_Basics/B._Basics_of_the_Sun/V._Air_Mass

[15] C. Honsberg and S. Bowden, "PV Education." Accessed November 15, 2021 [Online]. Available: https://www.pveducation.org/

[16] SunPower Corporation, More power. A better investment. [Online]. Available: https://silo.tips/download/more-power-a-better-investment

[17] M. Lammert and R. Schwartz, "Silicon solar cells for high concentration applications" in *Proc. Electron Devices Mtg*, 1975, pp. 350–352. [Online]. doi: 10.1109/IEDM.1975.188896

[18] S. Green, "Interdigitated back-surface-contact solar cell modeling using Silvaco ATLAS," M.S. thesis, Dept. of Elec. & Comp. Eng., NPS, Monterey, CA, USA, 2015. [Online]. Available: https://calhoun.nps.edu/handle/10945/45861

[19] A. Bates, "Novel optimization technique for multijunction solar cell design using Silvaco ATLAS," M.S. thesis, Dept. of Elec. & Comp. Eng., NPS, Monterey, CA, USA, 2004. [Online]. Available: https://calhoun.nps.edu/handle/10945/46458

[20] W. Shafarman and L. Stolt, Handbook of Photovoltaic Science and Engineering, John. Wiley & Sons, 2003, ch. 13, pp. 567–616. [Online]. doi: 10.10002/0470014008

[21] M. Contreras, L. Mansfield, B. Egaas, J. Li, M. Romero, R. Noufi, E. Rudiger-Voigt, and W. Mannstadt, "Improved energy conversion efficiency in wide-bandgap Cu(In, GA)Se2 solar cells" in *37th IEEE Photo. Spec. Conf.*, 2011, pp. 26–31. [Online]. doi: 10.1109/PVSC.2011.6185837

[22] K. Nagaich, S. Campbell and E. Aydil, "Wide band-gap CuIn1−XGaXSe2 based chalcopyrite absorbers for tandem cell applications," in *37th IEEE Photo. Spec. Conf.*, 2011, pp. 425–429. [Online]. doi: 10.1109/PVSC.2011.6185984

[23] Circuits Today, "Thin film solar cell," Accessed April 28, 2022 [Online]. Available: https://www.circuitstoday.com/thin-film-solar-cell

[24] M. Richter, C. Schubbert, P. Eraerds, I. Riedel, J. Keller, J. Parisi, T. Dalibor, and A. Avellan-Hampe, “Optical characterization and modeling of Cu(In, GA)(Se, S)2 solar cells with spectroscopic ellipsometry and coherent numerical simulation” *Thin Solid Films*, vol *535*, 2013, pp. 331–335. [Online]. doi: 10.1016/j.tsf.2012.11.078

[25] M. Hsieh, S. Kuo, F. Lai, M. Kao, P. Huang, H. Wang, M. Tsai, and H. Kuo, “Optimization of CdS buffer layer on the performance of copper indium gallium selenide solar cells” in 2011 Conference on Lasers and Electro-Optics Pacific Rim, 2011. [Online]. Available: https://opg.optica.org/abstract.cfm?uri=cleopr2011-C765

[26] C. Larez, C. Bellabarba, and C. Rincon, “Alloy composition and temperature dependence of the fundamental absorption edge in CuGaxIn1-xSe2” in Applied Physics Letters 65, 1994, pp. 1650-1652. [Online]. doi: 10.1063/1.112944

[27] T. M. Cioppa and T. W. “Lucas. Efficient nearly orthogonal and space-filling Latin hypercubes.” Technometrics, 49(1):45–55, 2007.

[28] P. J. Sanchez. 2018. Datafarming (Version 1.3.0): RubyGem. [Online]. Available: https://rubygems. org/gems/datafarming

[29] Silvaco, Inc., Atlas User Manual, Santa Clara, CA, 2020.

THIS PAGE INTENTIONALLY LEFT BLANK

INITIAL DISTRIBUTION LIST

1. Defense Technical Information Center
   Ft. Belvoir, Virginia

2. Dudley Knox Library
   Naval Postgraduate School
   Monterey, California